Department of Computer Science

AGH University of Science and Technology in Krakow

Three-Dimensional Oil-Industry Applications Using a Goal-Oriented hp-Finite Element Method

D. Pardo, M. Paszynski, C. Torres-Verdín, M. J. Nam, Ch. Michler, L. Demkowicz

Collaborators: W. Rachowicz, A. Zdunek, L.E. Garcia-Castillo,
I. Gomez-Revuleto, J. Kurtz, R. Abdollah-Pour

September 4, 2007

Department of Petroleum and Geosystems Engineering

THE UNIVERSITY OF TEXAS AT AUSTIN

OVERVIEW

1. **Motivation:** Simulation of borehole logging measurements.
2. **One Dimension (1D):** Brief introduction to hp-finite elements (FE).
3. **Two Dimensions (2D):**
   - Methodology: A goal-oriented self-adaptive hp-FE method.
   - Numerical simulations of 2D electromagnetic measurements.
   - Numerical simulations of 2.5D sonic measurements.
4. **Three Dimensions (3D):**
   - Methodology: A Fourier series expansion in a non-orthogonal system of coordinates with a 2D hp goal-oriented FE method.
   - Numerical simulations of 3D electromagnetic measurements.
5. **Conclusions and future work.**

MOTIVATION (APPLICATIONS)

Logging Instruments: Definition

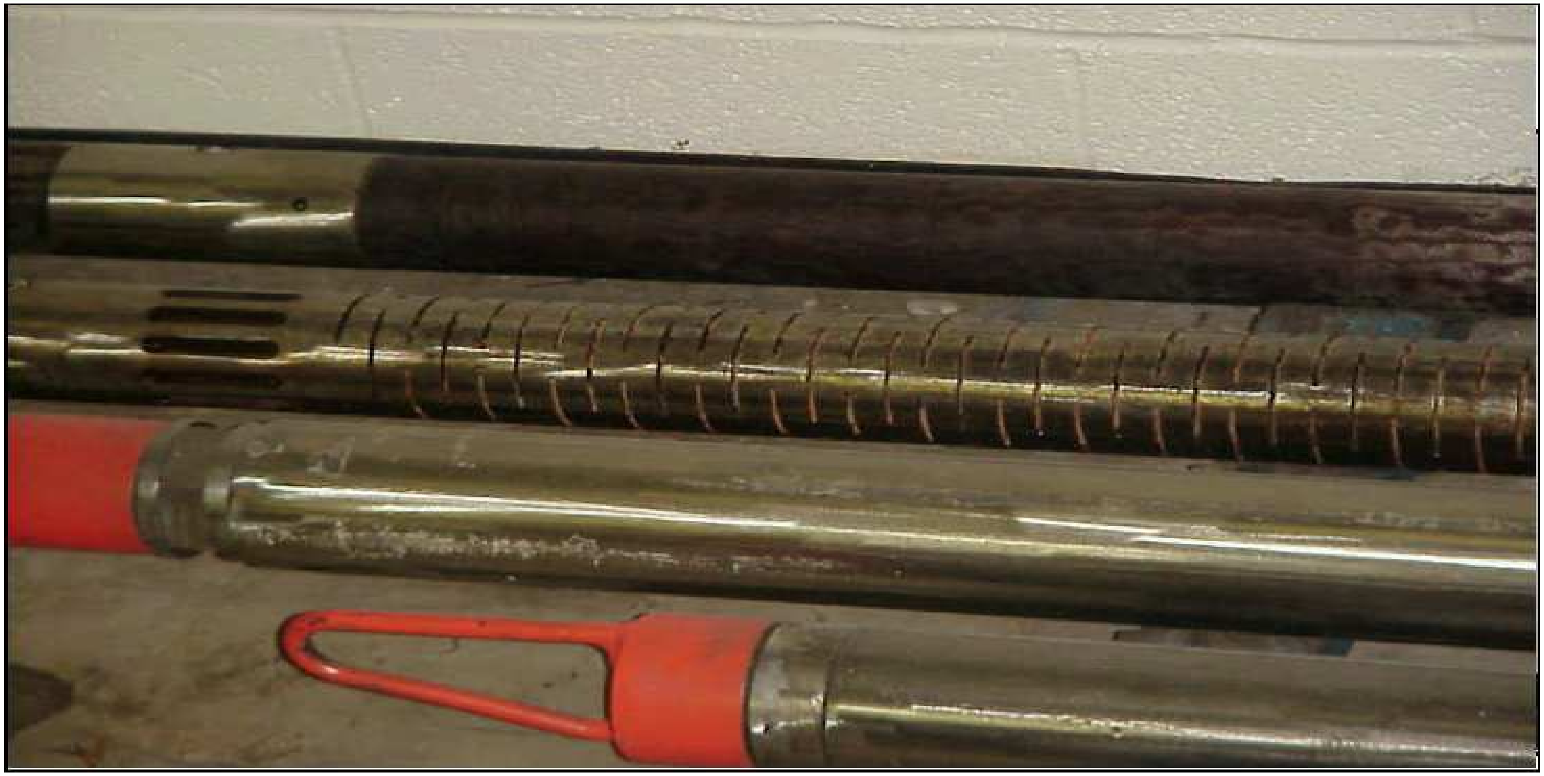

MOTIVATION (APPLICATIONS)

Utility of Logging Instruments

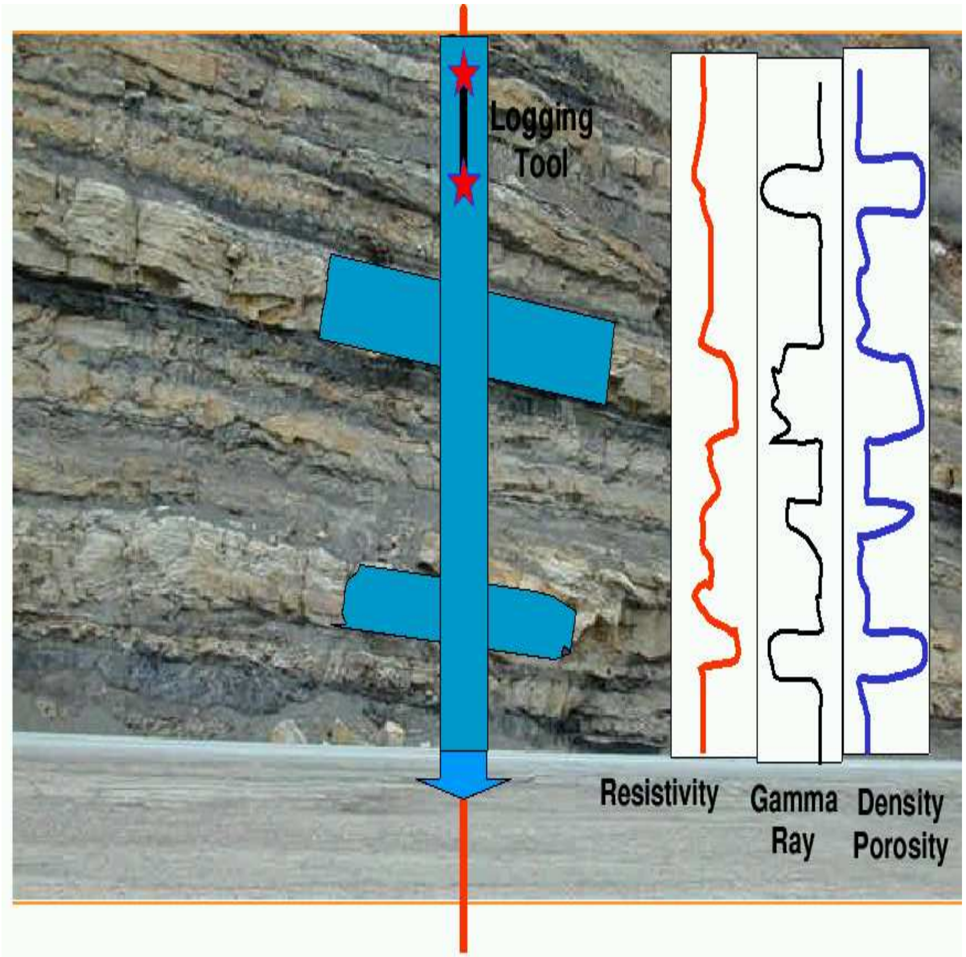

OBJECTIVES: To determine

- **Payzones (oil and gas).**
- **Amount of oil/gas.**
- **Ability to extract oil/gas.**

$

MOTIVATION (APPLICATIONS)

Main Objective: To Solve an Inverse Problem

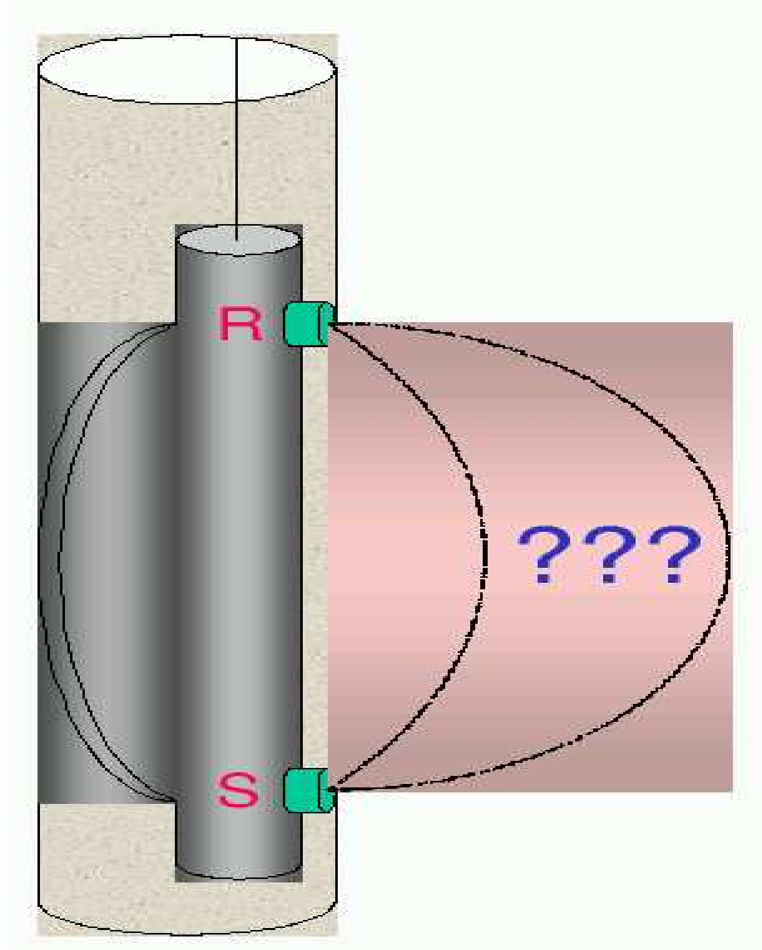

A software for solving the DIRECT problem is essential in order to solve the INVERSE problem

MOTIVATION (APPLICATIONS)

Resistivity Logging Instruments

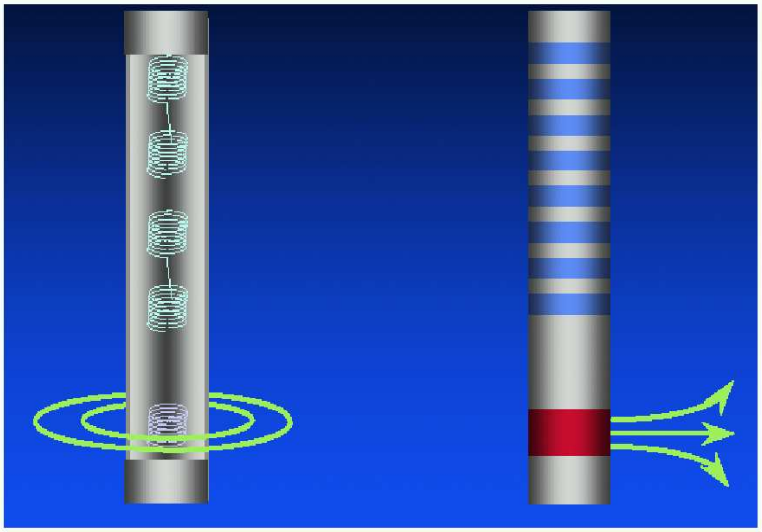

1D: INTRODUCTION TO HP-FEM

Fully automatic *hp*-adaptive strategy

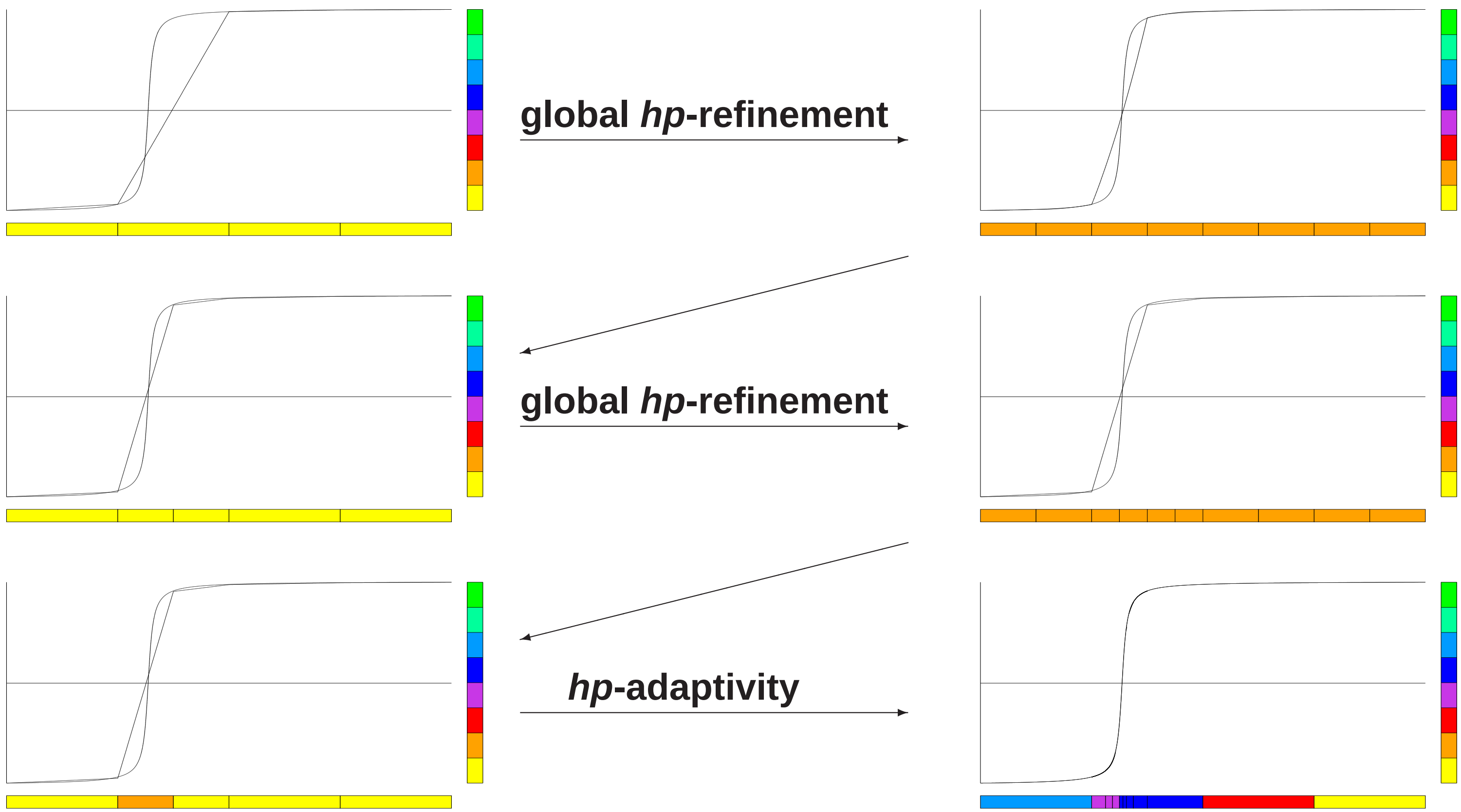

2D: SELF-ADAPTIVE HP-FEM

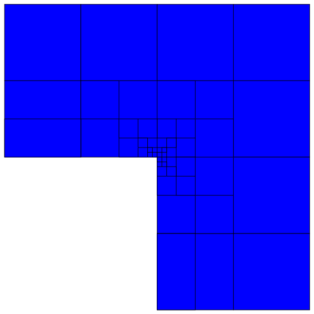

The h-Finite Element Method

1. **Convergence limited by the polynomial degree, and large material contrasts.**
2. **Optimal h-grids do NOT converge exponentially in real applications.**
3. **They may "lock" (100$\%$ error).**

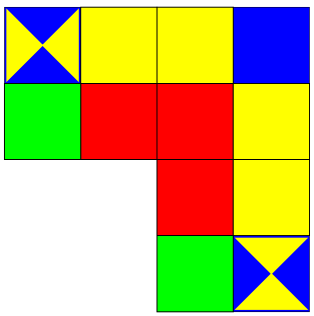

The p-Finite Element Method

1. **Exponential convergence feasible for analytical ("nice") solutions.**
2. **Optimal *p*-grids do NOT converge exponentially in real applications.**
3. **If initial *h*-grid is not adequate, the *p*-method will fail miserably.**

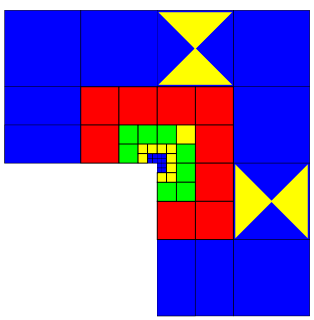

The hp-Finite Element Method

1. **Exponential convergence feasible for ALL solutions.**
2. **Optimal *hp*-grids DO converge exponentially in real applications.**
3. **If initial *hp*-grid is not adequate, results will still be great.**

2D: SELF-ADAPTIVE HP-FEM

Energy norm based fully automatic *hp*-adaptive strategy

Coarse grids (hp) **Fine grids** ($h/2, p+1$)

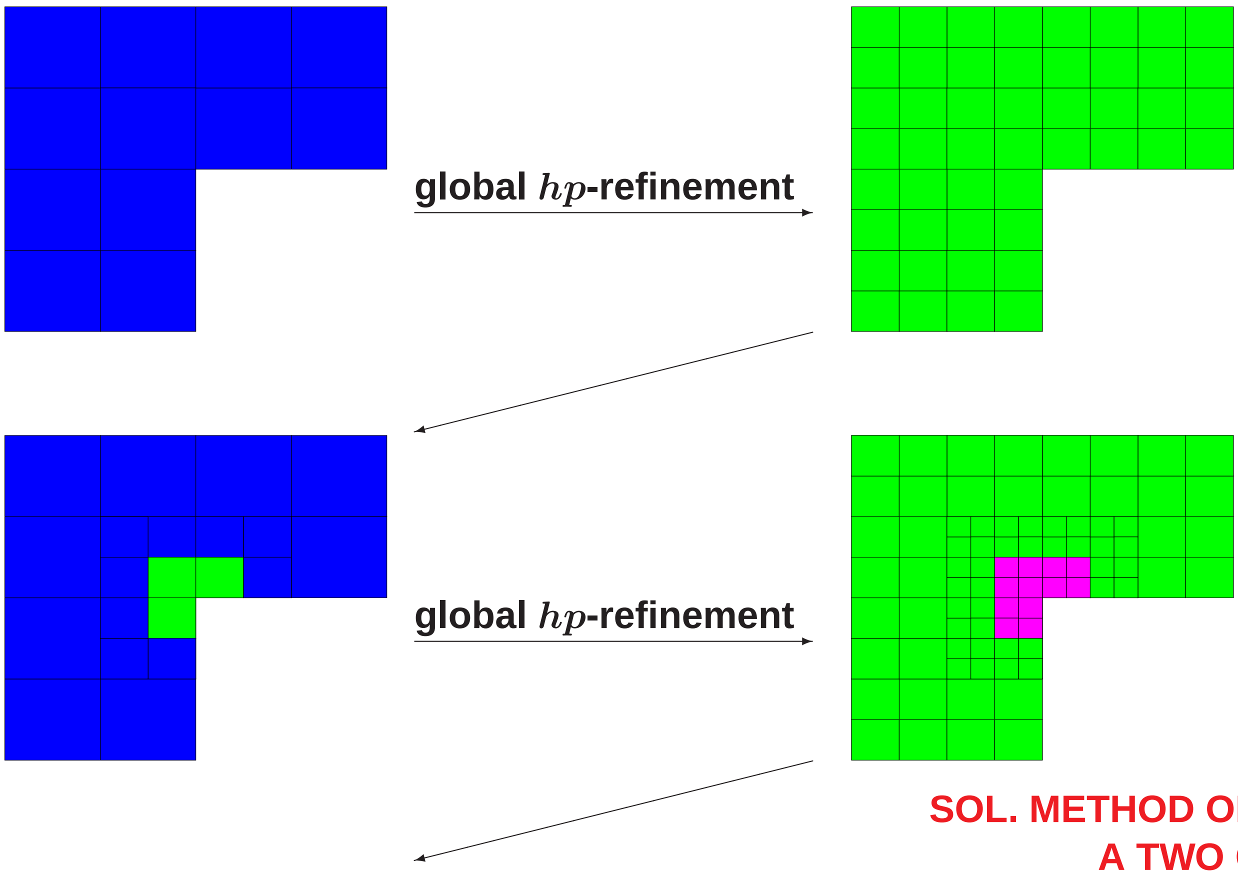

SOL. METHOD ON FINE GRIDS:
A TWO GRID SOLVER

2D: GOAL-ORIENTED ADAPTIVITY

Motivation (Goal-Oriented Adaptivity)

Test Problem

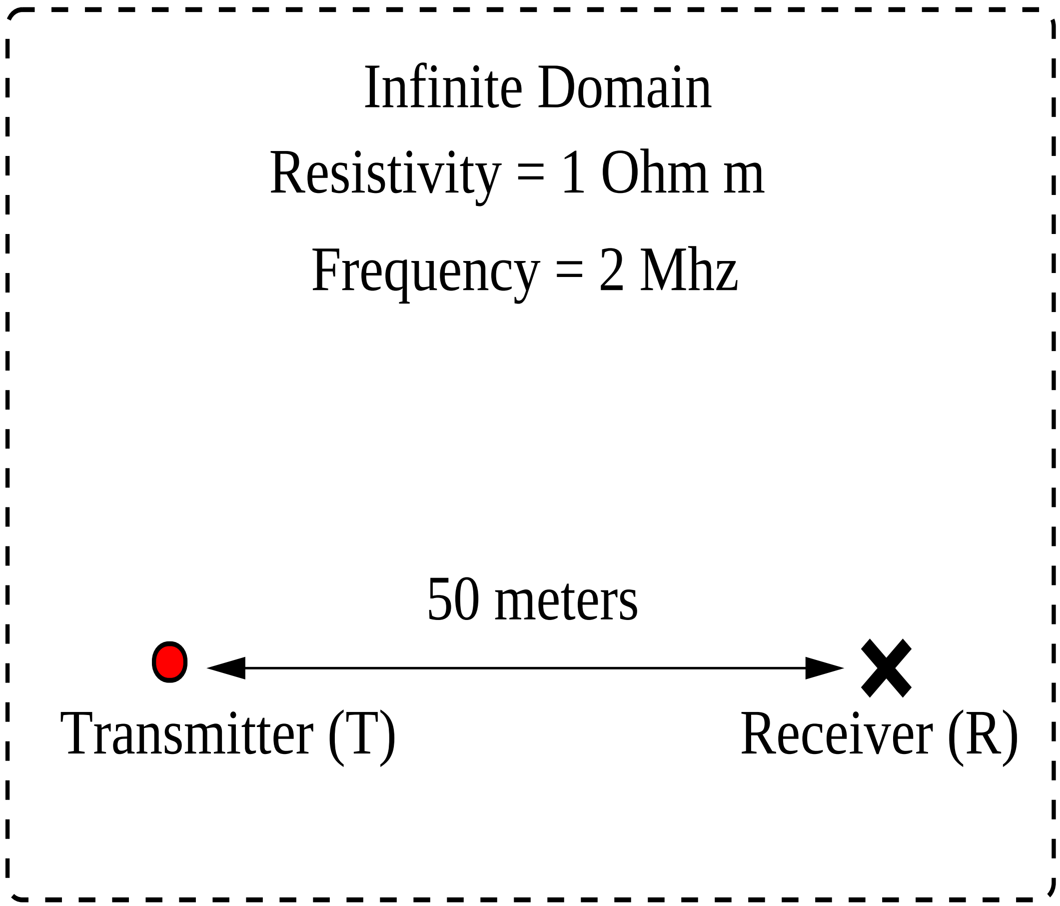

2D: GOAL-ORIENTED ADAPTIVITY

Motivation (Goal-Oriented Adaptivity)

Test Problem

Problema Modelo

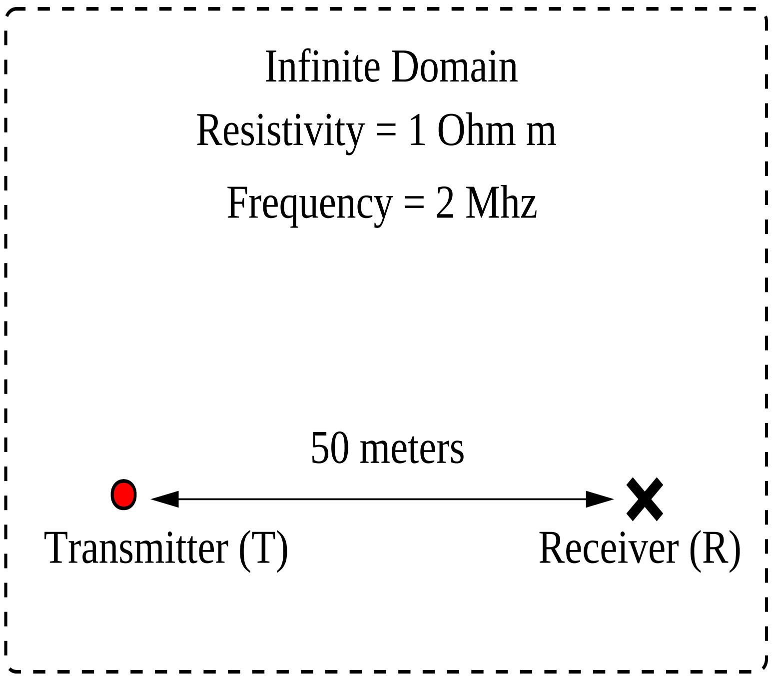

- **Solution decays exponentially.**
- $\dfrac{|E(T)|}{|E(R)|} \approx 10^{60}$
- **Results using energy-norm adaptivity:**
  - **Energy-norm error:** 0.001%
  - **Relative error in the quantity of interest** $> 10^{30}$ **%.**

2D: GOAL-ORIENTED ADAPTIVITY

Motivation (Goal-Oriented Adaptivity)

Test Problem

Problema Modelo

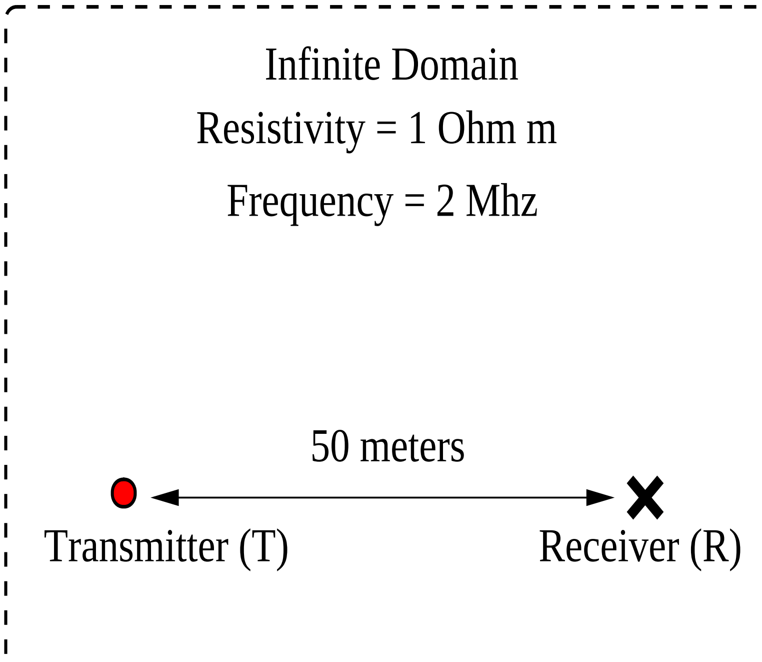

- **Solution decays exponentially.**
- $\dfrac{|E(T)|}{|E(R)|} \approx 10^{60}$
- **Results using energy-norm adaptivity:**
  - **Energy-norm error:** 0.001%
  - **Relative error in the quantity of interest** $> 10^{30}$ **%.**

Goal-oriented adaptivity is needed

Becker-Rannacher (1995,1996), Rannacher-Stuttmeier (1997), Cirak-Ramm (1998), Paraschivoiu-Patera (1998), Peraire-Patera (1998), Prudhomme-Oden (1999, 2001), Heuveline-Rannacher (2003), Solin-Demkowicz (2004).

2D: GOAL-ORIENTED ADAPTIVITY

Motivation (Goal-Oriented Adaptivity)

Test Problem

Problema Modelo

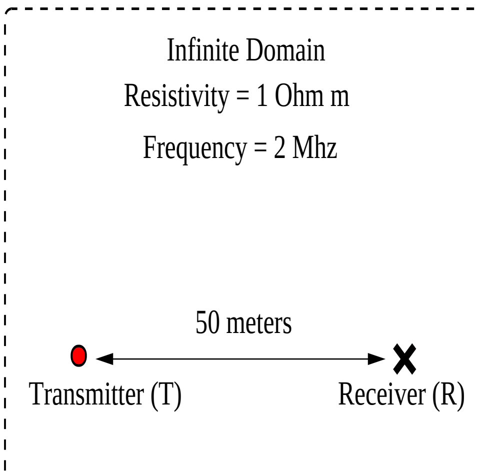

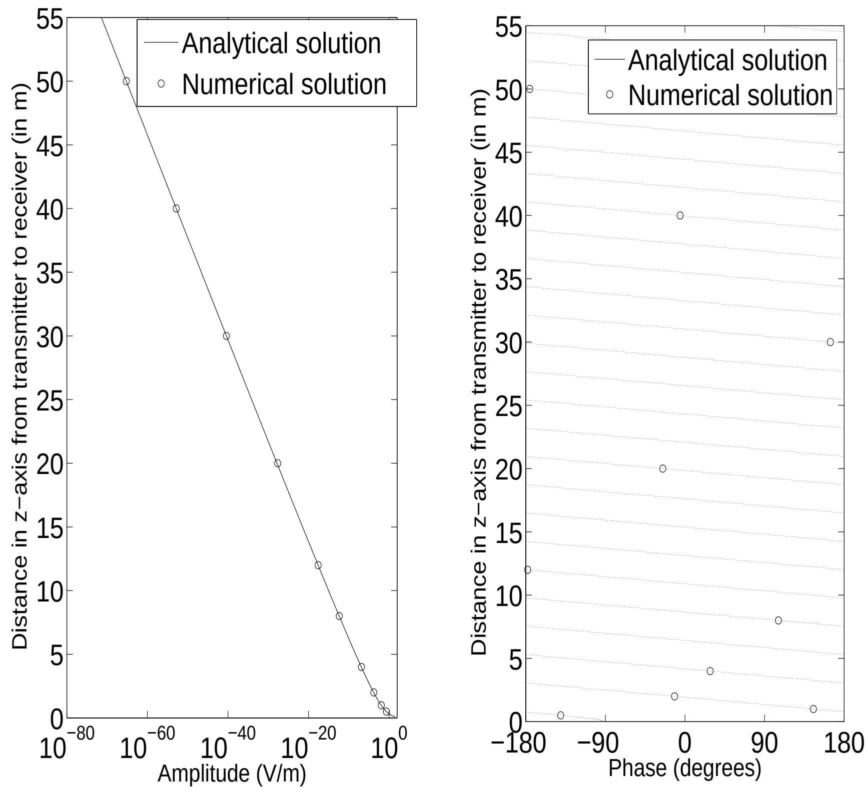

Goal-oriented adaptivity is needed

2D: GOAL-ORIENTED ADAPTIVITY

Mathematical Formulation (Goal-Oriented Adaptivity)

We consider the following problem (in variational form):

$$\begin{cases} \text{Find } L(\Psi)\text{, where } \Psi \in V \text{ such that :} \\ b(\Psi, \xi) = f(\xi) \quad \forall \xi \in V \ . \end{cases}$$

We define residual $r_e(\xi) = b(e, \xi)$. We seek for solution G of:

$$\begin{cases} \text{Find } G \in V'' \sim V \text{ such that :} \\ G(r_e) = L(e) \ . \end{cases}$$

This is necessarily solved if we find the solution of the *dual* problem:

$$\begin{cases} \text{Find } G \in V \text{ such that :} \\ b(\Psi, G) = L(\Psi) \quad \forall \Psi \in V \ . \end{cases}$$

Notice that $L(e) = b(e, G)$.

2D: GOAL-ORIENTED ADAPTIVITY

Mathematical Formulation (Goal-Oriented Adaptivity)

DIRECT PROBLEM **DUAL PROBLEM**

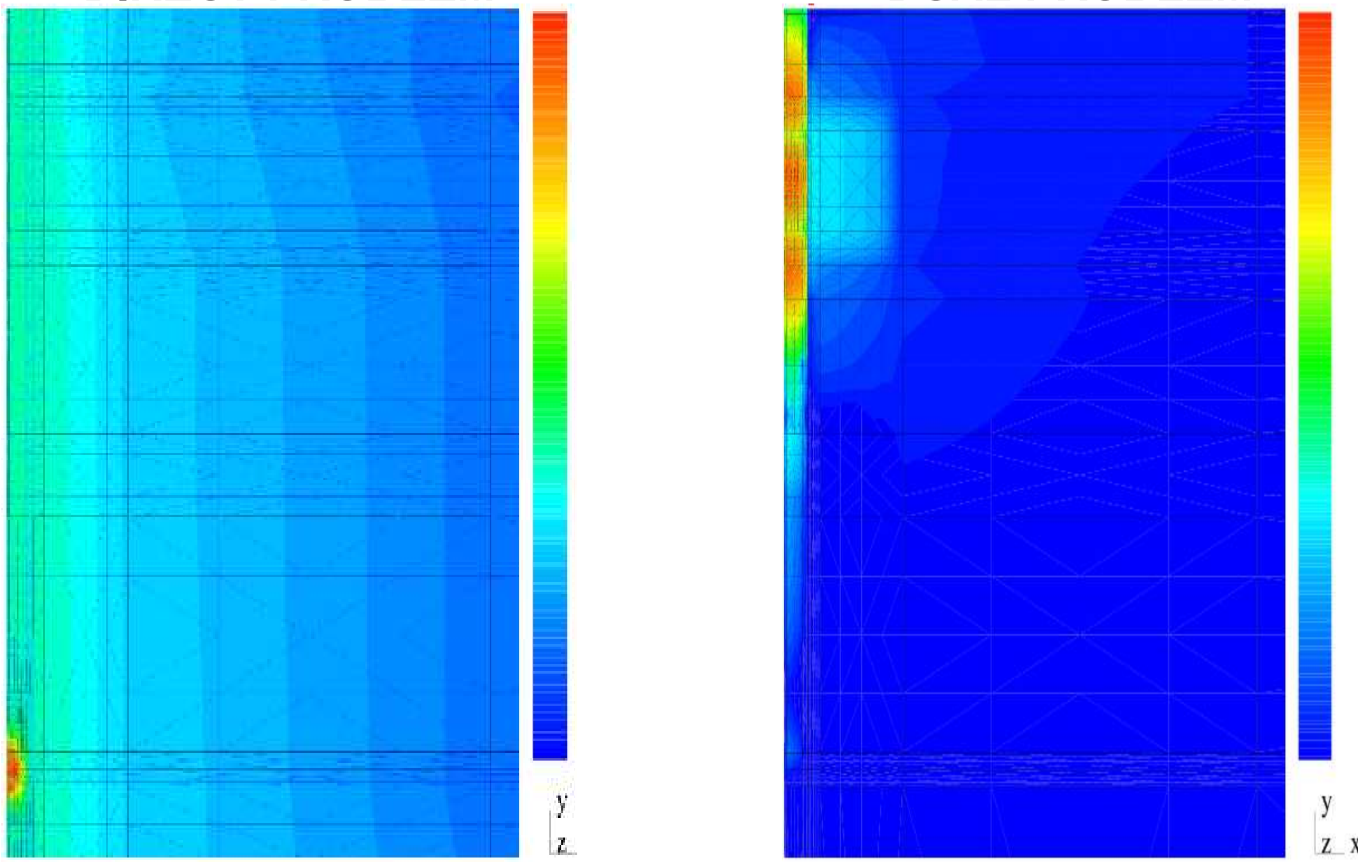

$$L(\Psi)=b(\Psi,G)$$

2D: GOAL-ORIENTED ADAPTIVITY

Algorithm for Goal-Oriented Adaptivity

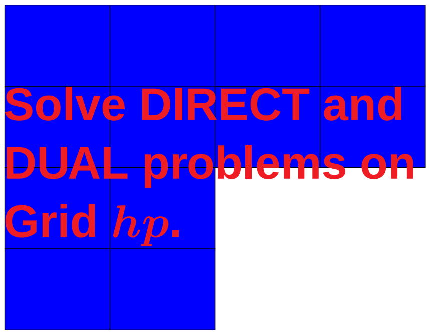

Solve DIRECT and DUAL problems on Grid hp.

$\longrightarrow$

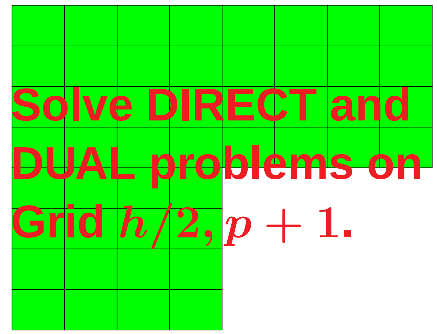

Solve DIRECT and DUAL problems on Grid $h/2, p+1$.

Compute $e = \Psi_{h/2,p+1} - \Psi_{hp}$, **and** $\tilde{e} = \Psi_{h/2,p+1} - \Pi_{hp}\Psi_{h/2,p+1}$.
Compute $\epsilon = G_{h/2,p+1} - G_{hp}$, **and** $\tilde{\epsilon} = G_{h/2,p+1} - \Pi_{hp}G_{h/2,p+1}$.

$$|L(e)| = |b(e,\epsilon)| \sim |b(\tilde{e},\tilde{\epsilon})| \leq \sum_K |b_K(\tilde{e},\tilde{\epsilon})| \leq \sum_K \| \tilde{e} \|_{E,K} \| \tilde{\epsilon} \|_{E,K}.$$

Apply the fully automatic hp-adaptive algorithm.

Solve DIRECT and DUAL problems on Grid hp.

$\longrightarrow$

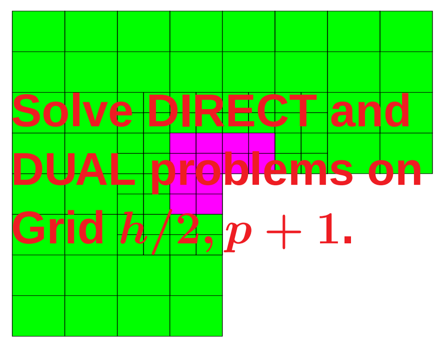

Solve DIRECT and DUAL problems on Grid $h/2, p+1$.

2D: ELECTROMAGNETIC SIMULATIONS

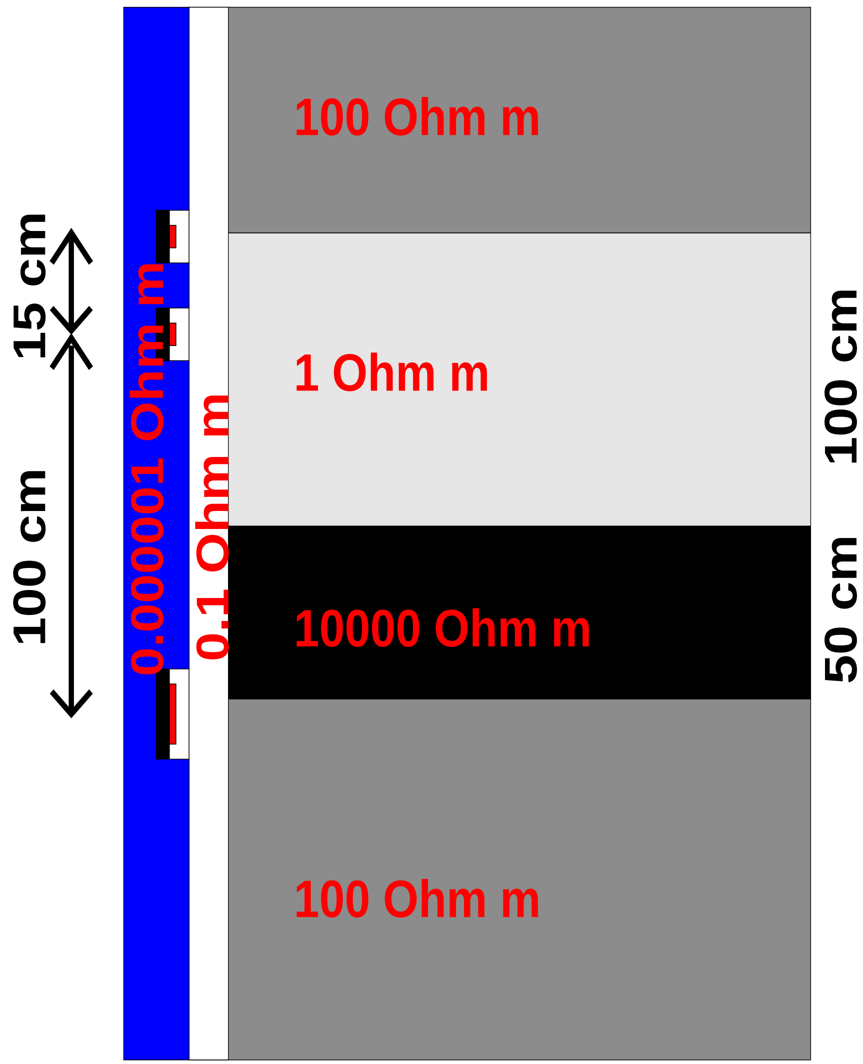

Description of Antennas

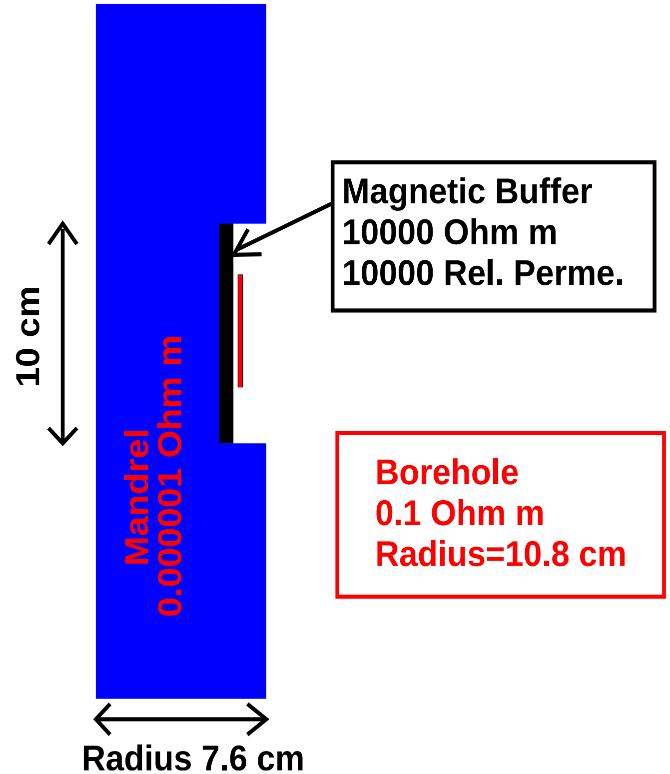

Goal: To Study the Effect of Invasion, Anistotropy, and Magnetic Permeability.

2D: ELECTROMAGNETIC SIMULATIONS

First Vert. Diff. H_ϕ for different antennas

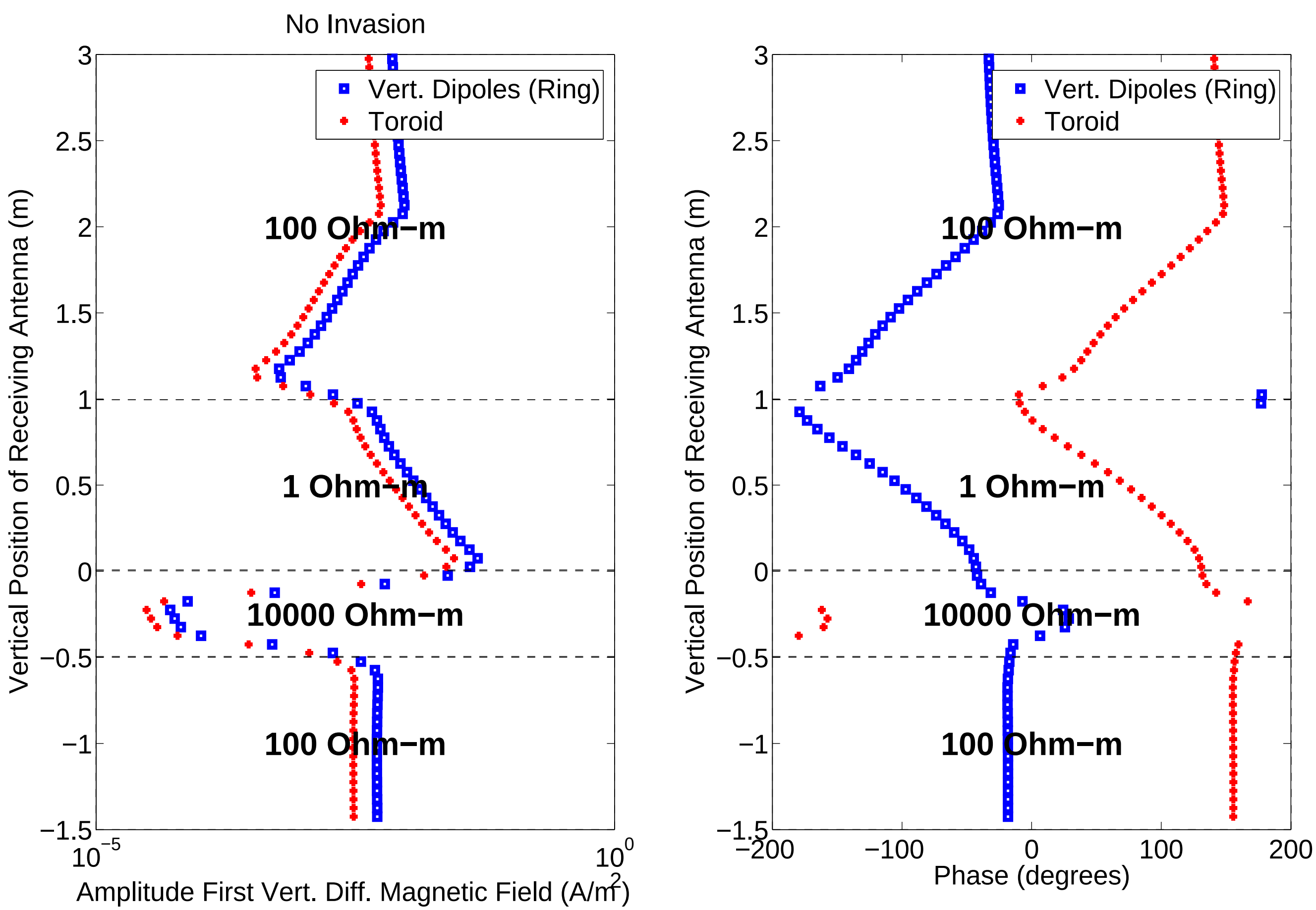

In LWD instruments, we obtain similar results using toroids or a ring of vert. dipoles

2D: ELECTROMAGNETIC SIMULATIONS

First Vert. Diff. E_z for a toroid antenna

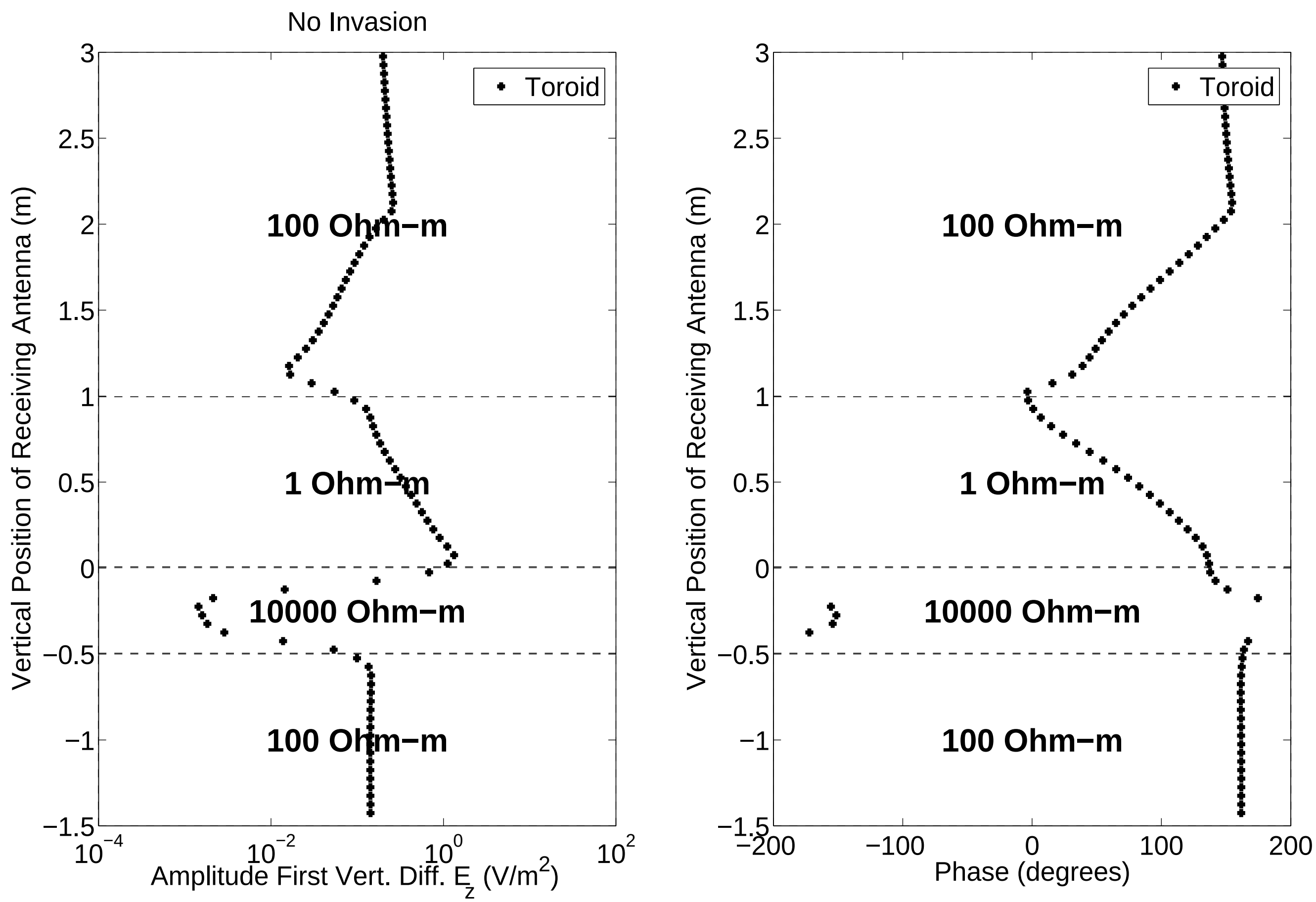

Toroids are adequate for identifying highly resistive layers

2D: ELECTROMAGNETIC SIMULATIONS

First Vert. Diff. E_ϕ for a solenoid antenna

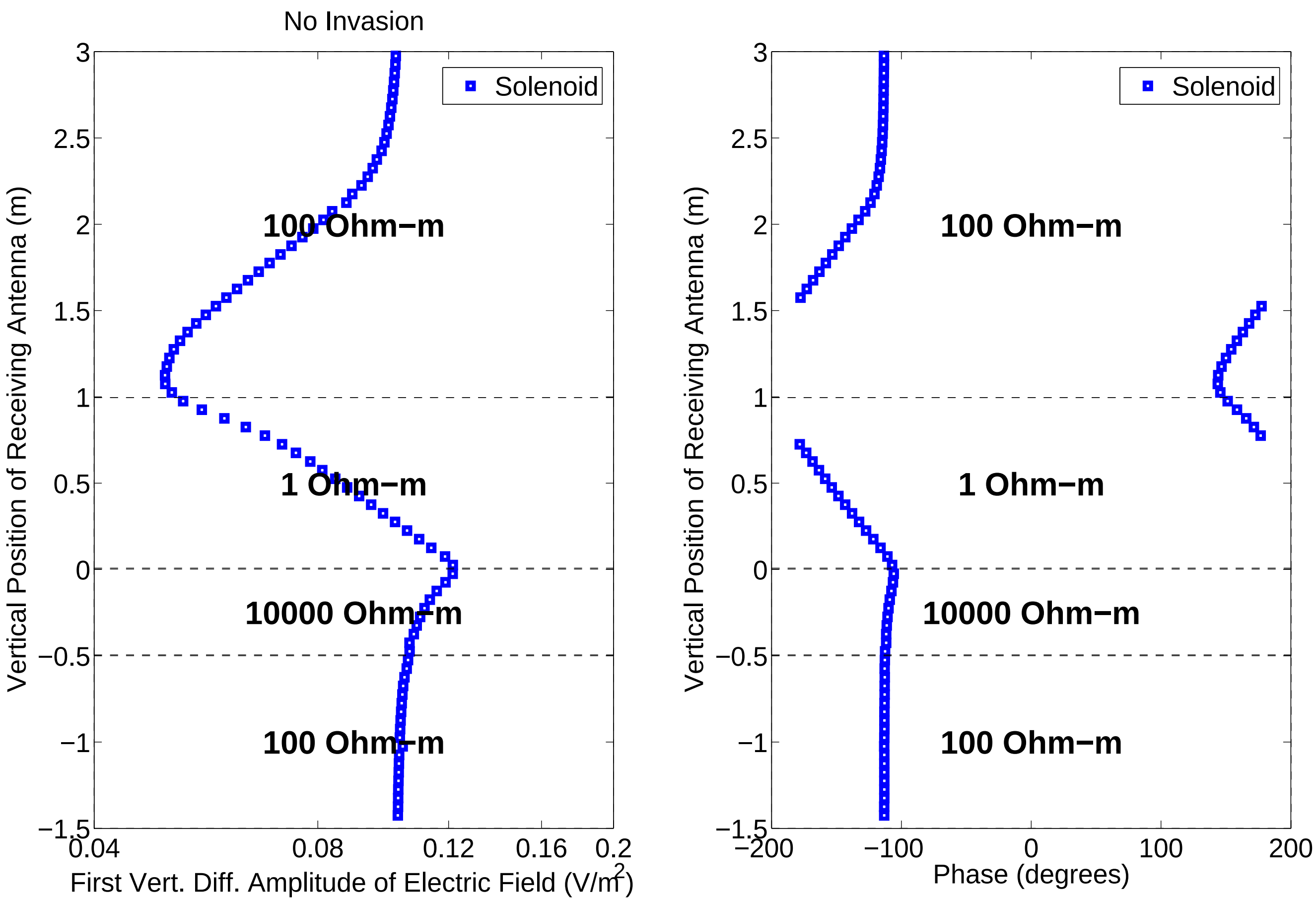

Solenoids are adequate for identifying low resistive layers

2D: ELECTROMAGNETIC SIMULATIONS

Use of Magnetic Buffers (E_ϕ for a solenoid)

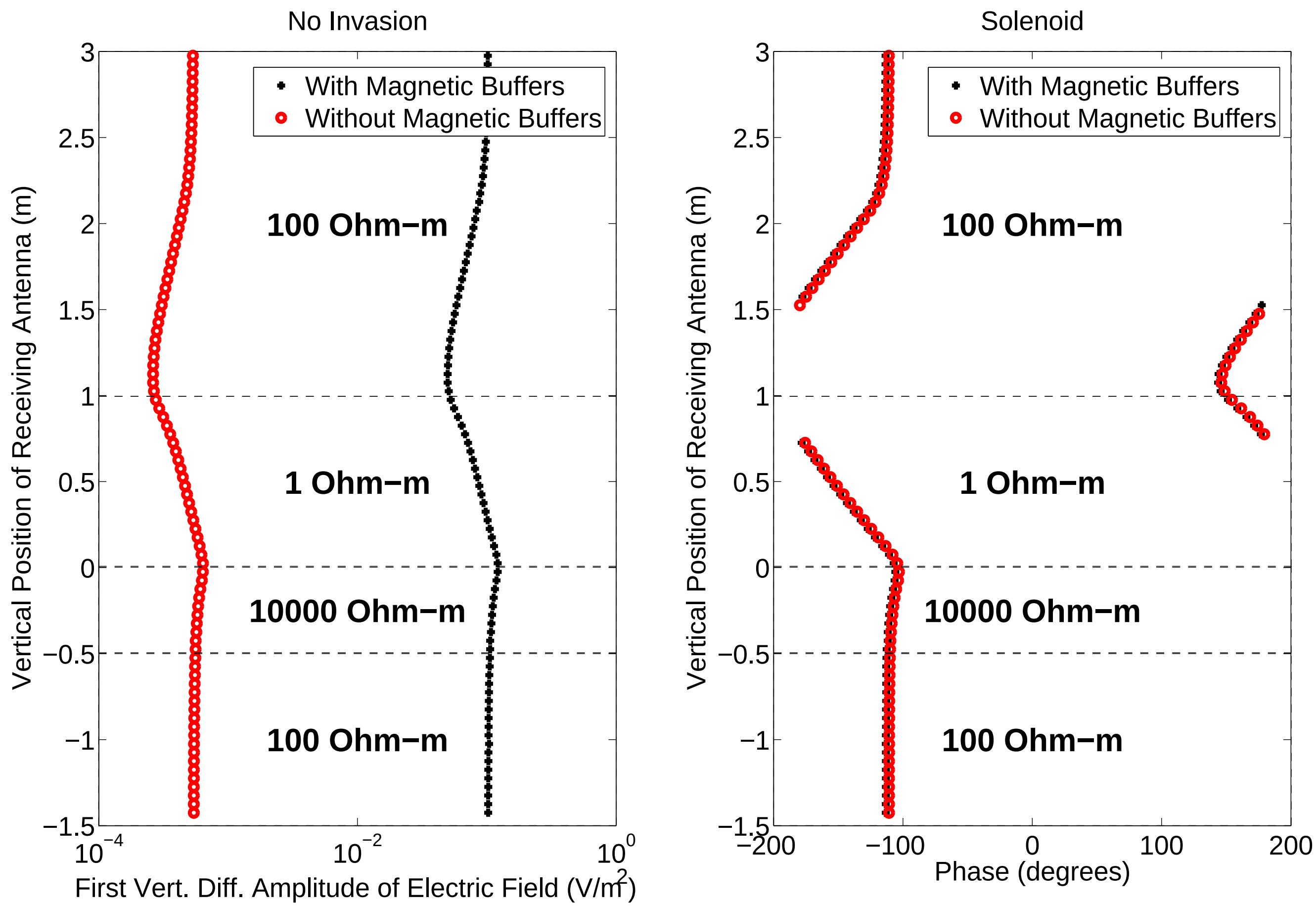

Use of magnetic buffers strengthen the signal in combination with solenoids

2D: ELECTROMAGNETIC SIMULATIONS

Use of Magnetic Buffers (H_ϕ for a toroid)

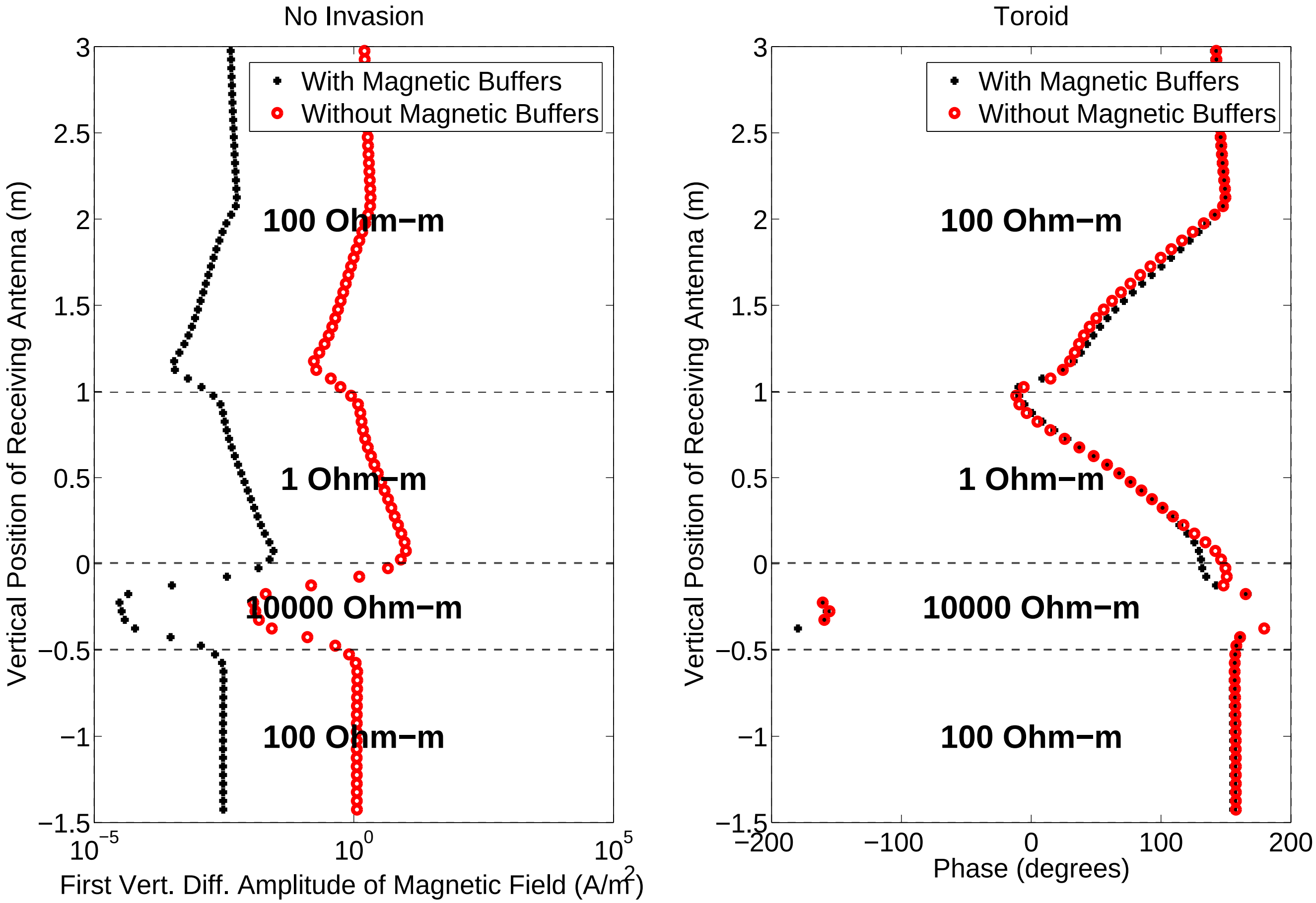

However, magnetic buffers weaken the signal in combination with toroids

2D: ELECTROMAGNETIC SIMULATIONS

Invasion study (E_ϕ for a solenoid)

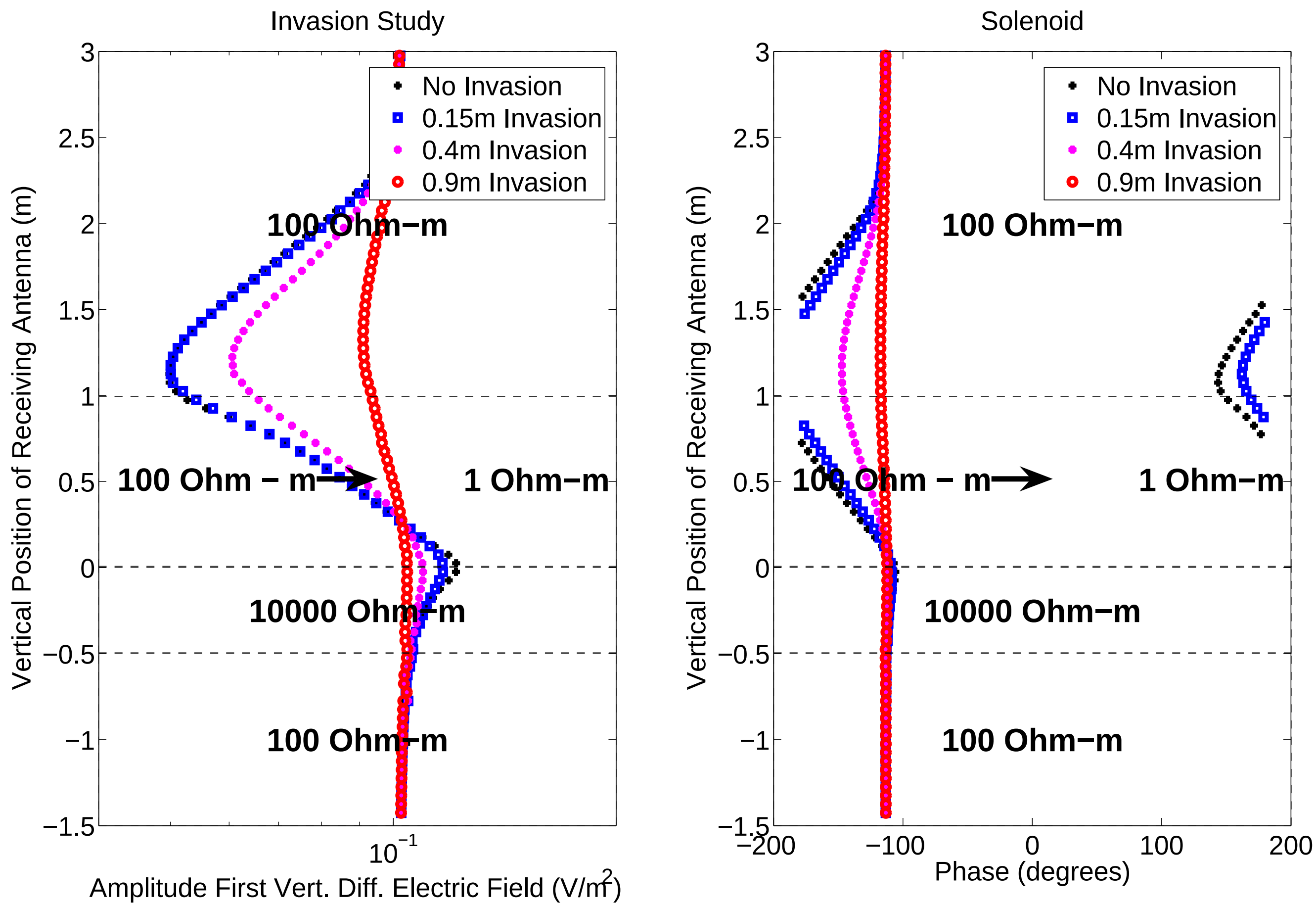

Large invasion effects can be sensed using solenoids

2D: ELECTROMAGNETIC SIMULATIONS

Invasion study (H_ϕ for a toroid)

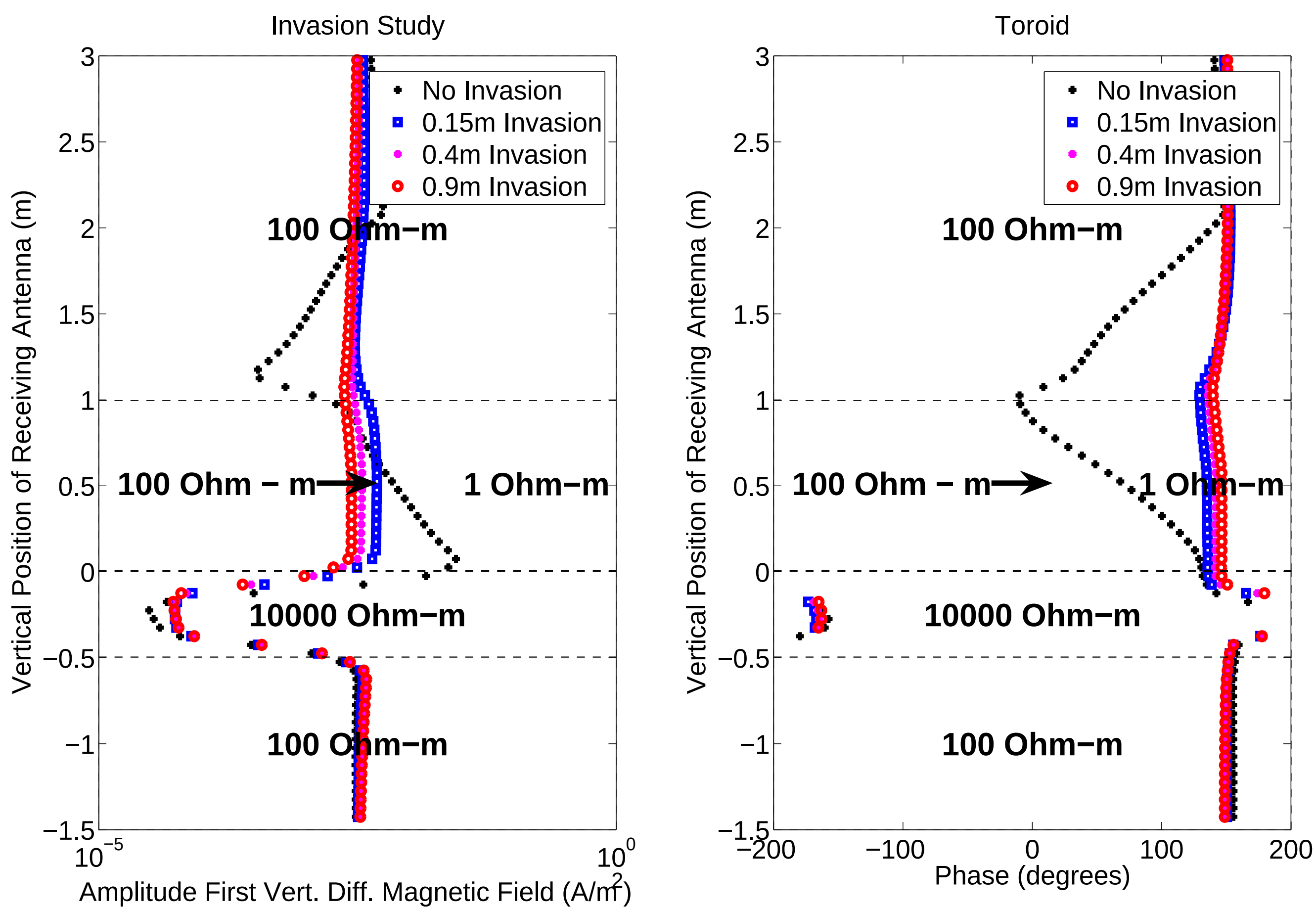

Small invasion effects can be sensed using toroids

2D: ELECTROMAGNETIC SIMULATIONS

Invasion study (E_ϕ for a solenoid)

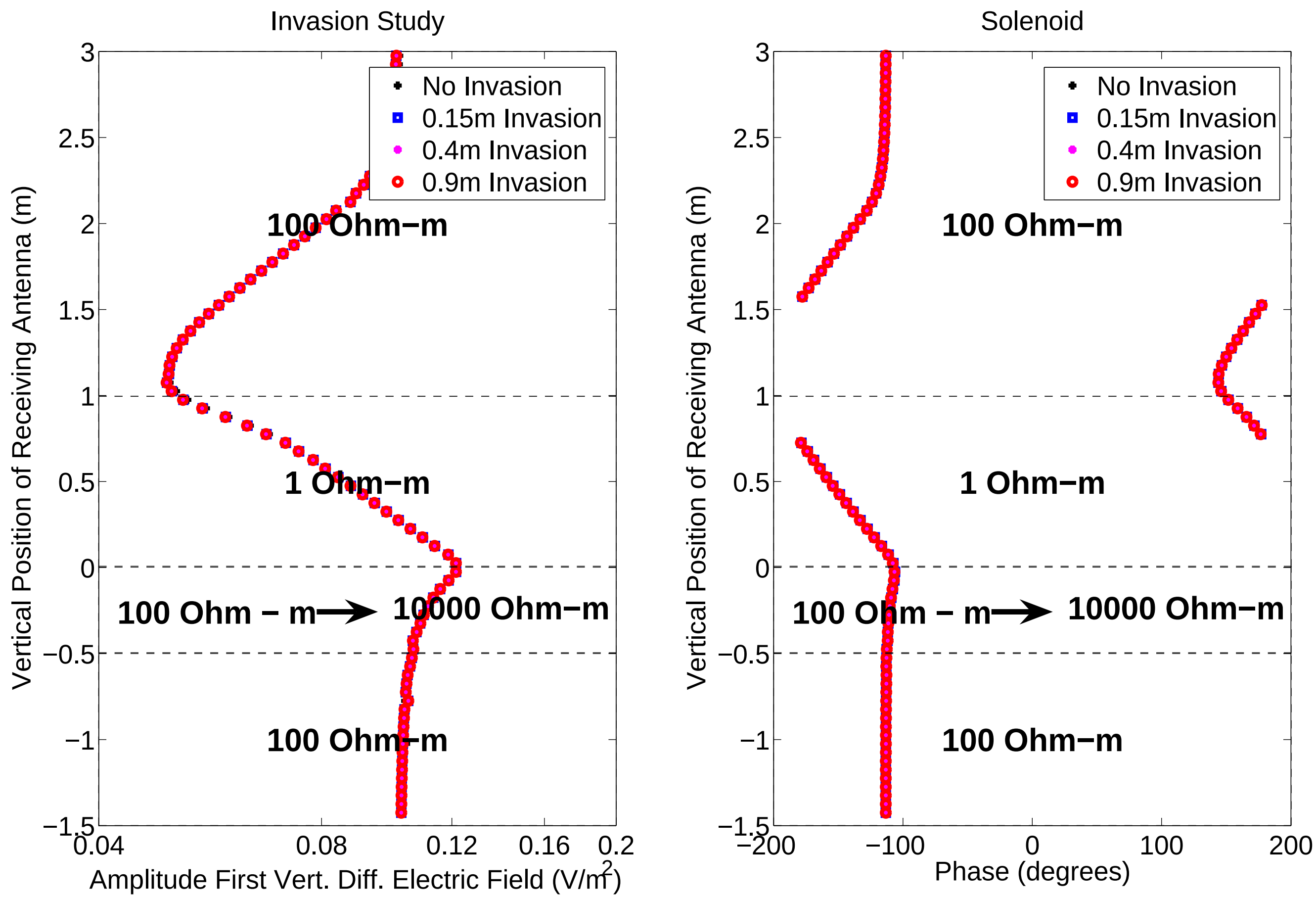

Invasion in resistive layers cannot be sensed using solenoids

2D: ELECTROMAGNETIC SIMULATIONS

Invasion study (H_ϕ for a toroid)

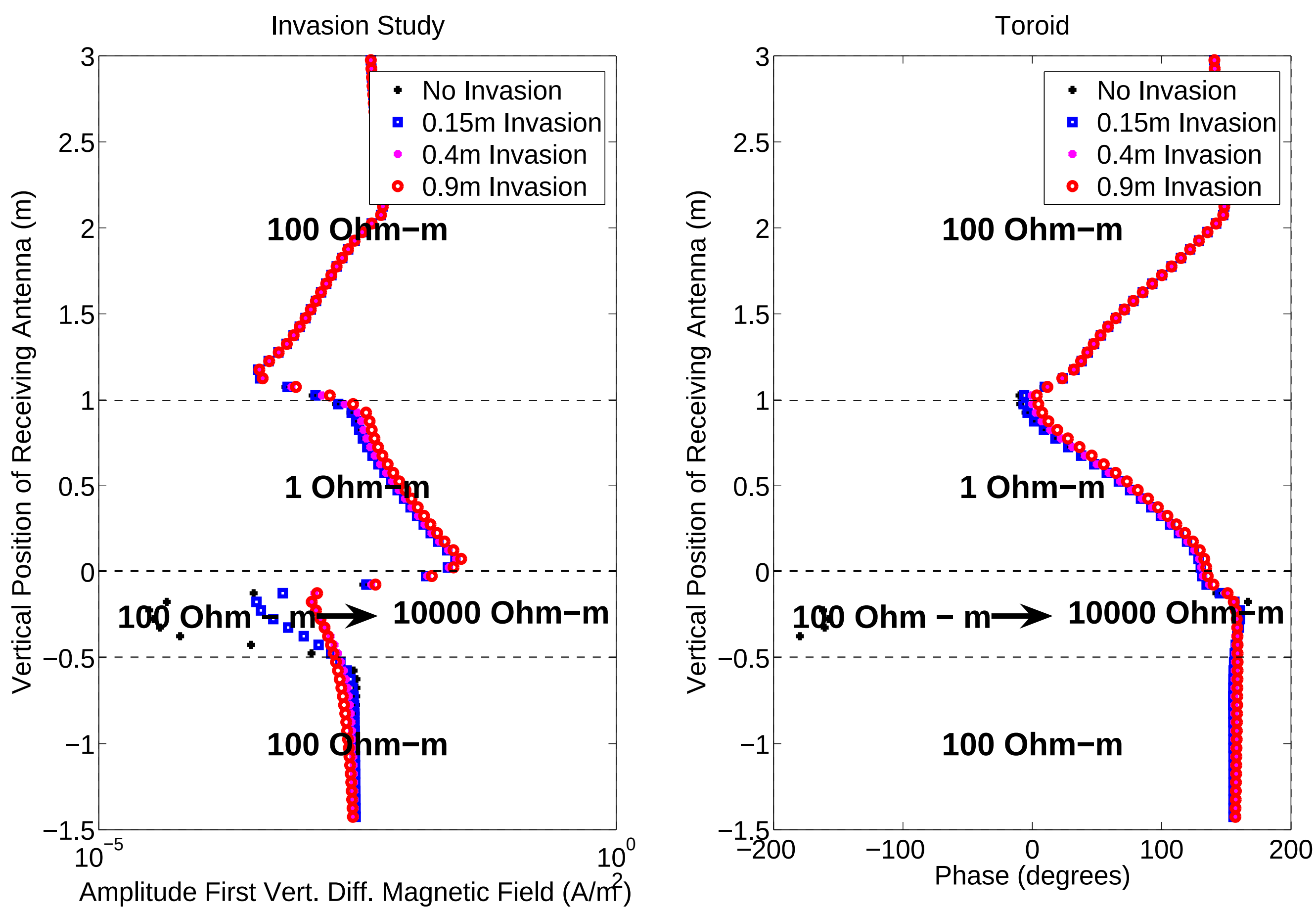

Invasion in resistive layers should be studied using toroids

2D: ELECTROMAGNETIC SIMULATIONS

Invasion and mandrel magnetic permeab. (E_ϕ)

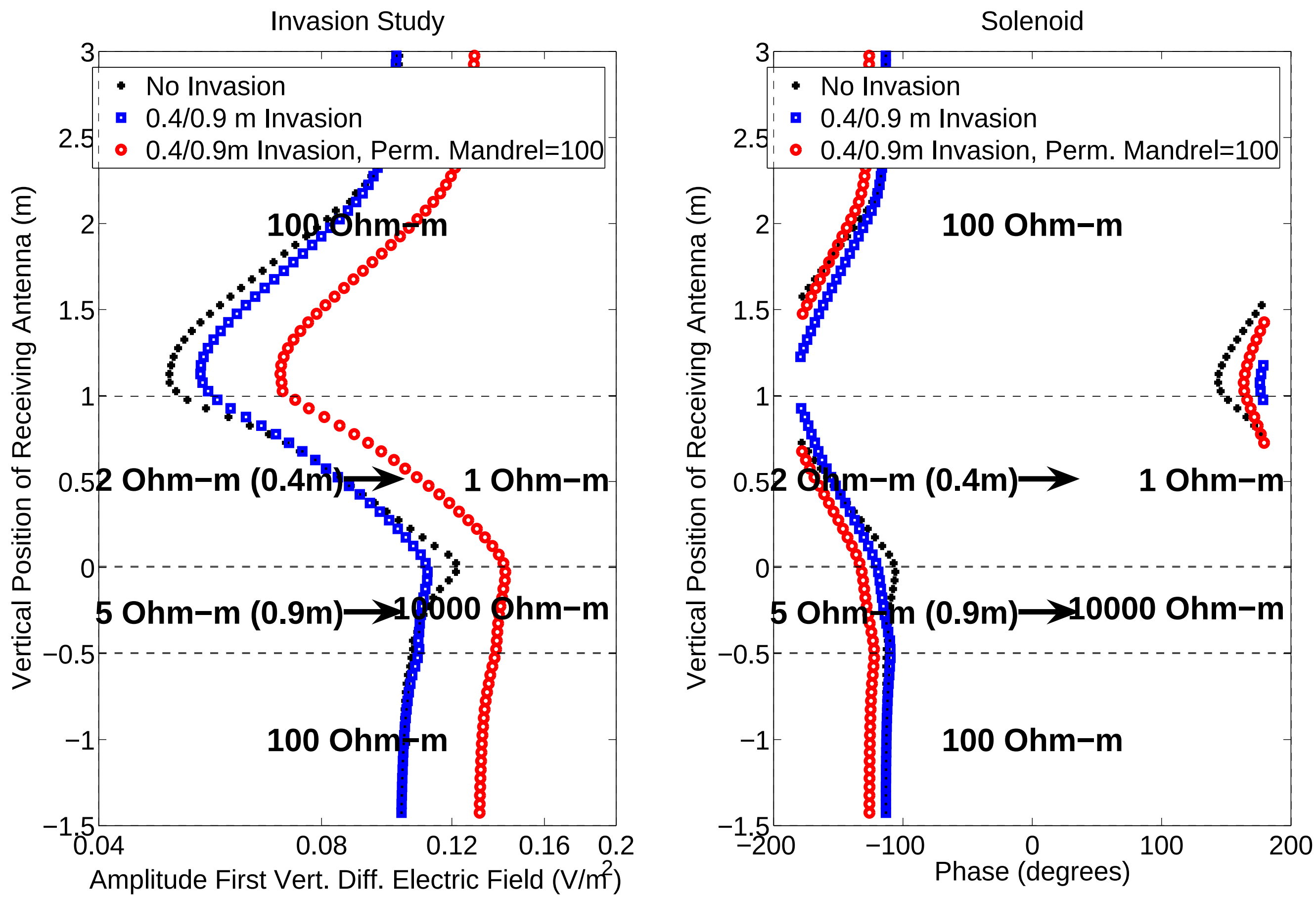

The effect of magnetic permeability on the mandrel is similar to the effect of magnetic buffers

2D: ELECTROMAGNETIC SIMULATIONS

Anisotropy (H_ϕ)

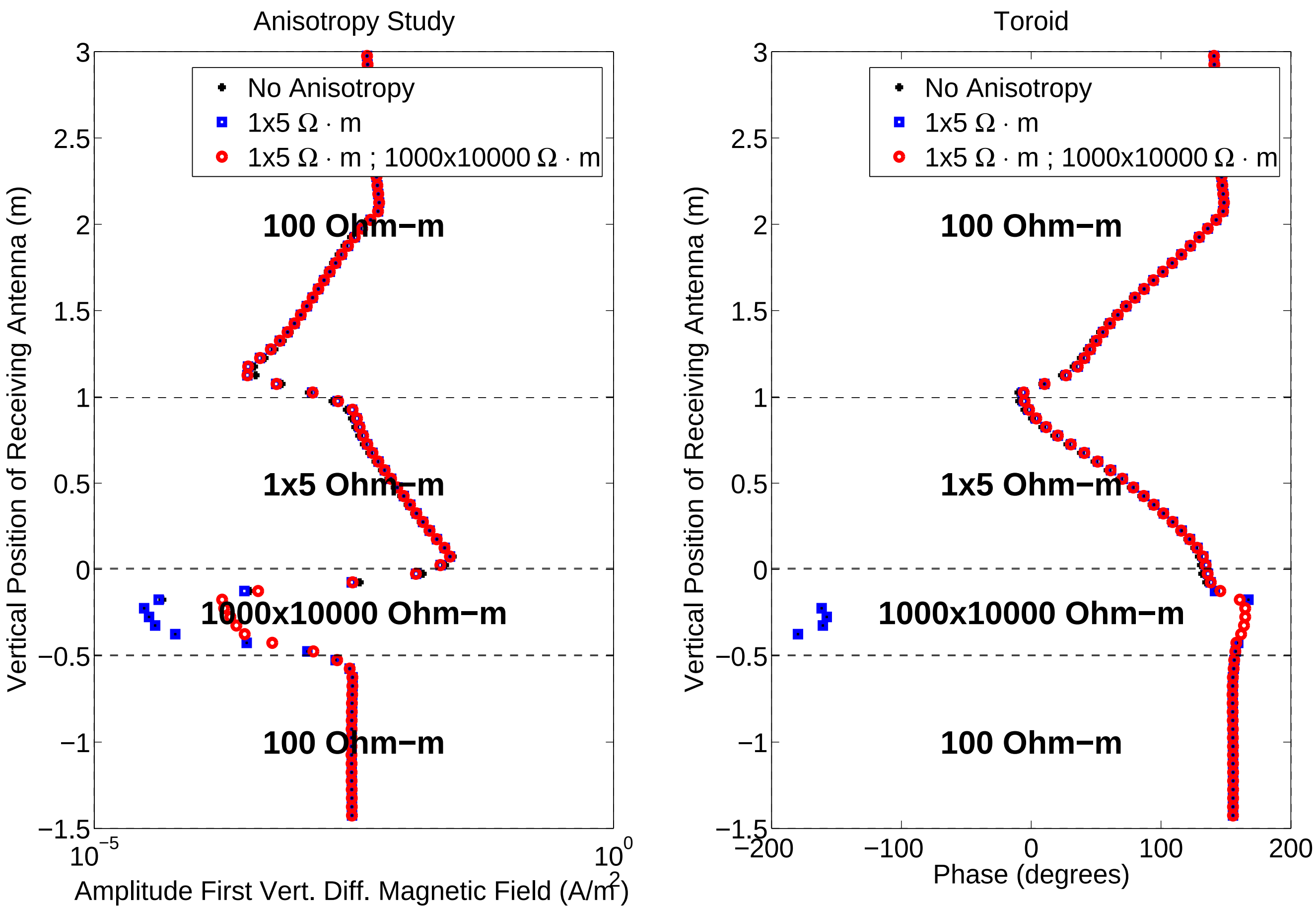

Anisotropy effects may be important when studying resistive layers

2D: ELECTROMAGNETIC SIMULATIONS

First. Vert. Diff. E_ϕ (solenoid). Position: 0.475m

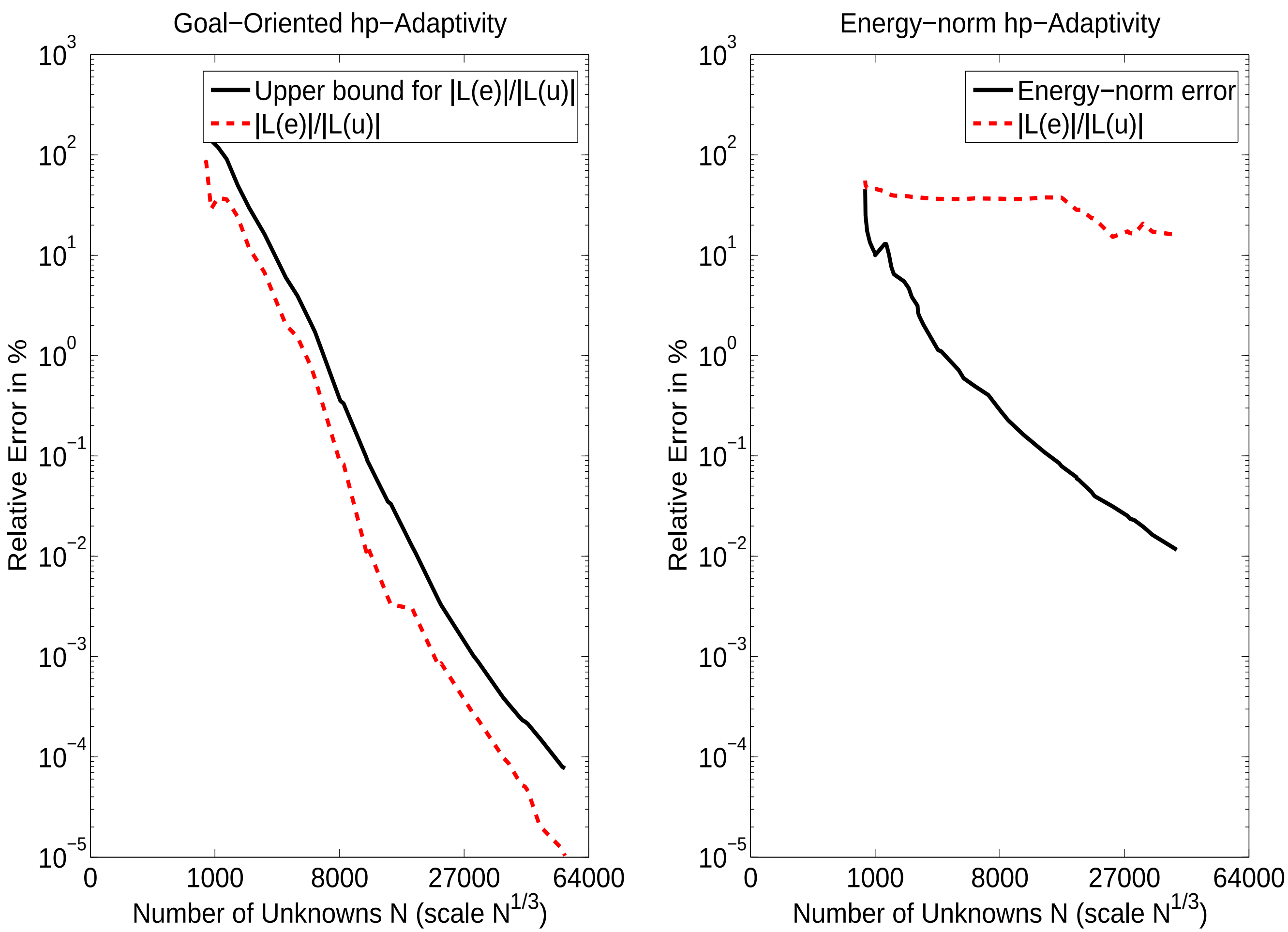

2D: ELECTROMAGNETIC SIMULATIONS

Goal-Oriented vs. Energy-norm hp-Adaptivity

Problem with Mandrel at 2 Mhz.

Continuous Elements (Goal-Oriented Adaptivity)

Quantity of Interest	Real Part	Imag Part
COARSE GRID	-0.1629862203E-01	-0.4016944732E-02
FINE GRID	-0.1629862347E-01	-0.4016944223E-02

Continuous Elements (Energy-norm Adaptivity)

Quantity of Interest	Real Part	Imag Part
0.01% ENERGY ERROR	-0.1382759158E-01	-0.2989492851E-02

It is critical to use GOAL-ORIENTED adaptivity.

2D: ELECTROMAGNETIC SIMULATIONS

First. Vert. Diff. E_ϕ (solenoid). Position: 0.475m

ENERGY-NORM HP-ADAPTIVITY

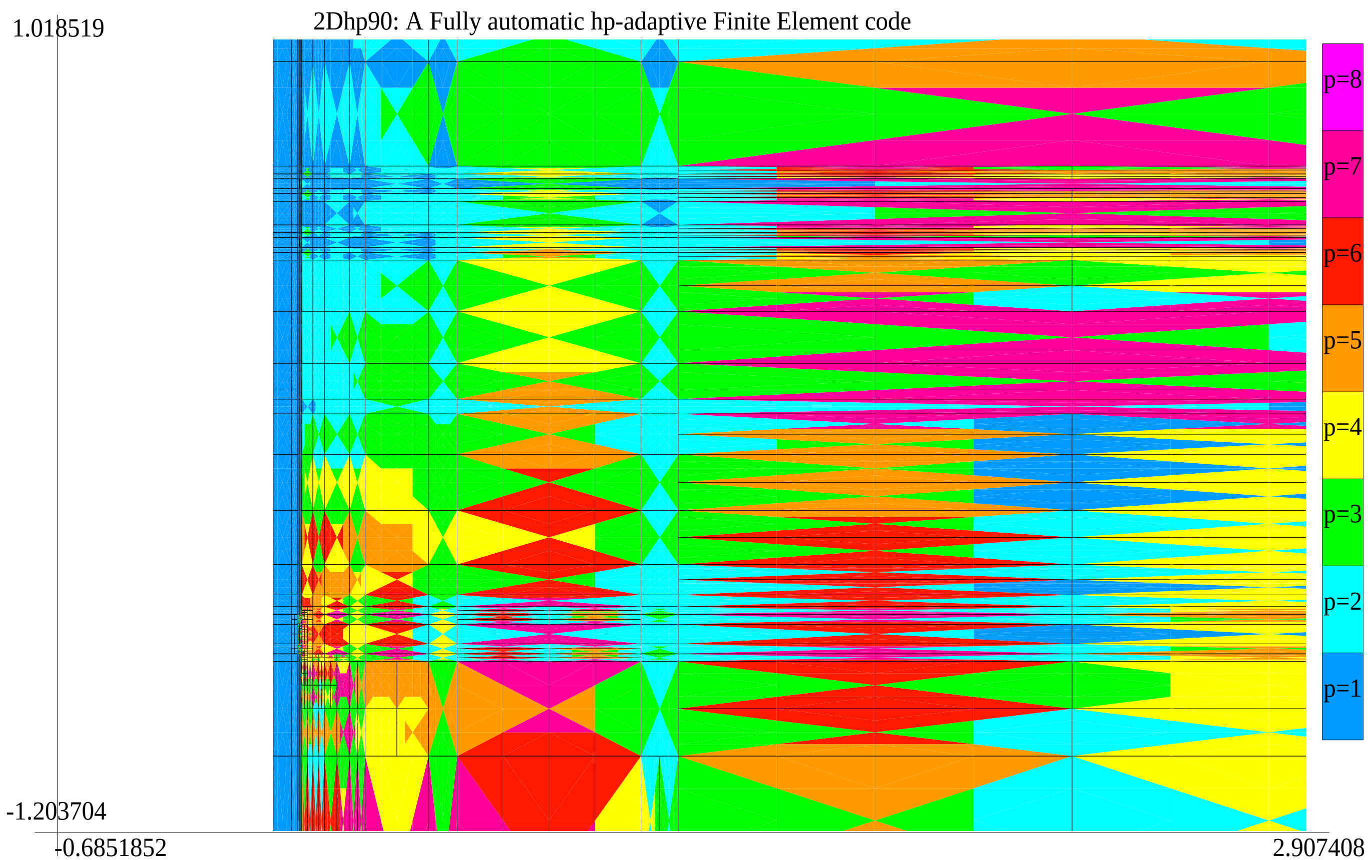

2D: ELECTROMAGNETIC SIMULATIONS

First. Vert. Diff. E_ϕ (solenoid). Position: 0.475m

GOAL-ORIENTED HP-ADAPTIVITY

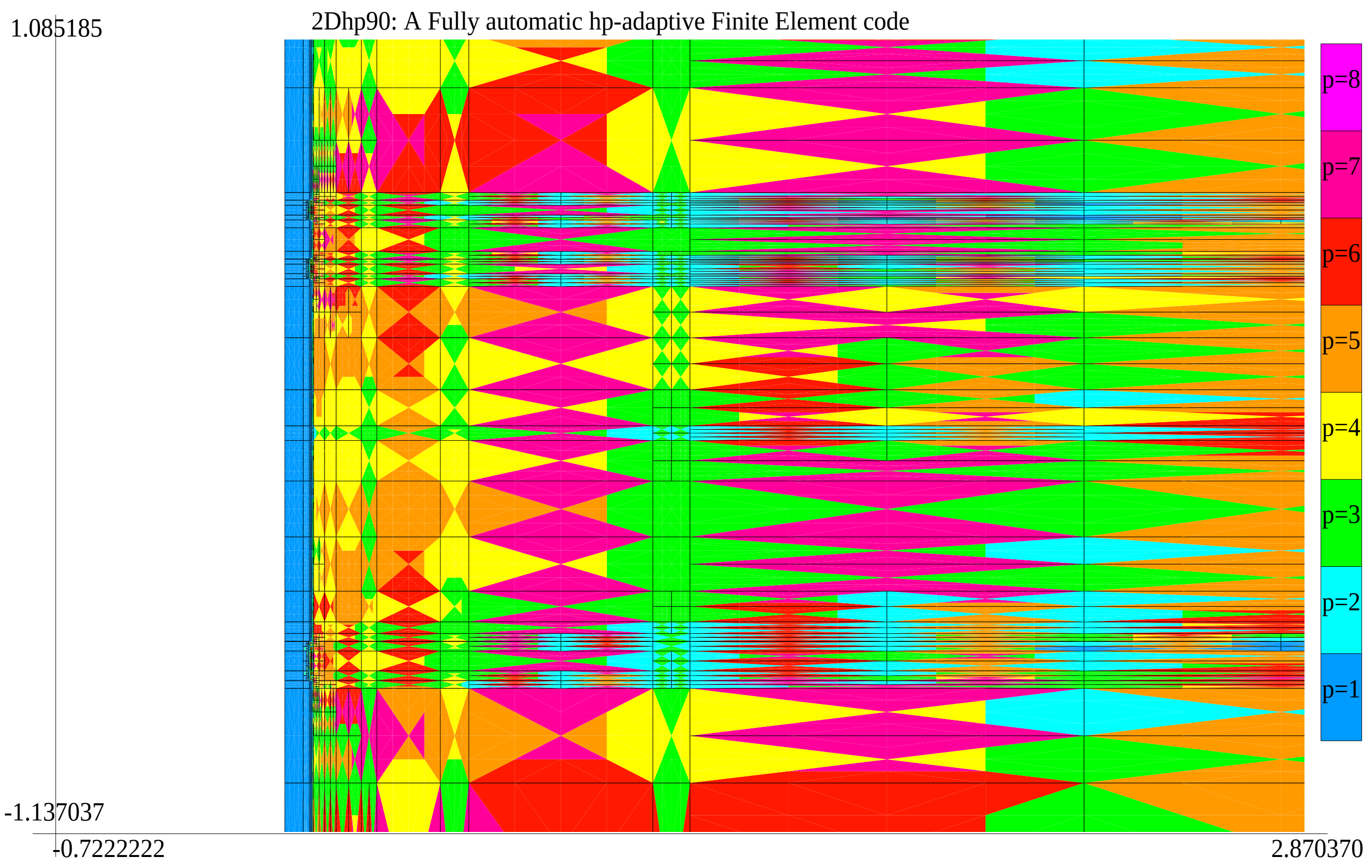

2D: ELECTROMAGNETIC SIMULATIONS

First. Vert. Diff. E_ϕ (solenoid). Position: 0.475m

GOAL-ORIENTED HP-ADAPTIVITY (ZOOM TOWARDS FIRST RECEIVER ANTENNA)

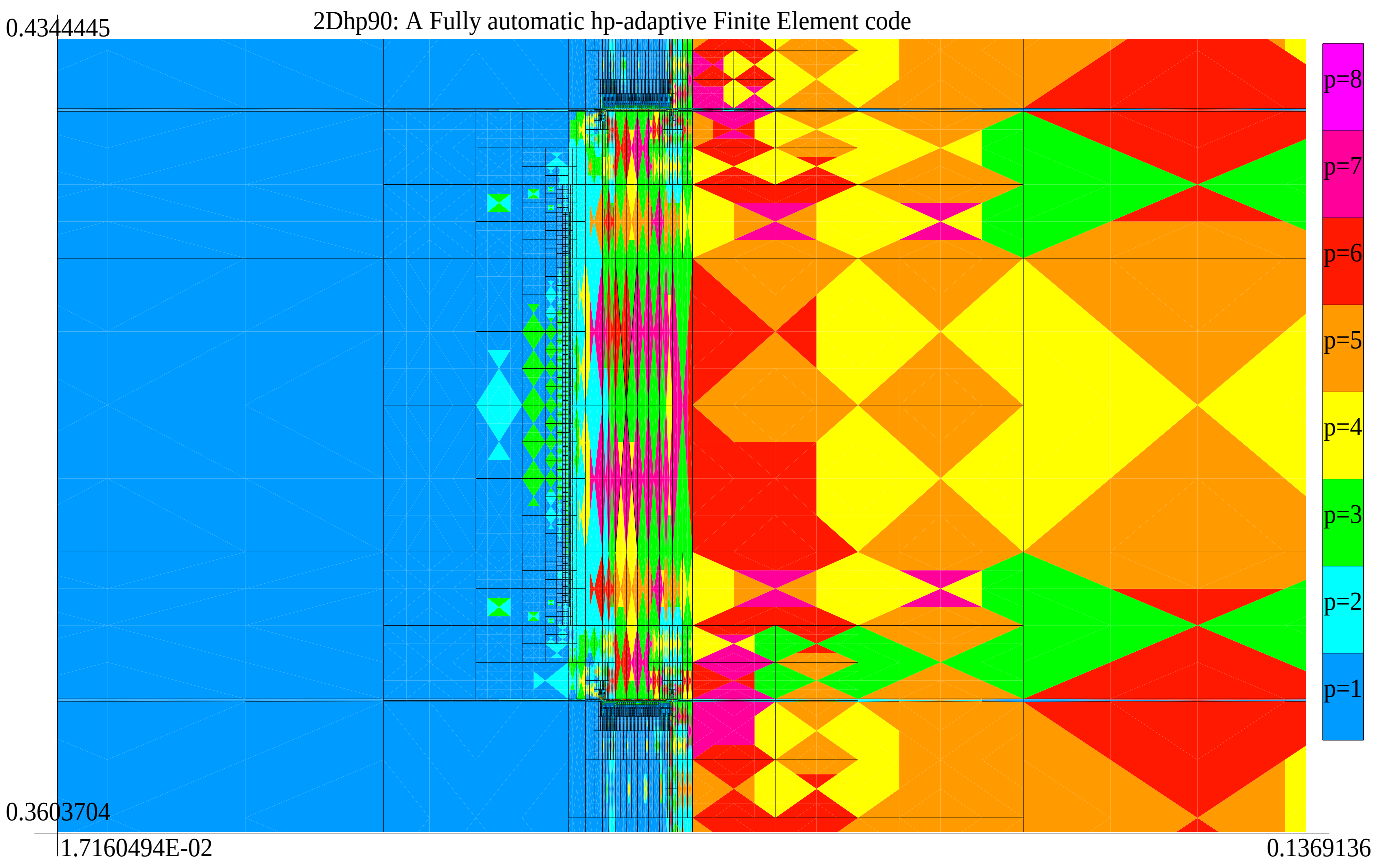

2D and 2.5D: SONIC SIMULATIONS

Axisymmetric problem setting in the frequency domain

- **Borehole fluid (lin. acoustics):**
  $-\omega^2 p - c^2 \Delta p = g$

- **Rock formation (lin. elasticity):**
  $-\omega^2 \rho \mathbf{u} - \nabla \cdot \boldsymbol{\sigma} = 0$
  $\boldsymbol{\sigma} = \lambda \mathbf{I}(\nabla \cdot \mathbf{u}) + 2\mu \boldsymbol{\epsilon}(\mathbf{u})$

- **Tool (logging instrument): lin. elasticity**

- **Interface conditions (compatib.):**
  $\nabla p \cdot \mathbf{n}_{\mathrm{f}} = \rho_{\mathrm{f}} \omega^2 \mathbf{u} \cdot \mathbf{n}_{\mathrm{f}}$
  $\boldsymbol{\sigma} \cdot \mathbf{n}_{\mathrm{s}} \;\; = -p \mathbf{n}_{\mathrm{s}}$

- **Fourier series expansion for the source:**

$$g(\zeta_1, \zeta_2, \zeta_3) = \sum_{k=-\infty}^{k=\infty} g_k(\zeta_1, \zeta_3) e^{-jk\zeta_2}$$

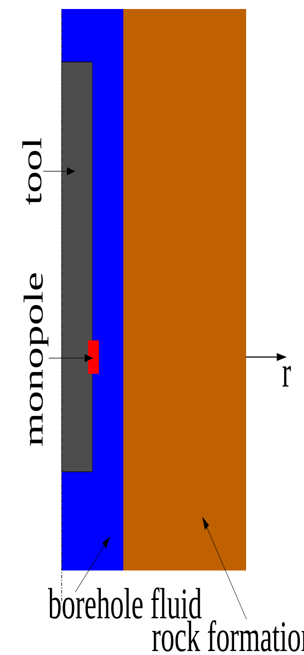

2D and 2.5D: SONIC SIMULATIONS

Sonic Logging (Coupled Acoustics/Elasticity)

Problem description:

	$\rho[kg/m^3]$	$V_p[m/s]$	$V_s[m/s]$
fluid	1000	1500	0
solid	2200	1700	1050
tool	7860	5240	2800

Material data of fluid, solid and tool

$$V_p = \left(\frac{\lambda + 2\mu}{\rho}\right)^{1/2}, \qquad V_s = \left(\frac{\mu}{\rho}\right)^{1/2}$$

R [m]	r [m]	a [m]
0.1	0.045	0.02

Geometrical data

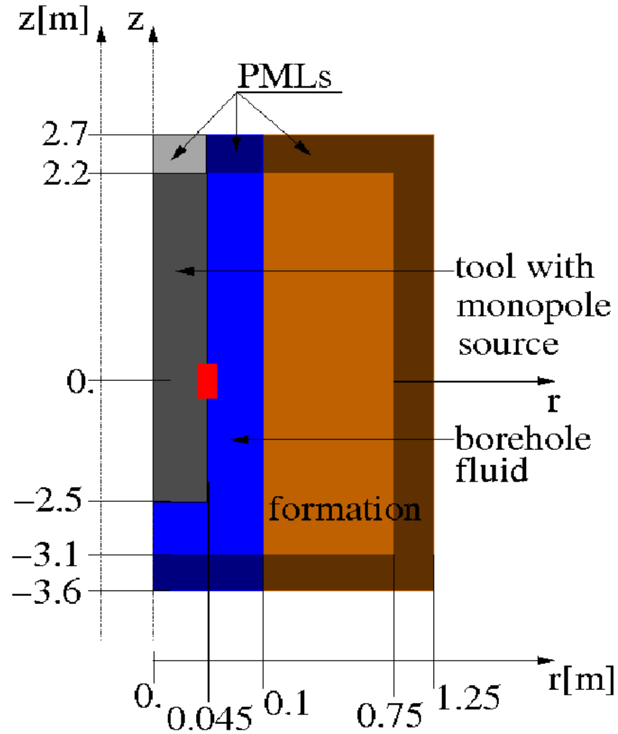

Multiple frequencies f [kHz]: 2, 4, 6

Excitation: $\dfrac{\partial p}{\partial r} = (2\pi f)^2 \rho_{\mathsf{f}} u_r$

Encompass computational domain with PML

2D and 2.5D: SONIC SIMULATIONS

Sonic Logging (Coupled Acoustics/Elasticity)

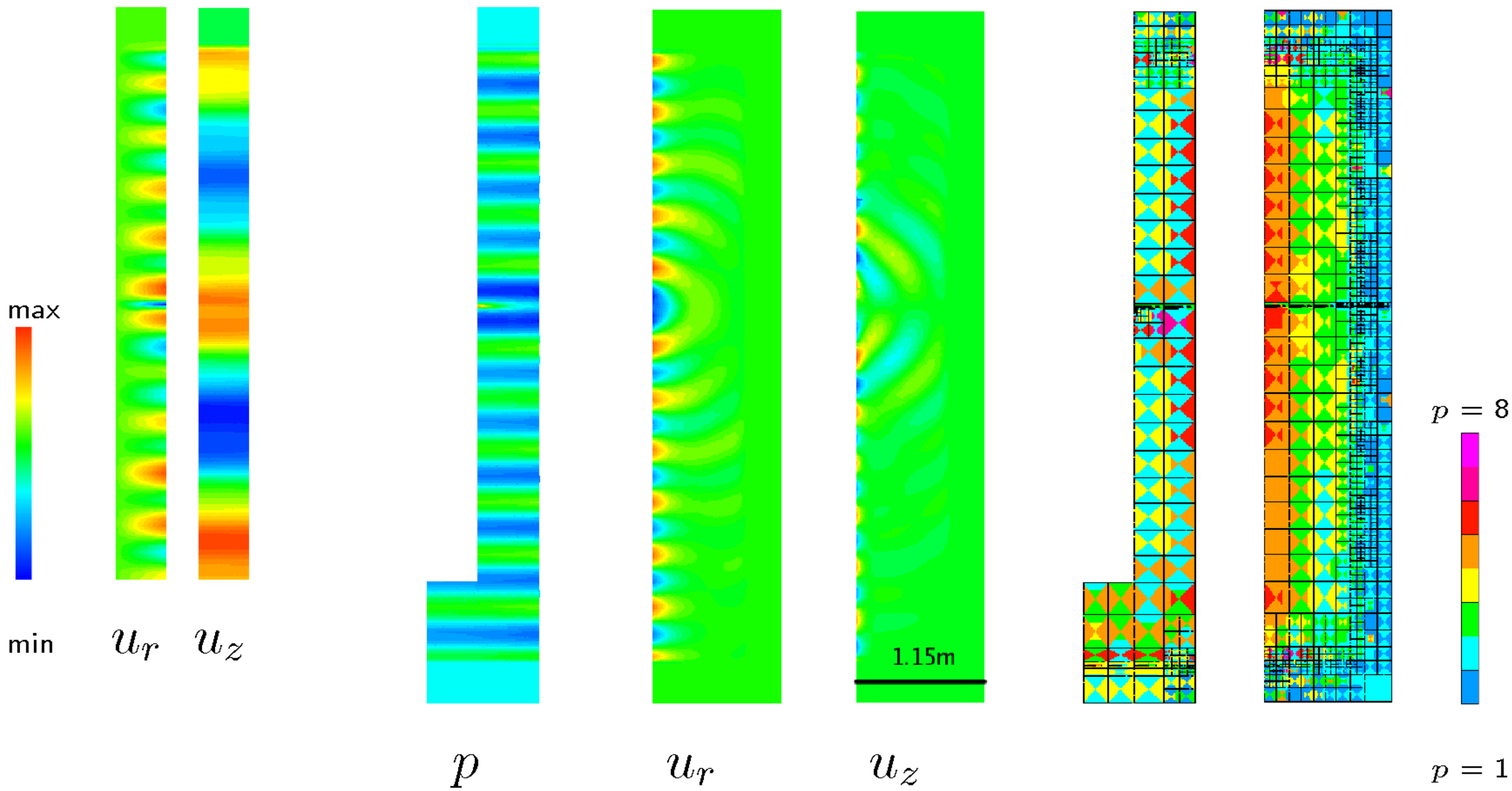

Tool Borehole Fluid Rock formation

2D and 2.5D: SONIC SIMULATIONS

Sonic Logging (Coupled Acoustics/Elasticity)

Monopole source at f = 4 kHz

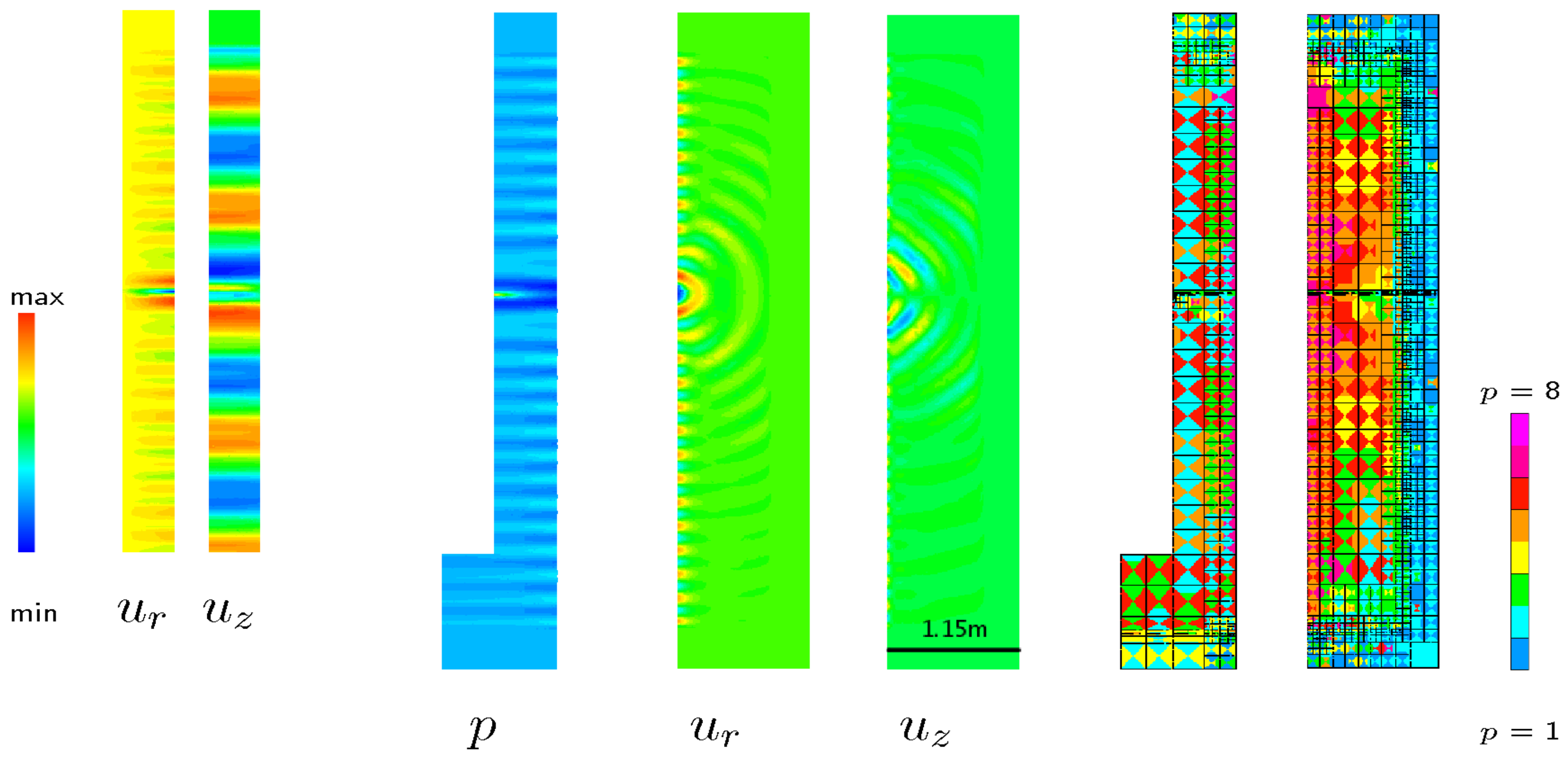

Tool Borehole Fluid Rock formation

2D and 2.5D: SONIC SIMULATIONS

Sonic Logging (Coupled Acoustics/Elasticity)

Monopole source at f = 6 kHz

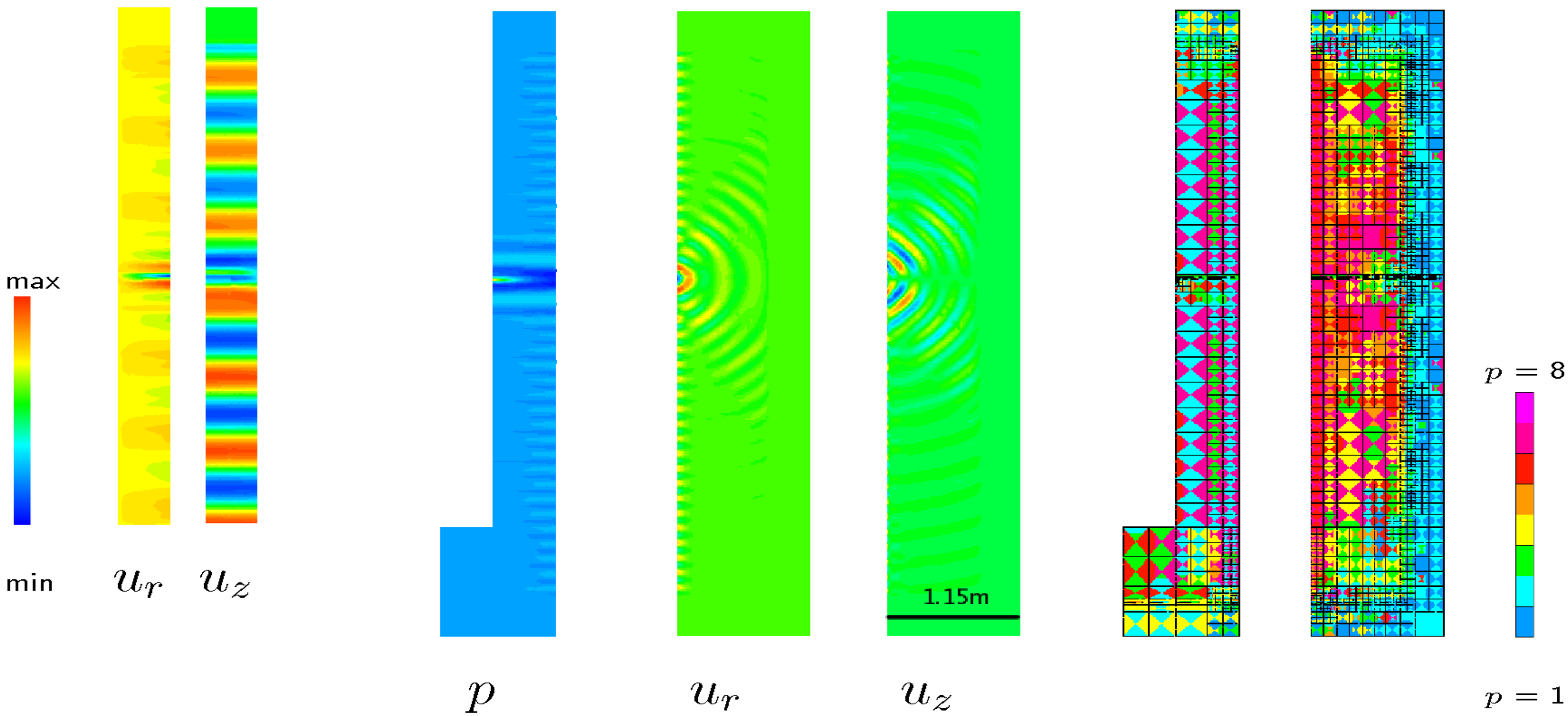

Tool Borehole Fluid Rock formation

2D and 2.5D: SONIC SIMULATIONS

Sonic Logging (Coupled Acoustics/Elasticity)

Problem description:

	$\rho[kg/m^3]$	$V_p[m/s]$	$V_s[m/s]$
fluid	1000	1500	0
solid(upper)	2200	1700	1050
solid(lower)	2900	3000	1300
tool	7860	5240	2800

Material data of fluid, solid and tool

R [m]	r [m]	a [m]
0.1	0.045	0.02

Geometrical data

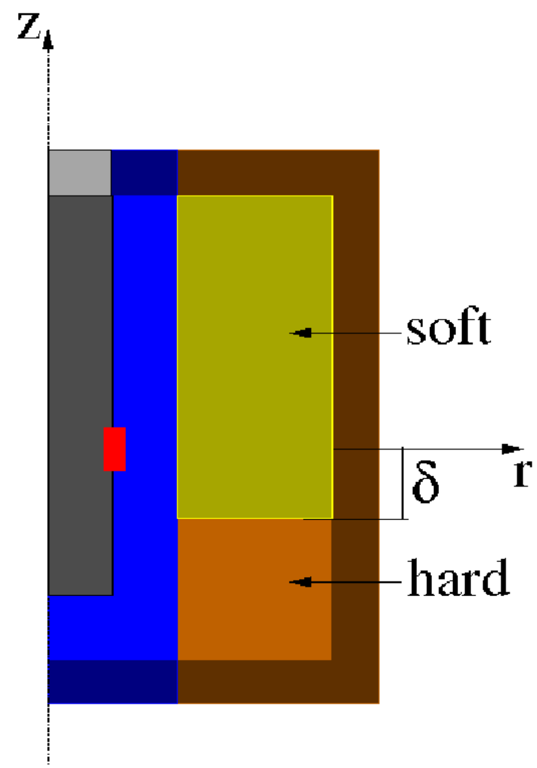

Single frequency: 6 kHz

Different positions of tool wrt. layer: δ

2D and 2.5D: SONIC SIMULATIONS

Sonic Logging (Coupled Acoustics/Elasticity)

Monopole at f $= 6$ kHz, $\delta = 0.0m$

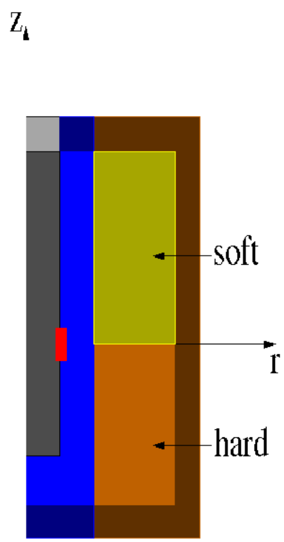

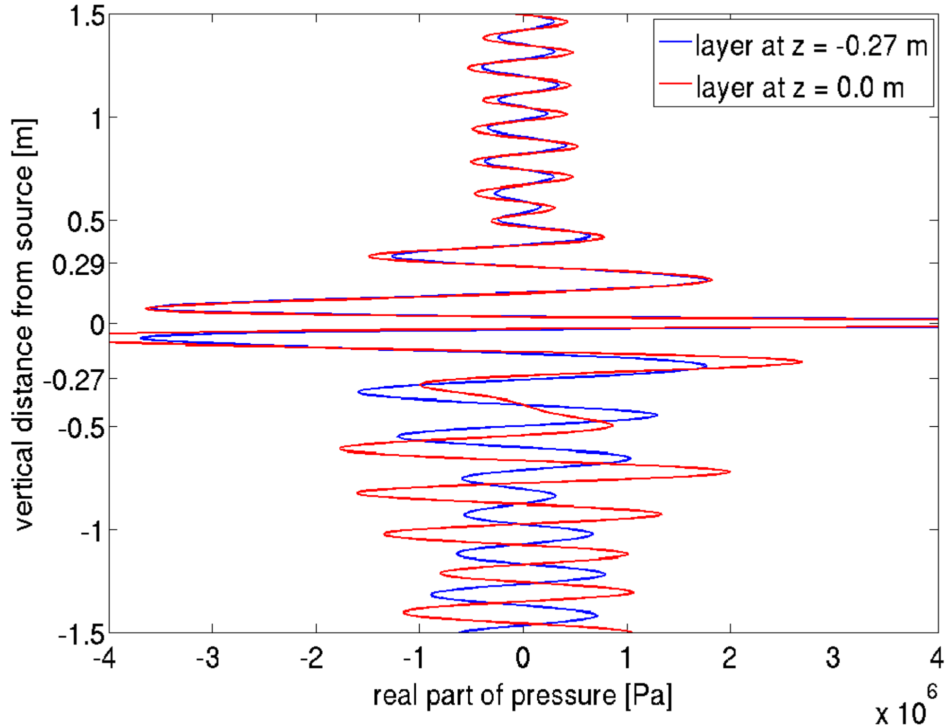

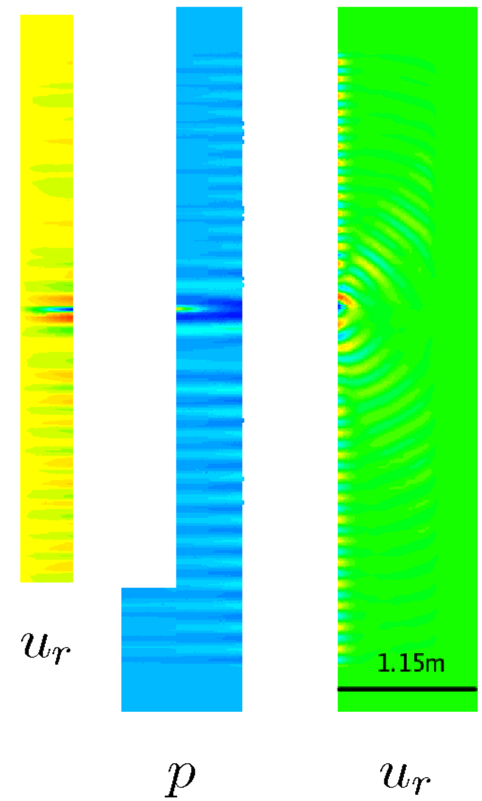

Tool Borehole Rock

2D and 2.5D: SONIC SIMULATIONS

Sonic Logging (Coupled Acoustics/Elasticity)

Comparison of the solution with (w/) and without (wo/) the tool

Homogeneous formation: $\rho = 2200$ kg/m^3, $V_p = 1700$ m/s, $V_s = 1050$ m/s

Monopole source at f = 4 kHz

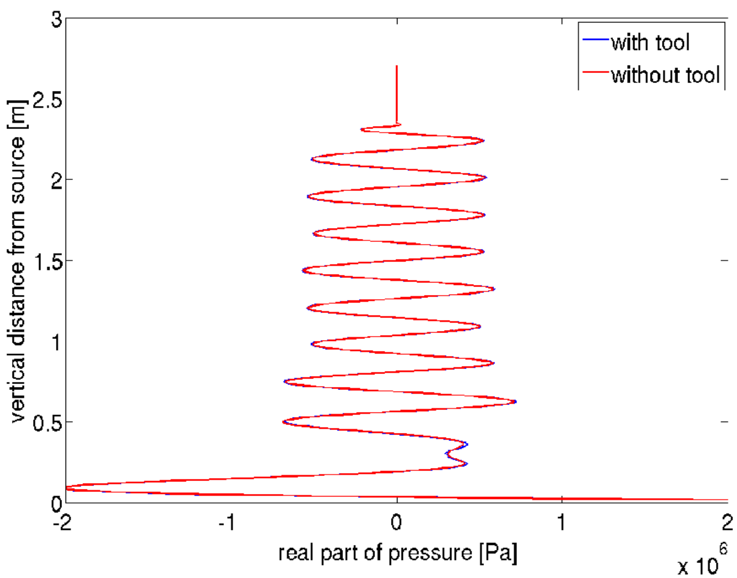

point source

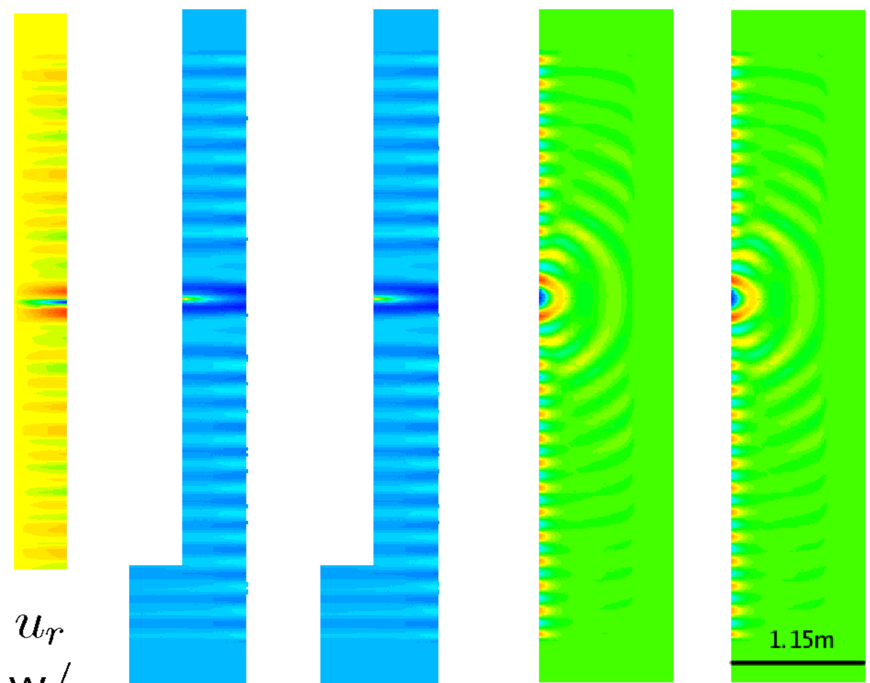

u_r w/

p w/ p wo/ u_r w/ u_r wo/

2D and 2.5D: SONIC SIMULATIONS

Sonic Logging (Coupled Acoustics/Elasticity)

Comparison of the solution with (w/) and without (wo/) the tool

Homogeneous formation: $\rho = 2200$ kg/m^3, $V_p = 1700$ m/s, $V_s = 1050$ m/s

Dipole source at f = 4 kHz (by Fourier-series exp. in azimuth)

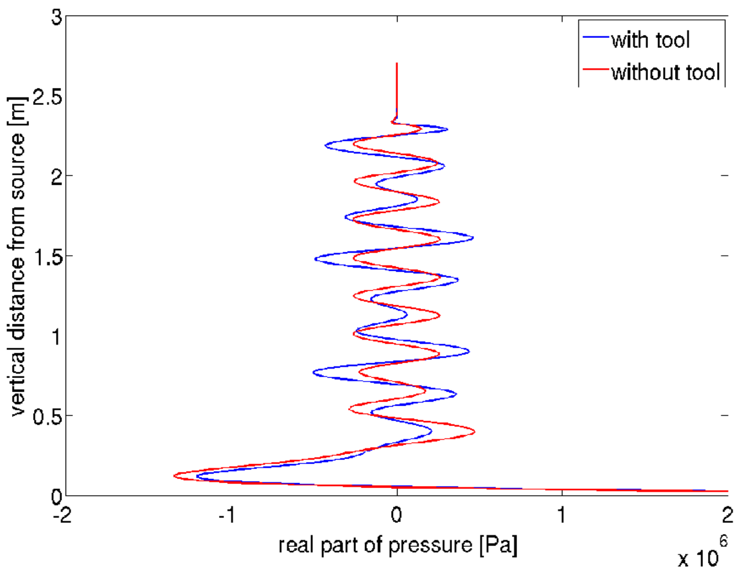

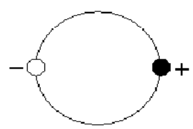

point source combination

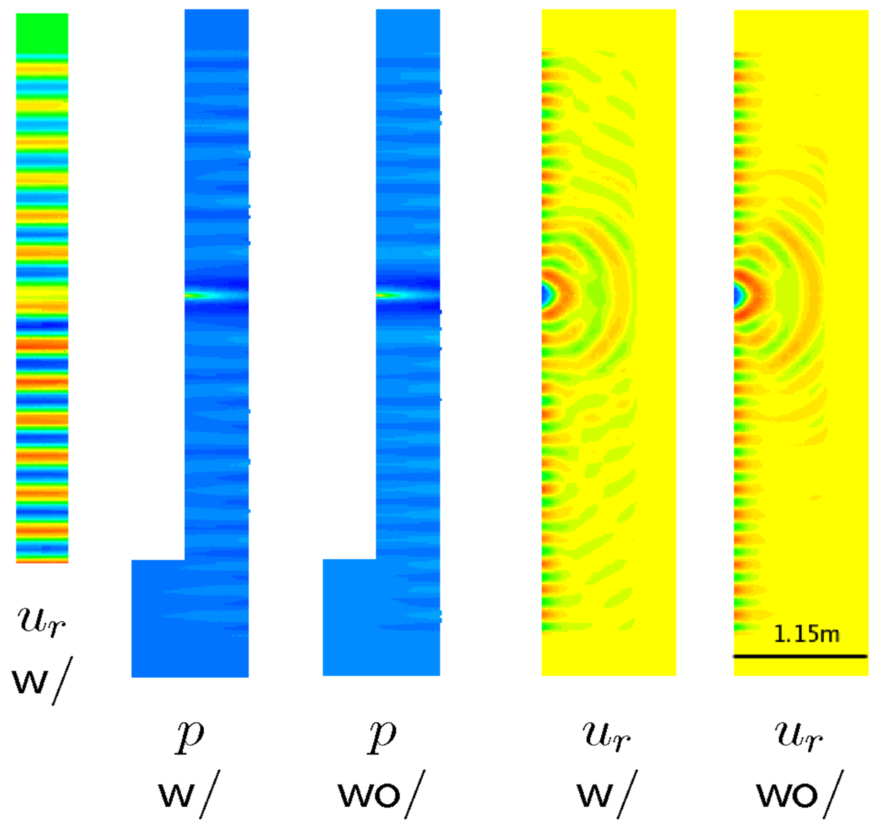

MULTI-PHYSICS APLICATIONS

De Rham diagram

De Rham diagram is critical to the theory of FE discretizations of multi-physics problems.

$$
\begin{tikzcd}
\mathbb{R} \arrow[r] \arrow[d, "id"] & W \arrow[r, "\nabla"] \arrow[d, "\Pi"] & Q \arrow[r, "\nabla\times"] \arrow[d, "\Pi^{\mathrm{curl}}"] & V \arrow[r, "\nabla\circ"] \arrow[d, "\Pi^{\mathrm{div}}"] & L^2 \arrow[r] \arrow[d, "P"] & 0 \\
\mathbb{R} \arrow[r] & W^{\mathrm{p}} \arrow[r, "\nabla"] & Q^{\mathrm{p}} \arrow[r, "\nabla\times"] & V^{\mathrm{p}} \arrow[r, "\nabla\circ"] & W^{\mathrm{p}-1} \arrow[r] & 0\,.
\end{tikzcd}
$$

This diagram relates two exact sequences of spaces, on both continuous and discrete levels, and corresponding interpolation operators.

3D: NON-ORTHOGONAL SYSTEM OF COORDINATES

Deviated Wells (Forward Problem)

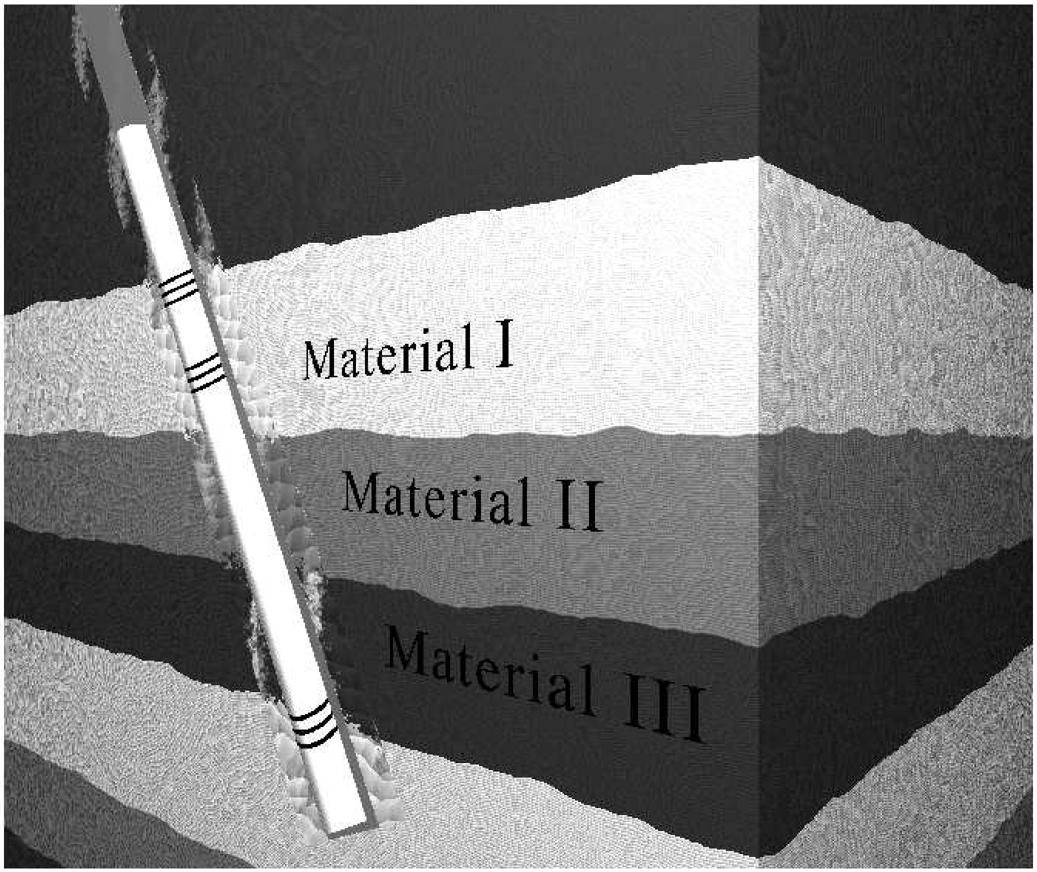

- Dip Angle
- Invasion
- Anisotropy
- Triaxial Induction
- Eccentricity
- Laterolog
- Through-Casing
- Induction-LWD
- Induction-Wireline
- Inverse Problems
- Multi-Physics

Objective: Find solution at the receiver antennas.

3D: NON-ORTHOGONAL SYSTEM OF COORDINATES

Example: Solution in a 60-degree deviated well ($-\nabla\sigma\nabla u = f$)

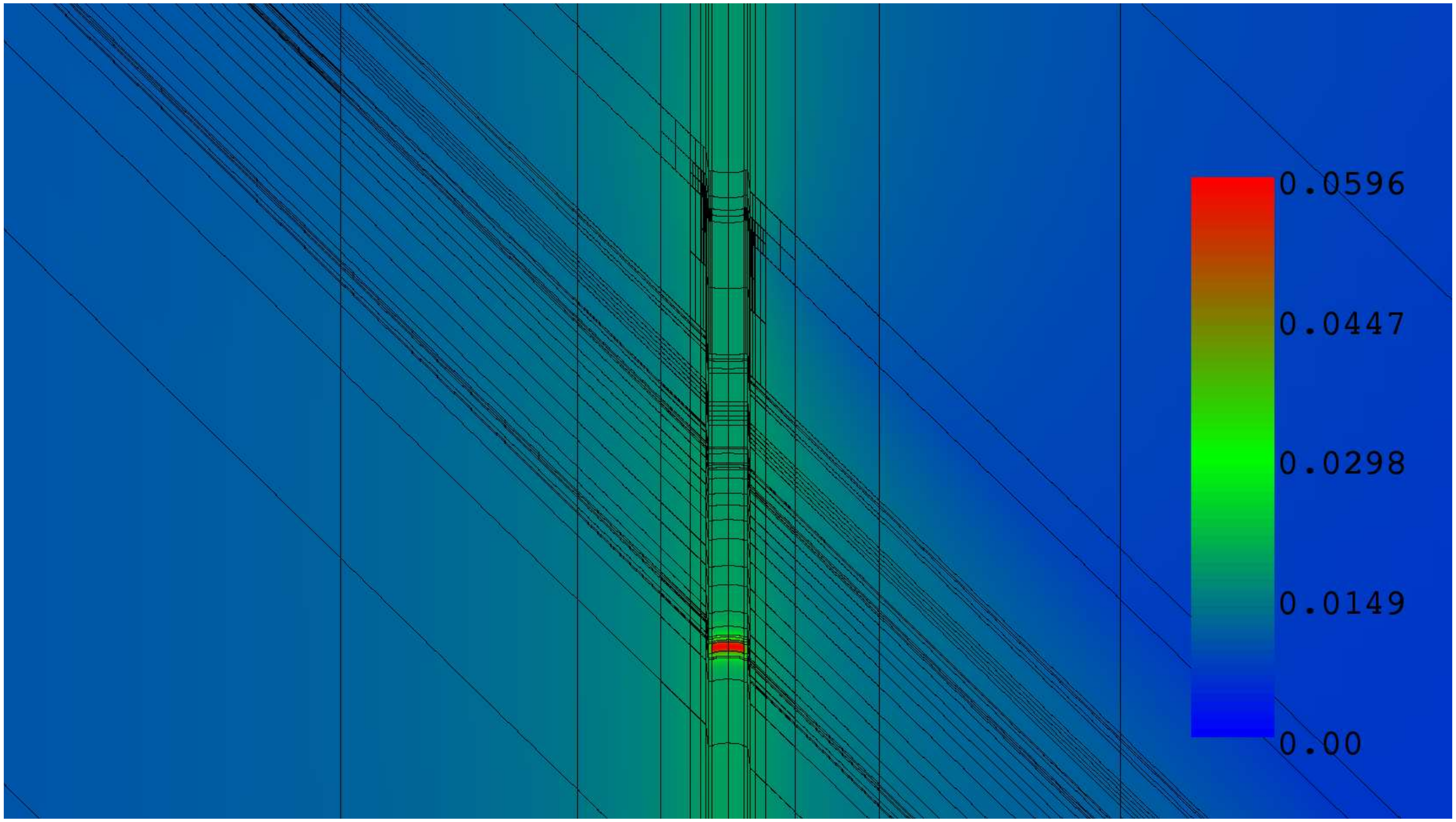

Several hours to obtain one solution (3D forward simulation).
Several months needed to solve the inverse problem.

3D: NON-ORTHOGONAL SYSTEM OF COORDINATES

Non-Orthogonal System of Coordinates

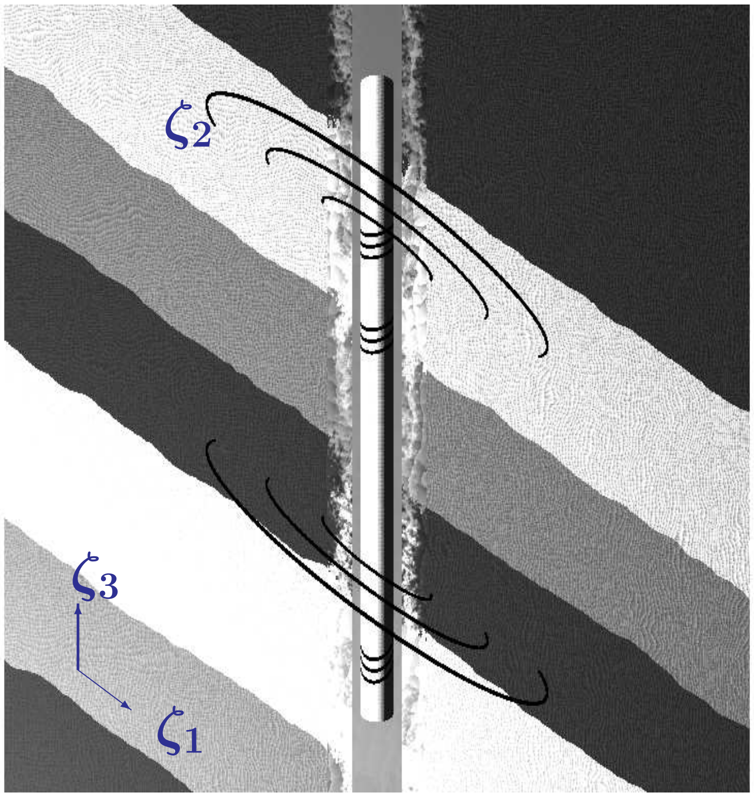

Material coefficients are constant with respect to the quasi-azimuthal direction ζ_2

Fourier Series Expansion in ζ_2

DC Problems: $-\nabla \sigma \nabla u = f$

$$u(\zeta_1, \zeta_2, \zeta_3) = \sum_{l=-\infty}^{l=\infty} u_l(\zeta_1, \zeta_3) e^{jl\zeta_2}$$

$$\sigma(\zeta_1, \zeta_2, \zeta_3) = \sum_{m=-\infty}^{m=\infty} \sigma_m(\zeta_1, \zeta_3) e^{jm\zeta_2}$$

$$f(\zeta_1, \zeta_2, \zeta_3) = \sum_{n=-\infty}^{n=\infty} f_n(\zeta_1, \zeta_3) e^{jn\zeta_2}$$

Fourier modes $e^{jl\zeta_2}$ are orthogonal high-order basis functions that are (almost) invariant with respect to the gradient operator.

3D: NON-ORTHOGONAL SYSTEM OF COORDINATES

Cartesian system of coordinates: $\mathrm{x} = (x_1, x_2, x_3)$.
New non-orthogonal system of coordinates: $\zeta = (\zeta_1, \zeta_2, \zeta_3)$.

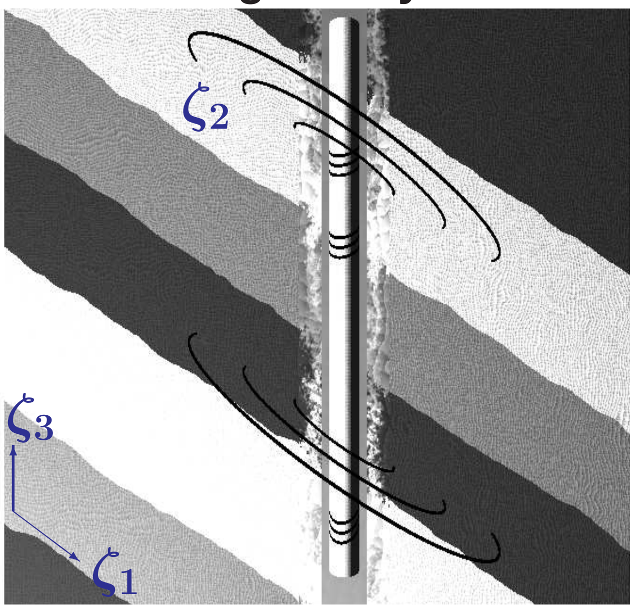

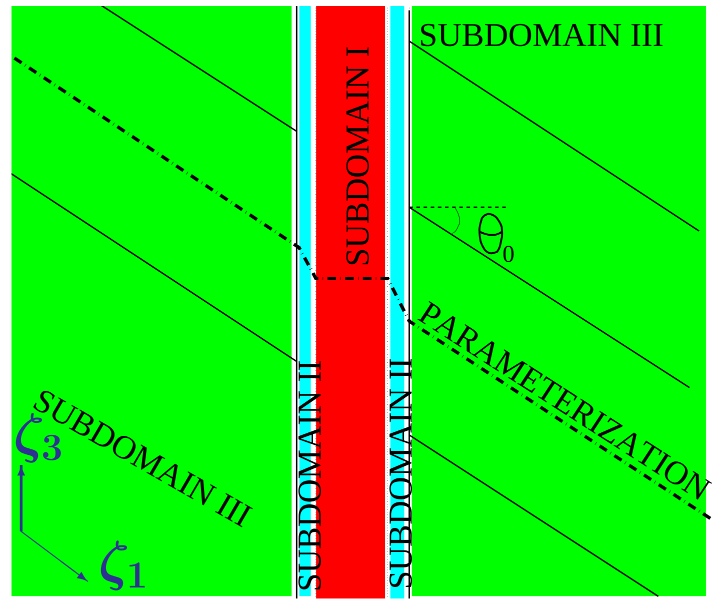

Subdomain I ; **Subdomain II** ; **Subdomain III**

$$\begin{cases} x_1 = \zeta_1 \cos \zeta_2 \\ x_2 = \zeta_1 \sin \zeta_2 \\ x_3 = \zeta_3 \end{cases} ; \quad \begin{cases} x_1 = \zeta_1 \cos \zeta_2 \\ x_2 = \zeta_1 \sin \zeta_2 \\ x_3 = \zeta_3 + \tan \theta_0 \dfrac{\zeta_1 - \rho_1}{\rho_2 - \rho_1} \rho_2 \end{cases} ; \quad \begin{cases} x_1 = \zeta_1 \cos \zeta_2 \\ x_2 = \zeta_1 \sin \zeta_2 \\ x_3 = \zeta_3 + \tan \theta_0 \zeta_1 \end{cases}$$

3D: NON-ORTHOGONAL SYSTEM OF COORDINATES

Final Variational Formulation

We define the Jacobian matrix $\mathcal{J} = \dfrac{\partial(x_1, x_2, x_3)}{\partial(\zeta_1, \zeta_2, \zeta_3)}$ **and its determinant** $|\mathcal{J}| = \det(\mathcal{J})$**.**

Variational formulation in the new system of coordinates:

$$\left\{ \begin{array}{l} \text{Find } u \in u_D + H_D^1(\Omega) \text{ such that:} \\ \left\langle \dfrac{\partial v}{\partial \zeta} \, , \, \tilde{\sigma} \dfrac{\partial u}{\partial \zeta} \right\rangle_{L^2(\Omega)} = \left\langle v \, , \, \tilde{f} \right\rangle_{L^2(\Omega)} \quad \forall v \in H_D^1(\Omega) \; , \end{array} \right.$$

where:

$$\tilde{\sigma} := \mathcal{J}^{-1} \sigma \mathcal{J}^{-1^T} |\mathcal{J}| \quad ; \quad \tilde{f} := f |\mathcal{J}| \; .$$

Same variational formulation with new materials and load data

3D: NON-ORTHOGONAL SYSTEM OF COORDINATES

For a mono-modal test function $v = v_k e^{jk\zeta_2}$, we have:

$$\left\{ \begin{array}{l} \text{Find } u \in u_D + H^1_D(\Omega) \text{ such that:} \\ \displaystyle\sum_{m,n} \left\langle \left(\frac{\partial v}{\partial \zeta}\right)_k e^{jk\zeta_2} \, , \, \tilde{\sigma}_m \left(\frac{\partial u}{\partial \zeta}\right)_n e^{j(m+n)\zeta_2} \right\rangle_{L^2(\Omega)} = \\ = \displaystyle\sum_l \left\langle v_k e^{jk\zeta_2} \, , \, \tilde{f}_l e^{jl\zeta_2} \right\rangle_{L^2(\Omega)} \quad \forall v_k e^{jk\zeta_2} \in H^1_D(\Omega) \end{array} \right.$$

Using the L^2-orthogonality of Fourier modes:

$$\left\{ \begin{array}{l} \text{Find } u \in u_D + H^1_D(\Omega) \text{ such that:} \\ \displaystyle\sum_{n} \left\langle \left(\frac{\partial v}{\partial \zeta}\right)_k \, , \, \tilde{\sigma}_{k-n} \left(\frac{\partial u}{\partial \zeta}\right)_n \right\rangle_{L^2(\Omega_{2D})} = \left\langle v_k \, , \, \tilde{f}_k \right\rangle_{L^2(\Omega_{2D})} \quad \forall v_k \end{array} \right.$$

3D: NON-ORTHOGONAL SYSTEM OF COORDINATES

Five Fourier modes are enough to represent EXACTLY the new material coefficients.

$$\tilde{\boldsymbol{\sigma}}(\zeta_1, \zeta_2, \zeta_3) = \sum_{m=-2}^{m=2} \tilde{\boldsymbol{\sigma}}_m(\zeta_1, \zeta_3) e^{jm\zeta_2}$$

3D: NON-ORTHOGONAL SYSTEM OF COORDINATES

Five Fourier modes are enough to represent EXACTLY the new material coefficients.

$$\tilde{\sigma}(\zeta_1, \zeta_2, \zeta_3) = \sum_{m=-2}^{m=2} \tilde{\sigma}_m(\zeta_1, \zeta_3) e^{jm\zeta_2}$$

Final Variational Formulation

$$\begin{cases} \text{Find } u \in u_D + H^1_D(\Omega) \text{ such that:} \\ \displaystyle\sum_{n=k-2}^{n=k+2} \left\langle \left(\frac{\partial v}{\partial \zeta}\right)_k , \tilde{\sigma}_{k-n} \left(\frac{\partial u}{\partial \zeta}\right)_n \right\rangle_{L^2(\Omega_{2D})} = \left\langle v_k , \tilde{f}_k \right\rangle_{L^2(\Omega_{2D})} \quad \forall v_k \end{cases}$$

3D: NON-ORTHOGONAL SYSTEM OF COORDINATES

Five Fourier modes are enough to represent EXACTLY the new material coefficients.

Direct Current:

$$\left\{\begin{array}{l} \textbf{Find } u \in u_D + H_D^1(\Omega) \textbf{ such that:} \\ \displaystyle\sum_{n=k-2}^{n=k+2} \left\langle \left(\frac{\partial v}{\partial \zeta}\right)_k , \tilde{\sigma}_{k-n} \left(\frac{\partial u}{\partial \zeta}\right)_n \right\rangle_{L^2(\Omega_{2D})} = \left\langle v_k , \tilde{f}_k \right\rangle_{L^2(\Omega_{2D})} \quad \forall v_k \end{array}\right.$$

Alternate Current:

$$\left\{\begin{array}{l} \textbf{Find } (\mathrm{E})_s \in H_{\Gamma_E}(\mathrm{curl};\Omega) \textbf{ such that:} \\ \displaystyle\sum_{n=s-2}^{n=s+2} \left\langle (\nabla^\zeta \times \mathrm{F})_s , (\tilde{\mu}^{-1})_{s-n} (\nabla^\zeta \times \mathrm{E})_l \right\rangle_{L^2(\Omega_{2D})} \\ \quad - \left\langle \mathrm{F}_s , (\tilde{k^2})_{s-n} \mathrm{E}_l \right\rangle_{L^2(\Omega_{2D})} = -j\omega \left\langle \mathrm{F}_s , (\tilde{\mathrm{J}}^{imp})_s \right\rangle_{L^2(\Omega_{2D})} \quad \forall\, \mathrm{F}_s \end{array}\right.$$

3D: NON-ORTHOGONAL SYSTEM OF COORDINATES

Example (7 Fourier Modes)

$$\sum_{n=k-2}^{n=k+2} \underbrace{\left\langle \left(\frac{\partial v}{\partial \zeta}\right)_k , \tilde{\sigma}_{k-n} \left(\frac{\partial u}{\partial \zeta}\right)_n \right\rangle_{L^2(\Omega_{2D})}}_{(k,k-n,n)} = \left\langle v_k , \tilde{f}_k \right\rangle_{L^2(\Omega_{2D})}$$

Stiffness Matrix:

$$\begin{pmatrix}
(-3,0,-3) & (-3,-1,-2) & (-3,-2,-1) & 0 & 0 & 0 & 0 \\
(-2,1,-3) & (-2,0,-2) & (-2,-1,-1) & (-2,-2,0) & 0 & 0 & 0 \\
(-1,2,-3) & (-1,1,-2) & (-1,0,-1) & (-1,-1,0) & (-1,-2,1) & 0 & 0 \\
0 & (0,2,-2) & (0,1,-1) & (0,0,0) & (0,-1,1) & (0,-2,2) & 0 \\
0 & 0 & (1,2,-1) & (1,1,0) & (1,0,1) & (1,-1,2) & (1,-2,3) \\
0 & 0 & 0 & (2,2,0) & (2,1,1) & (2,0,2) & (2,-1,3) \\
0 & 0 & 0 & 0 & (3,2,1) & (3,1,2) & (3,0,3)
\end{pmatrix}$$

3D: NON-ORTHOGONAL SYSTEM OF COORDINATES

A Self-Adaptive Goal-Oriented hp-FEM

Optimal 2D Grid
(Through Casing Resistivity Problem)

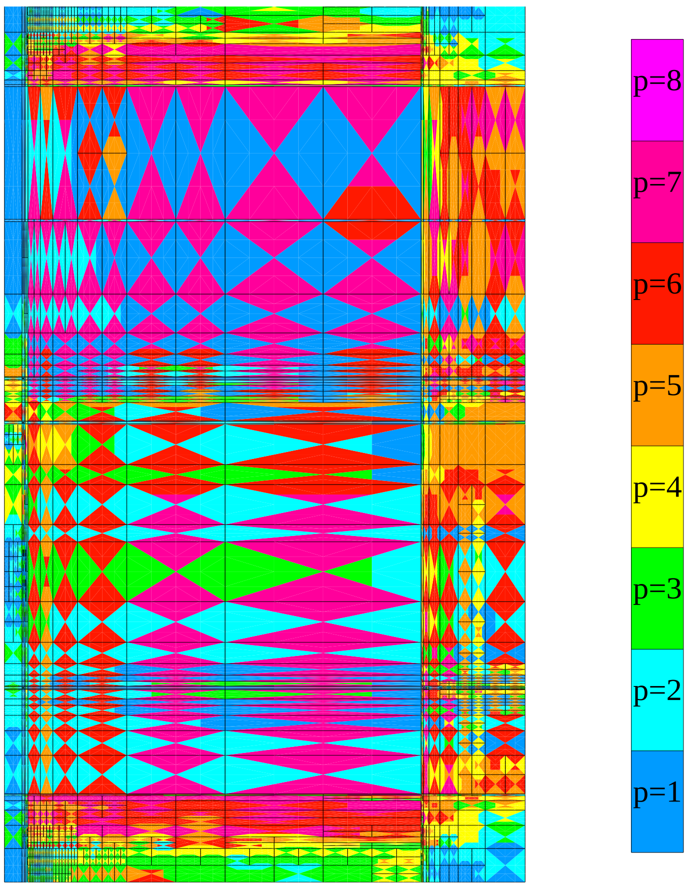

We vary locally the element size h and the polynomial order of approximation p throughout the grid.

Optimal grids are automatically generated by the computer.

The self-adaptive goal-oriented hp-FEM provides exponential convergence rates in terms of the CPU time vs. the error in a user prescribed quantity of interest.

3D: PARALLEL IMPLEMENTATION

We Use Shared Domain Decomposition

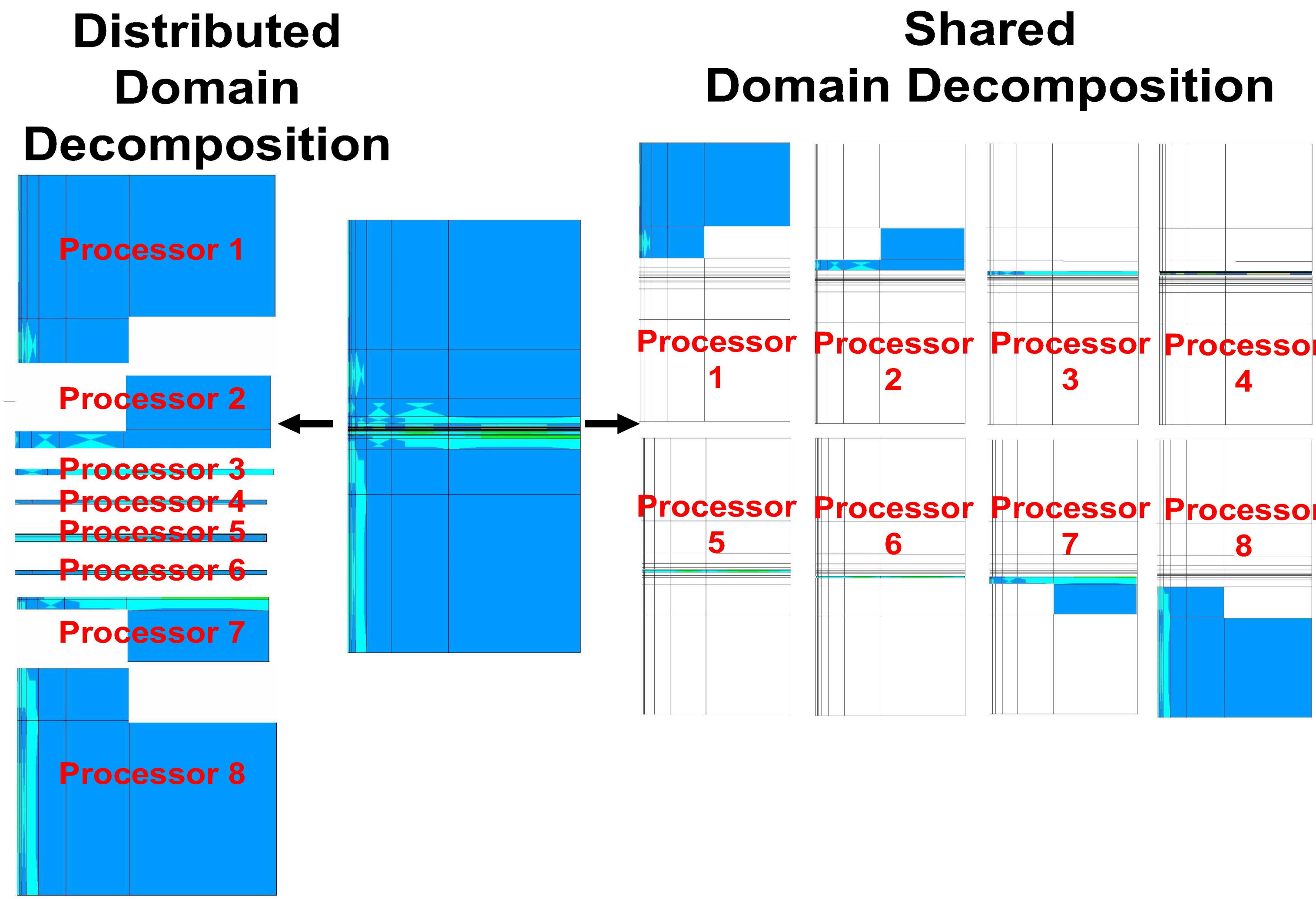

3D: PARALLEL IMPLEMENTATION

Scalability of the Parallel Multi-Frontal Solver

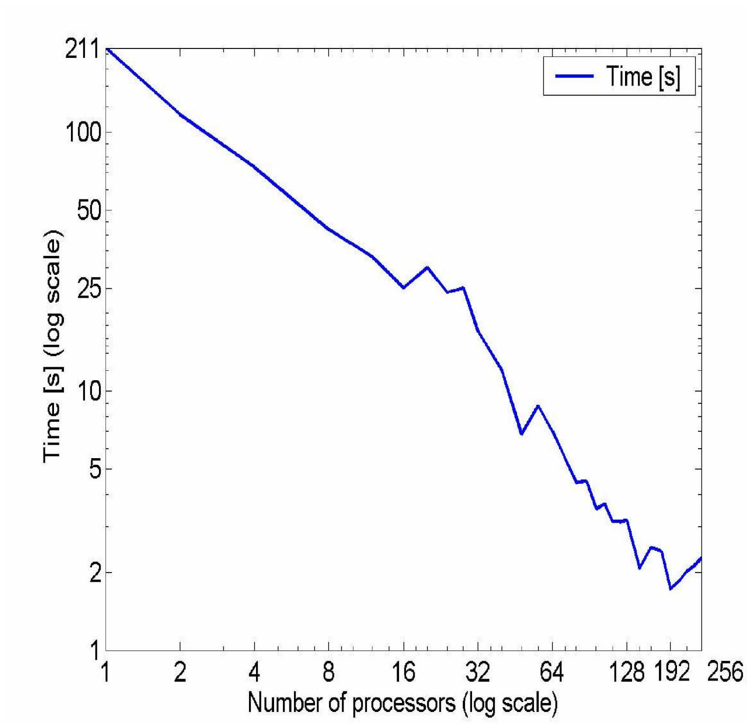

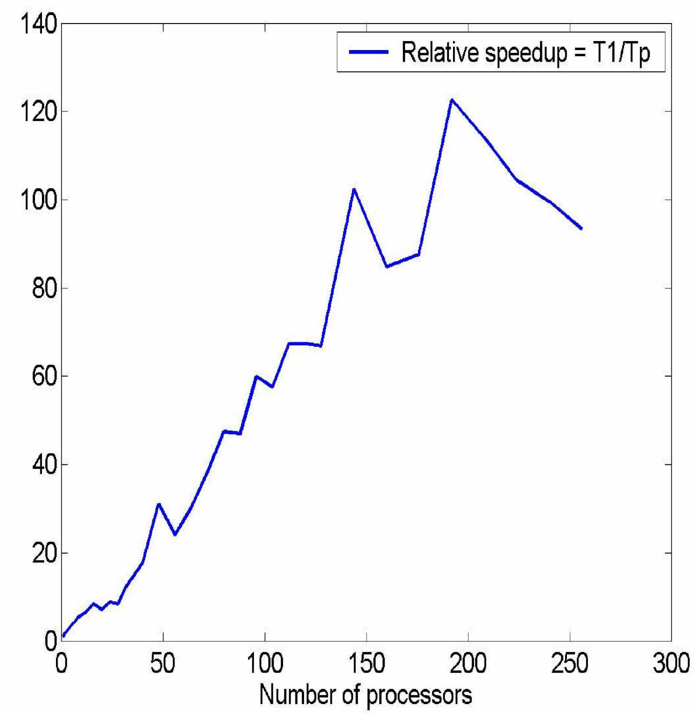

Parallel computations performed on Texas Advanced Computing Center (TACC) 60 % relative efficiency up to 200 processors.
Parallel solver is 125 times faster on 200 processors.

3D: ELECTROMAGNETIC SIMULATIONS

Three Model Problems

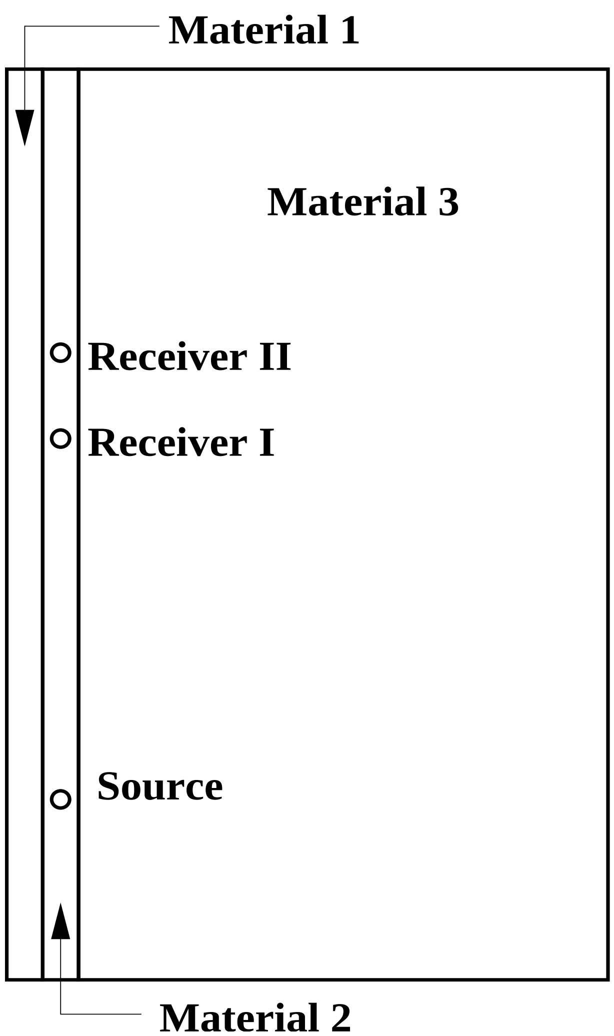

Problem I **(Uniform Materials)**

Material 1:1 Ω−m
Material 2:1 Ω−m
Material 3:1 Ω−m

Problem II

Material 1:0.00001 Ω−m
Material 2:10 Ω−m
Material 3:1 Ω−m

Problem III

Material 1:10000 Ω−m
Material 2: 0.2 Ω−m
Material 3:1 Ω−m

3D: ELECTROMAGNETIC SIMULATIONS

Three Model Problems (DC)

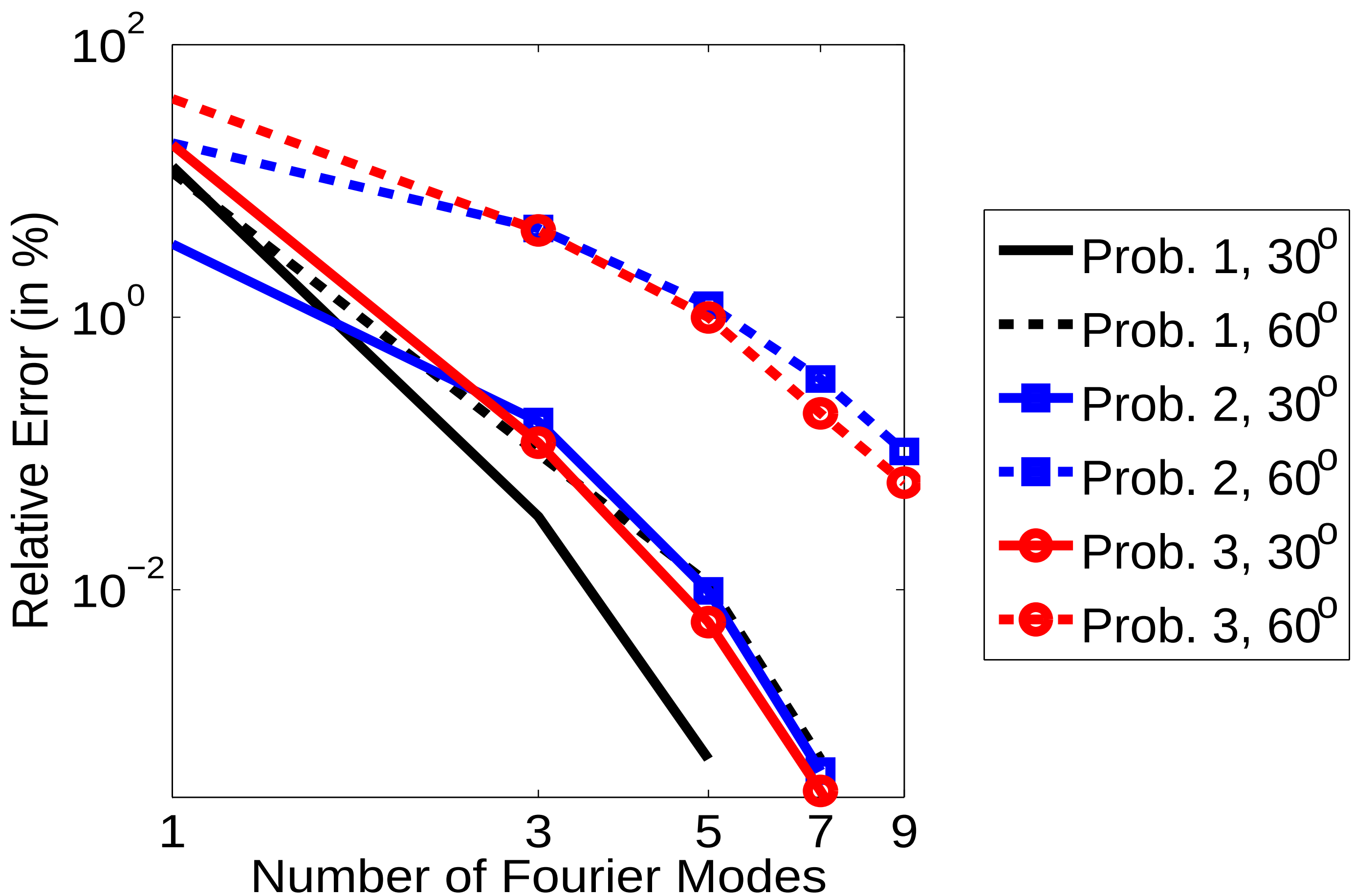

Exponential Convergence in terms of the Number of Fourier Modes

3D: ELECTROMAGNETIC SIMULATIONS

Simulation of Through Casing Resistivity Measurements

Casing resistivity: $10^{-5} - 10^{-7}\Omega\cdot$ m
Casing thickness: 0.0127 m

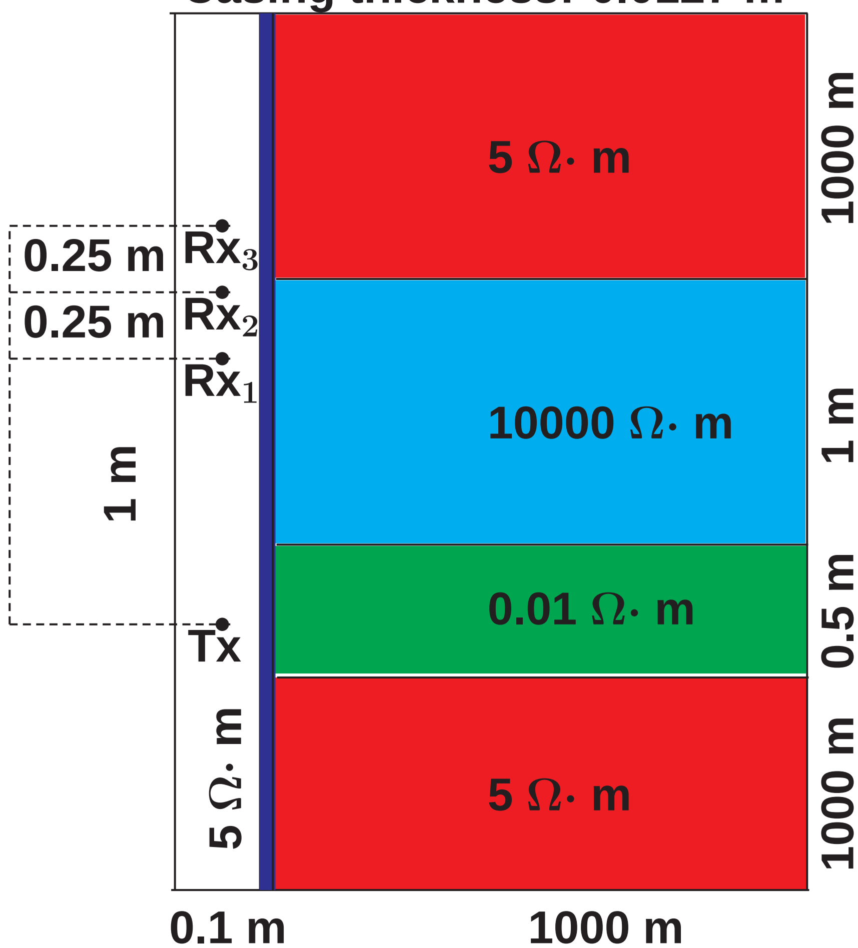

Left Figure:
- Axial-symmetric model
- One current electrode (emitter)
- Three voltage electrodes (collectors)

Objective:
- Compute second diff. of potential for various depth angles and possibly with water invasion

Method of solution:
- Fourier series expansion + change of coordinates + 2D goal-oriented hp-FEM

3D: ELECTROMAGNETIC SIMULATIONS

Simulation of Through Casing Resistivity Measurements

Algorithm (Case) Number	I	II	III	IV	V	VI	VII	VIII
1 Fourier mode used for adaptivity	X	X	X	X				
5 Fourier modes used for adaptivity					X	X	X	X
Final hp-grid NOT p-enriched	X		X		X		X	
Final hp-grid globally p-enriched		X		X		X		X
9 Fourier modes used for the final solution	X	X			X	X		
15 Fourier modes used for the final solution			X	X			X	X

Different algorithms provide different levels of accuracy

3D: ELECTROMAGNETIC SIMULATIONS

Through Casing Resistivity Measurements (60-Degree Deviated Well)

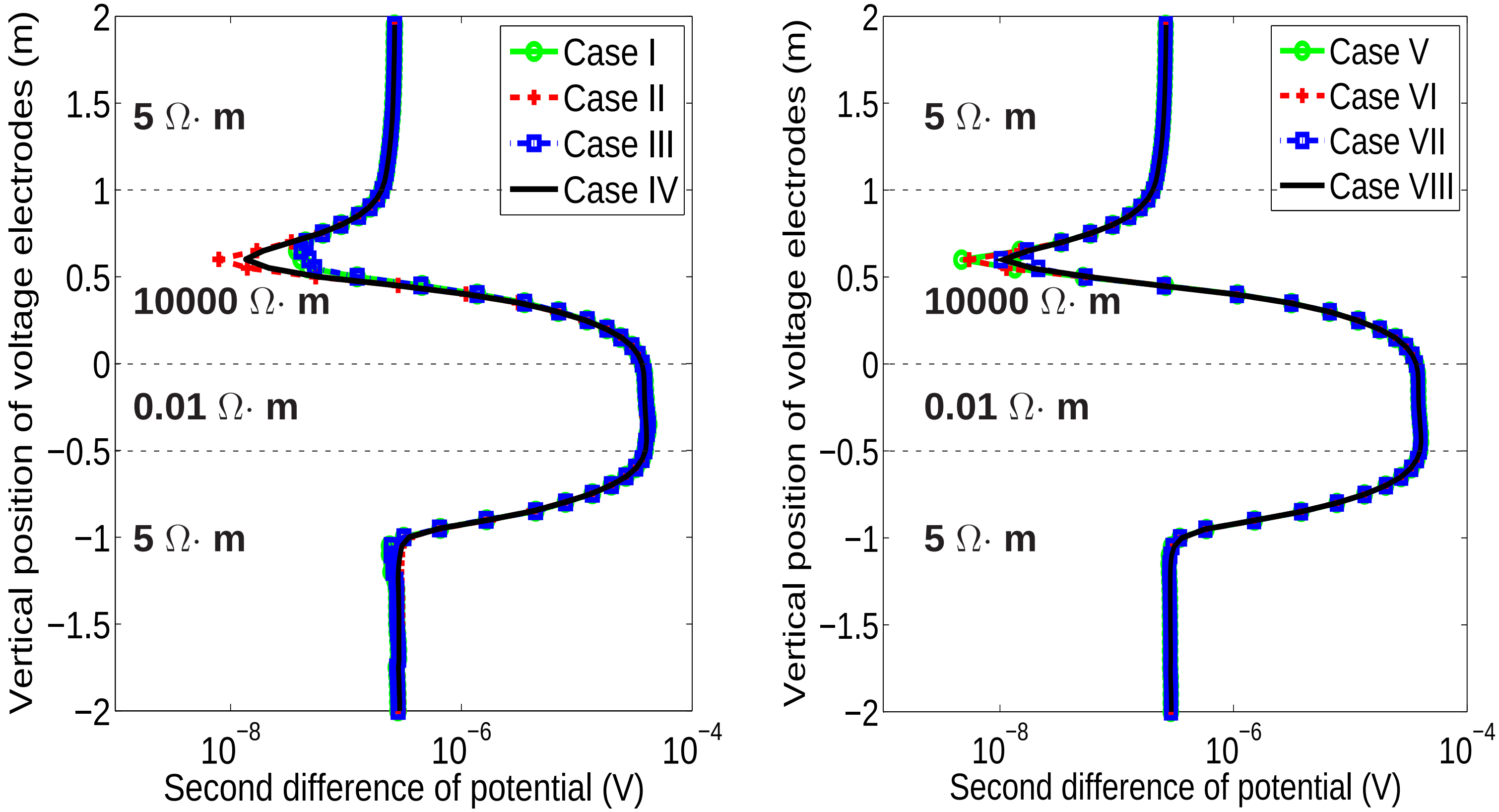

Case Number	I	II	III	IV	V	VI	VII	VIII
Total Time (minutes)	21’	40’	39’	109’	244’	290’	286’	432’

3D: ELECTROMAGNETIC SIMULATIONS

Through Casing Resistivity Measurements (60-Degree Deviated Well)

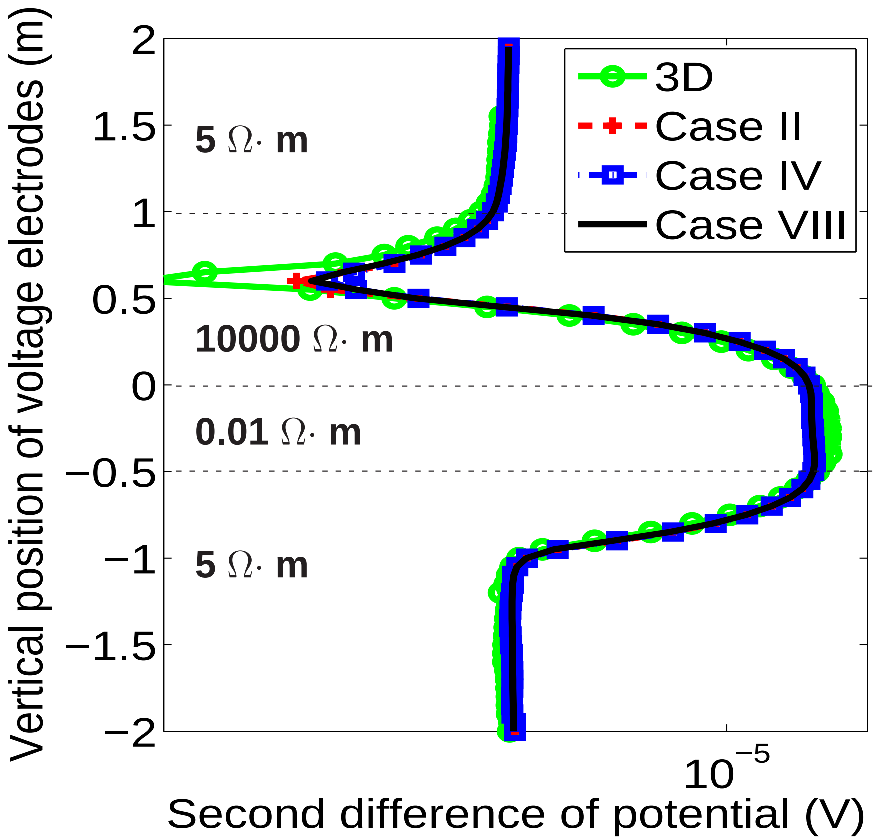

Results with the new methodology seem more accurate than those obtained with the 3D software. In addition, with the new methology we reduce the CPU time from several days to two hours.

3D: ELECTROMAGNETIC SIMULATIONS

Through Casing Resistivity Measurements (Casing Conductivity)

Casing Resistivity=$10^{-5}\Omega\cdot$ m **Casing Resistivity=$2.3\times10^{-7}\Omega\cdot$ m**

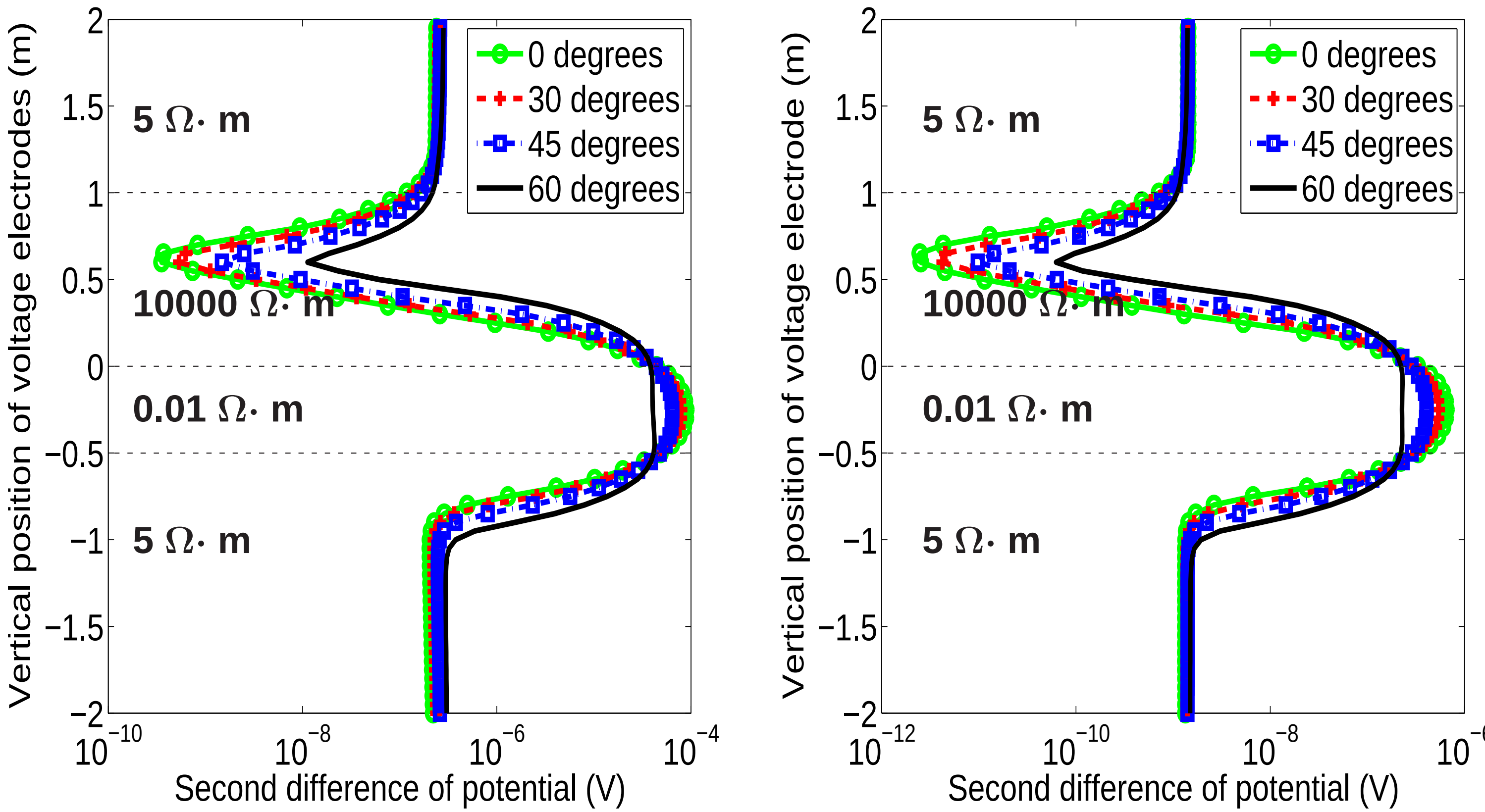

Qualitatively, results for various casing conductivities are similar even for deviated wells.

3D: ELECTROMAGNETIC SIMULATIONS

Through Casing Resistivity Measurements (Invasion)

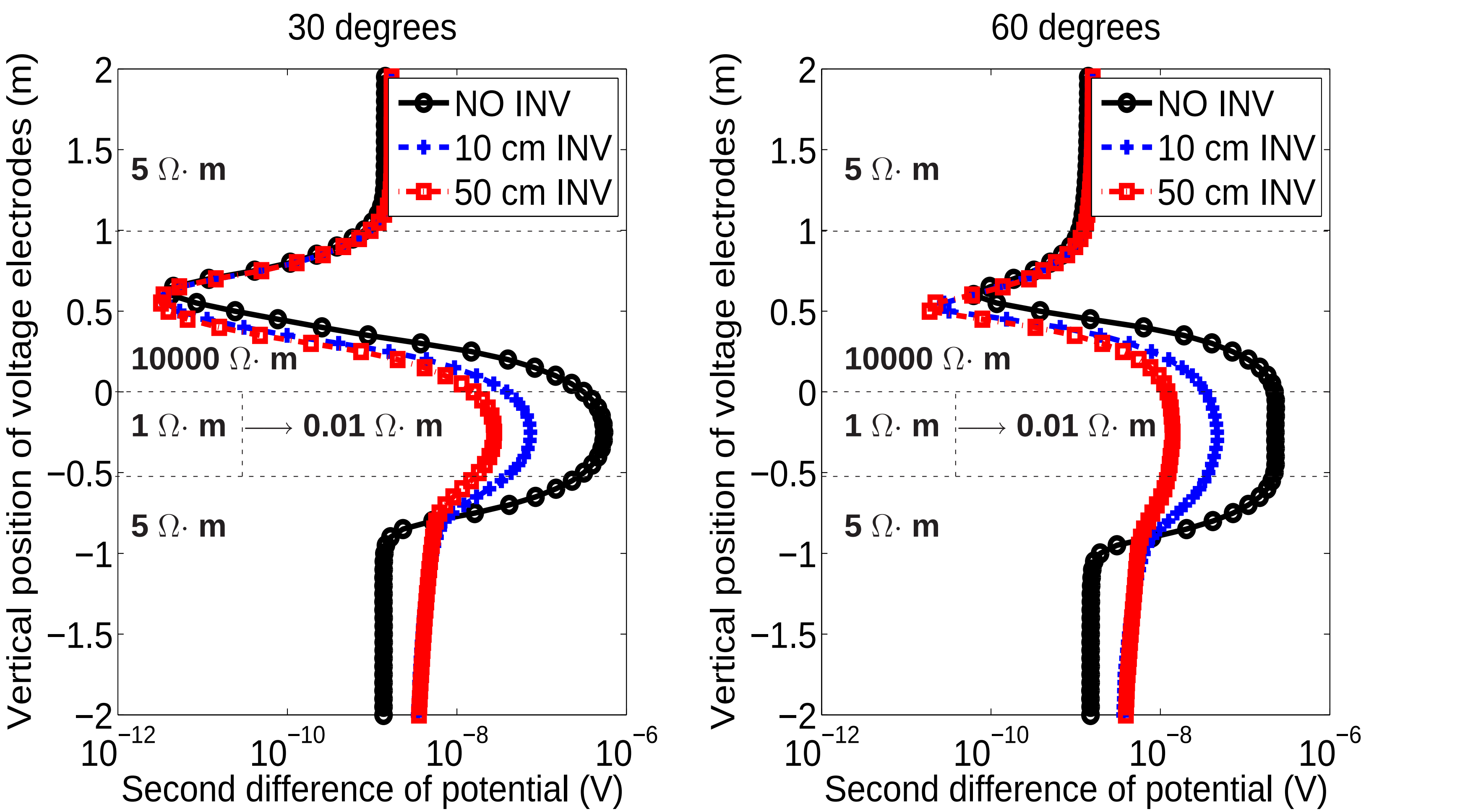

3D: ELECTROMAGNETIC SIMULATIONS

Through Casing Resistivity Measurements (Invasion)

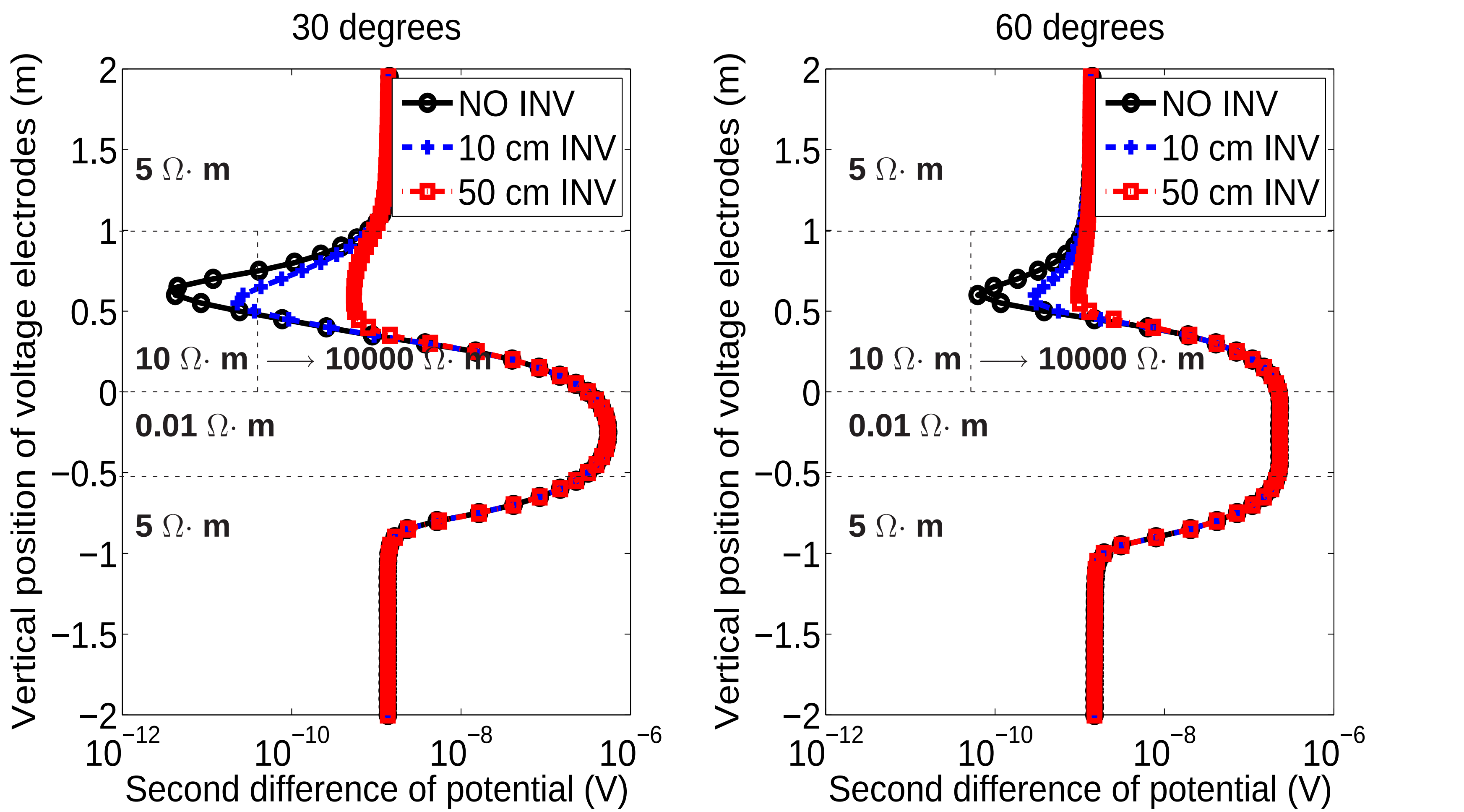

3D: ELECTROMAGNETIC SIMULATIONS

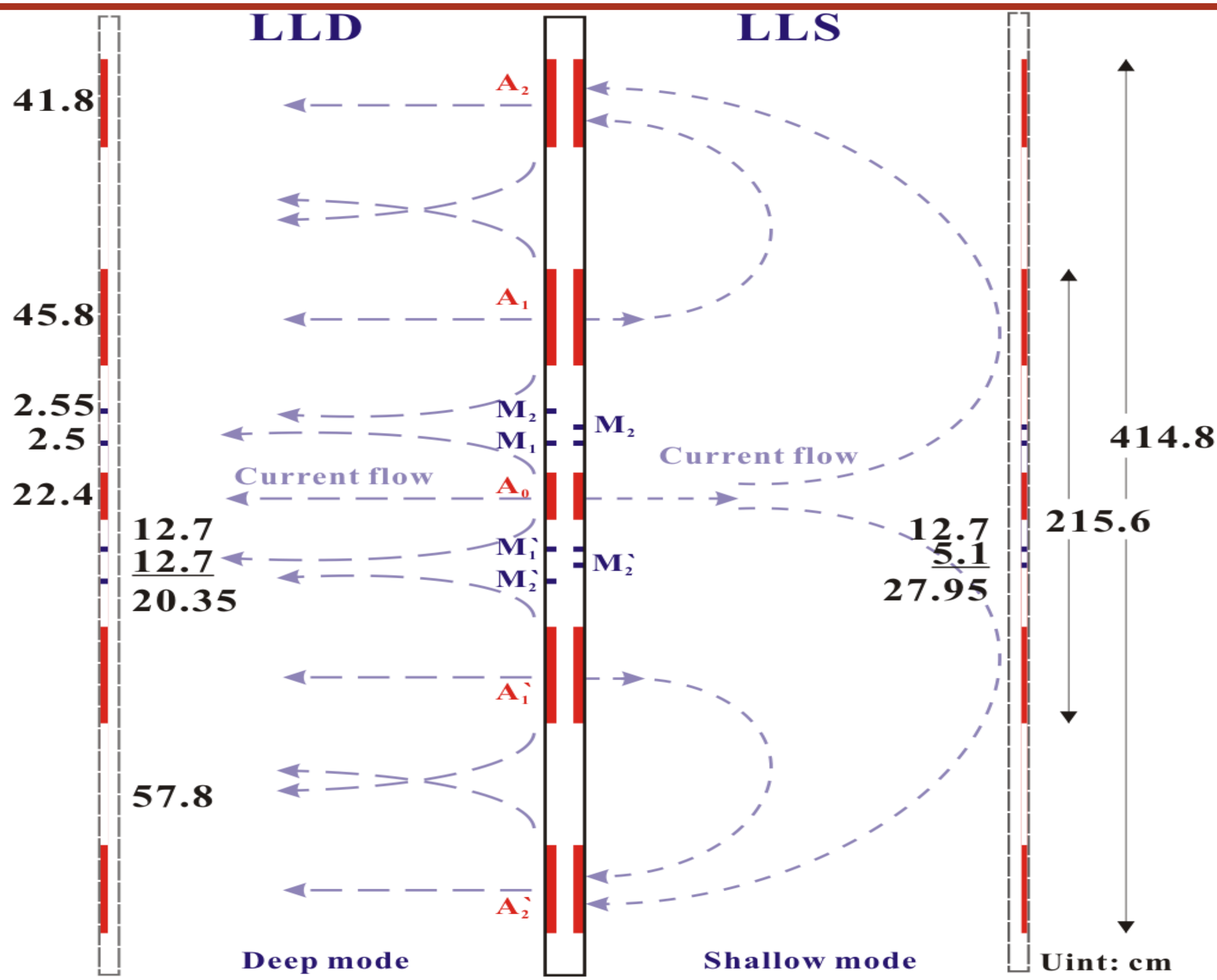

DUAL LATEROLOG - Halliburton Energy Services

3D: ELECTROMAGNETIC SIMULATIONS

Laterolog Measurements

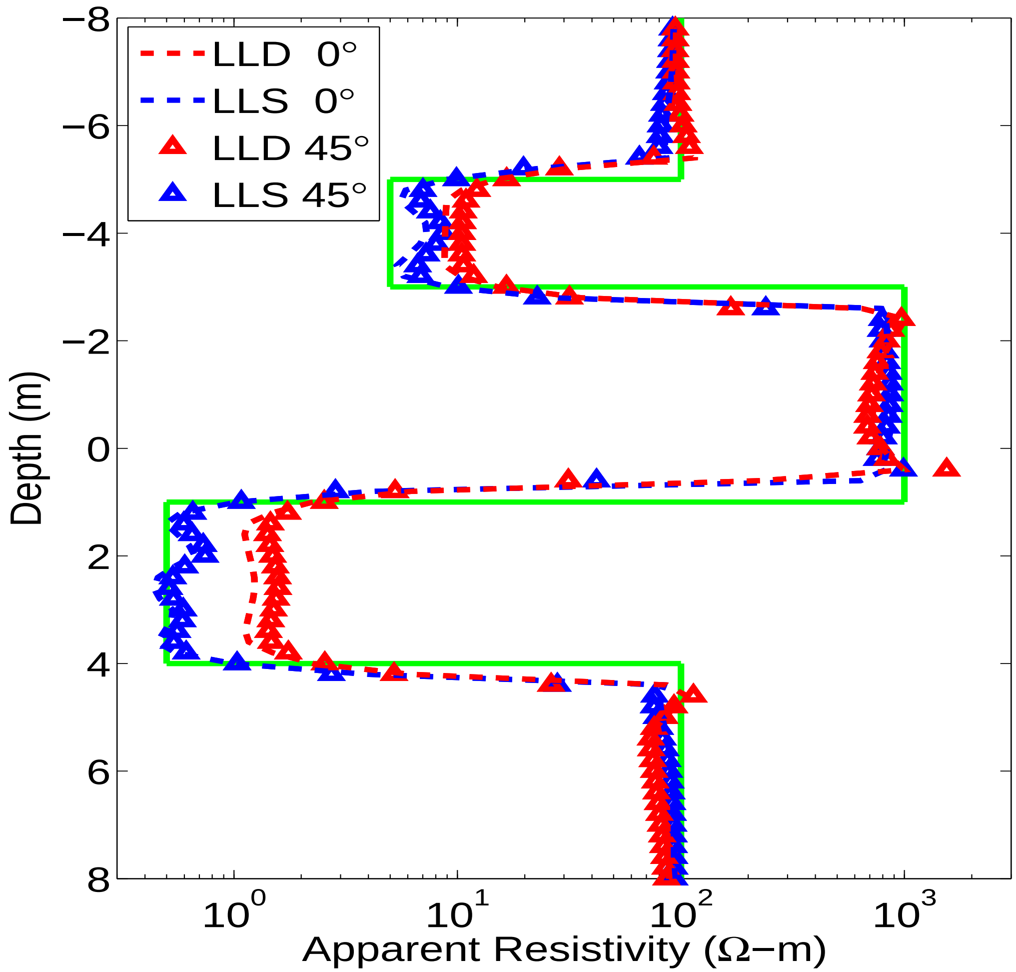

3D: ELECTROMAGNETIC SIMULATIONS

Model Problem and Verification

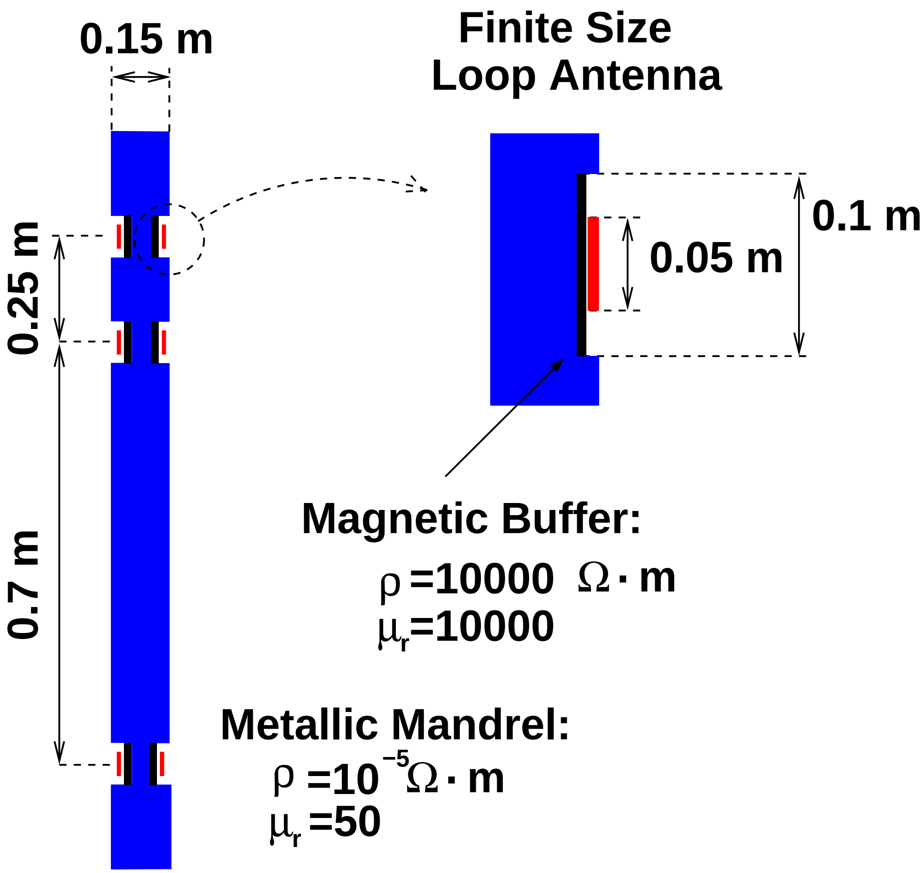

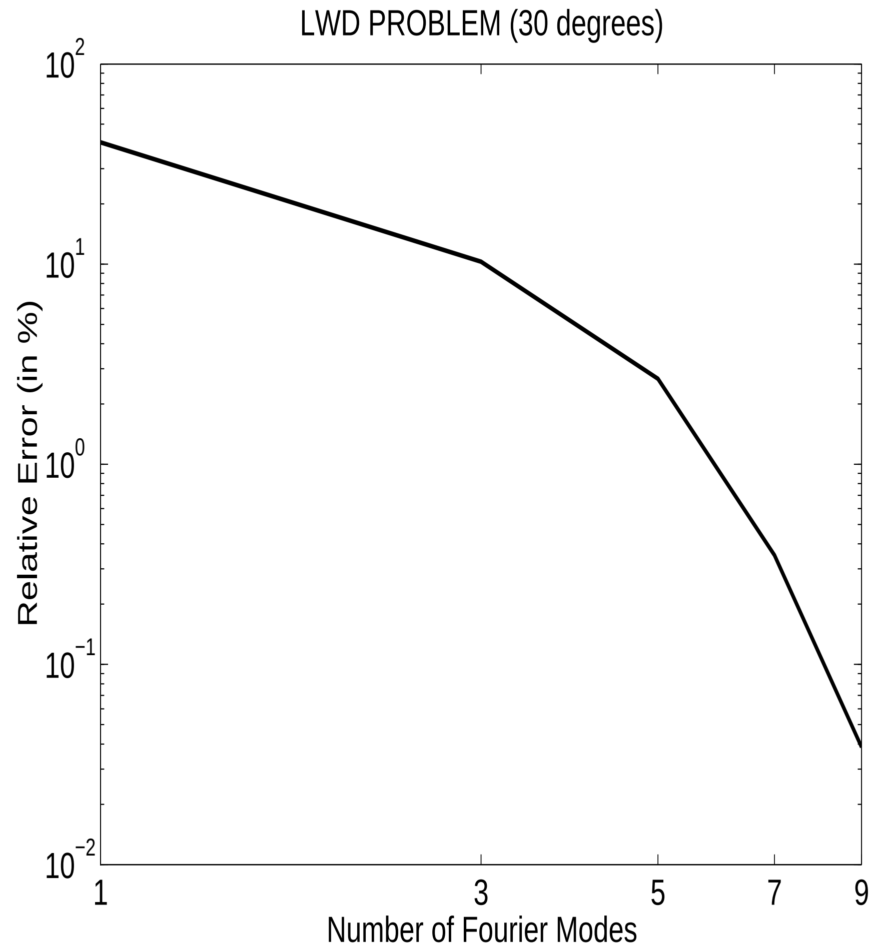

3D: ELECTROMAGNETIC SIMULATIONS

Dip Angle

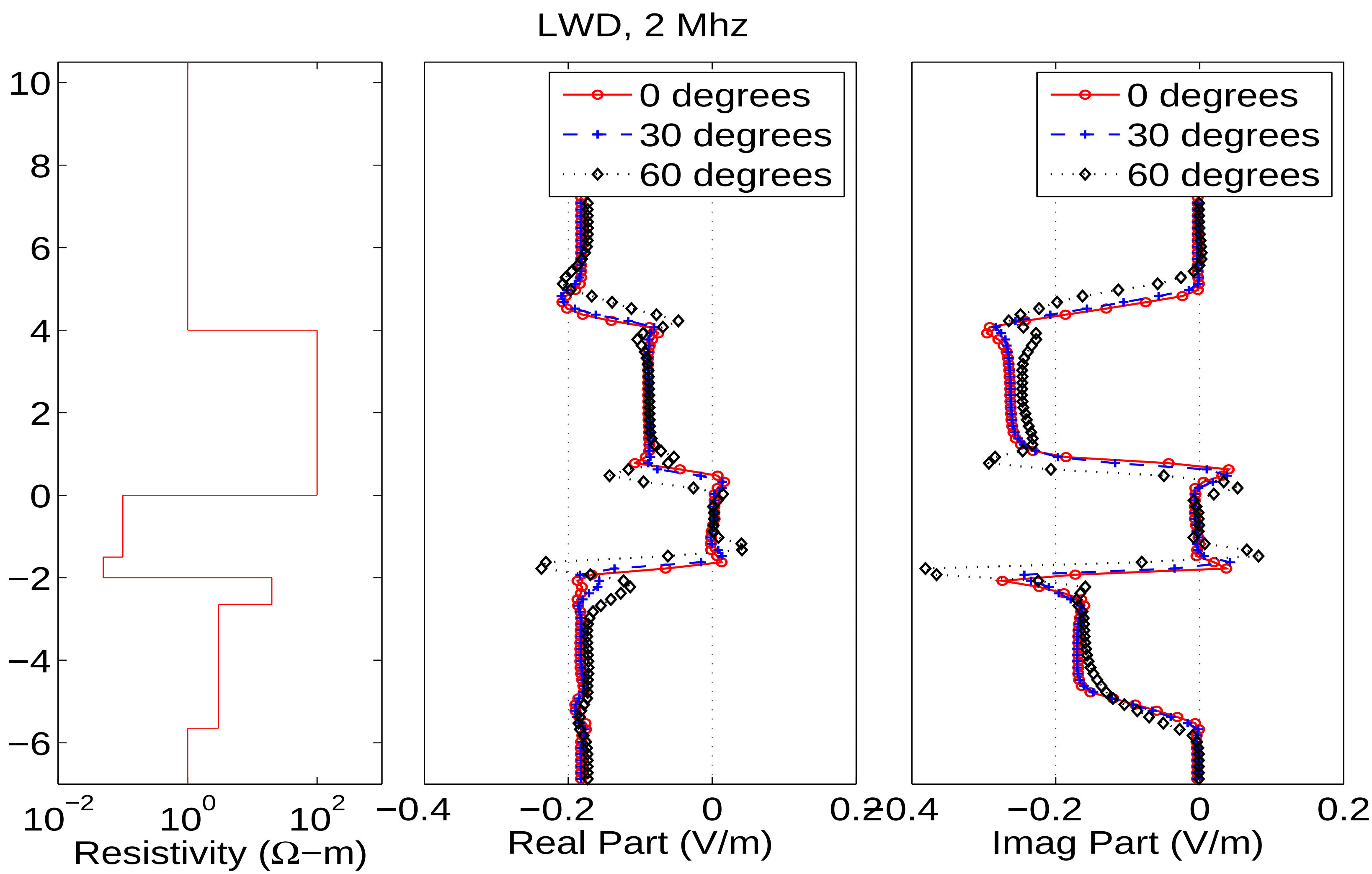

3D: ELECTROMAGNETIC SIMULATIONS

Dip Angle + Invasion

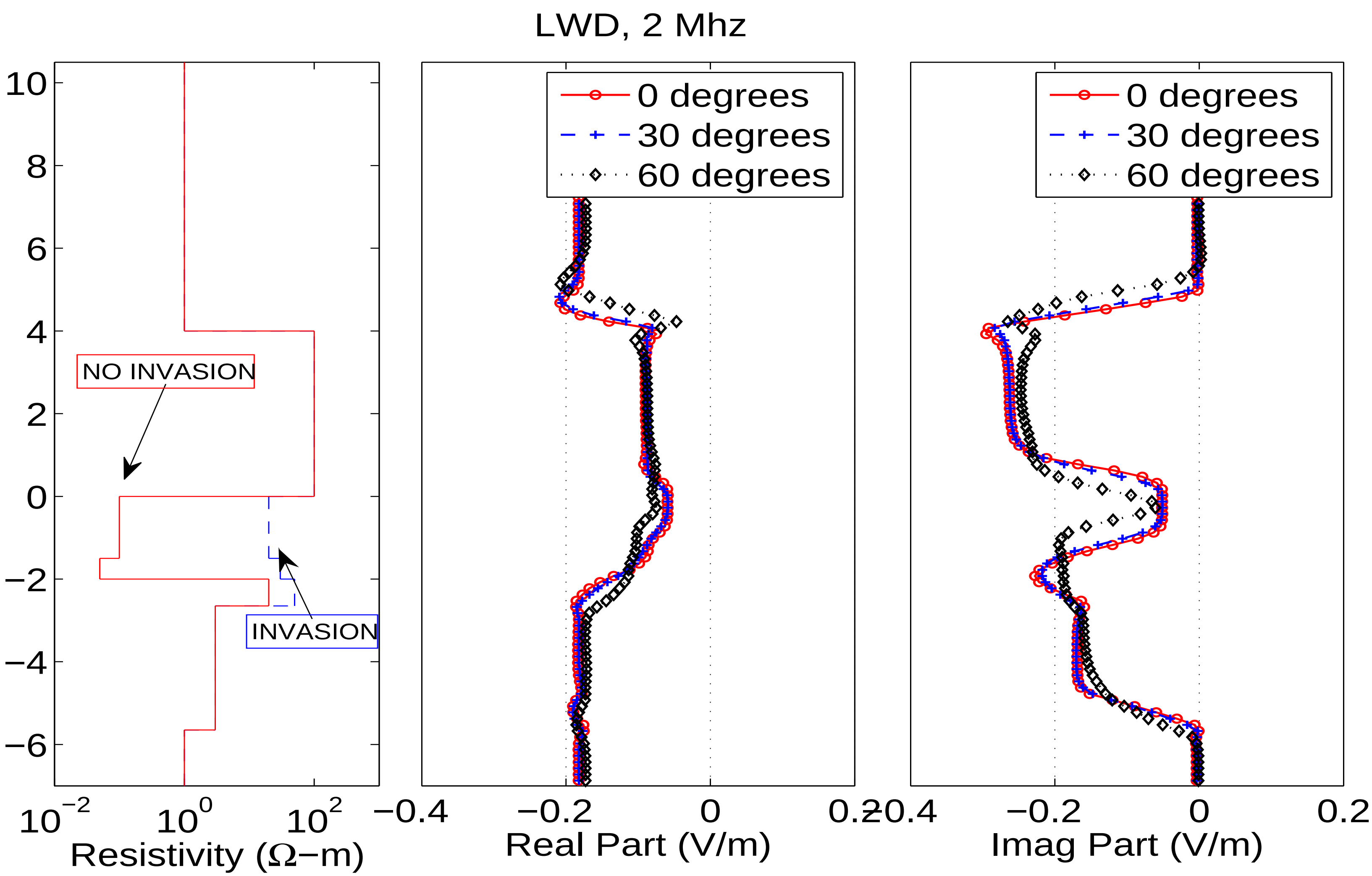

3D: ELECTROMAGNETIC SIMULATIONS

Dip Angle + Anisotropy

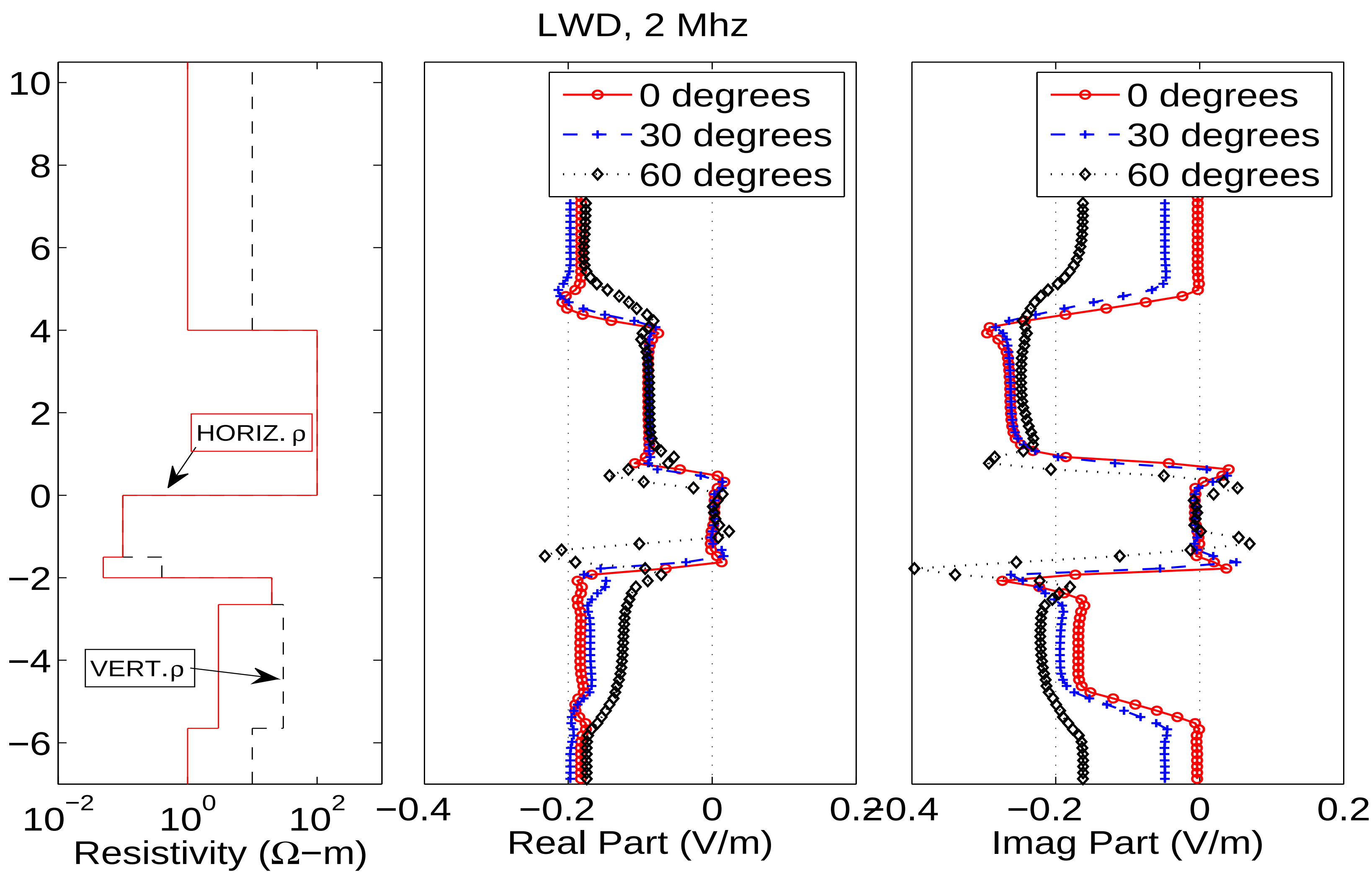

3D: ELECTROMAGNETIC SIMULATIONS

Dip Angle + Invasion + Anisotropy

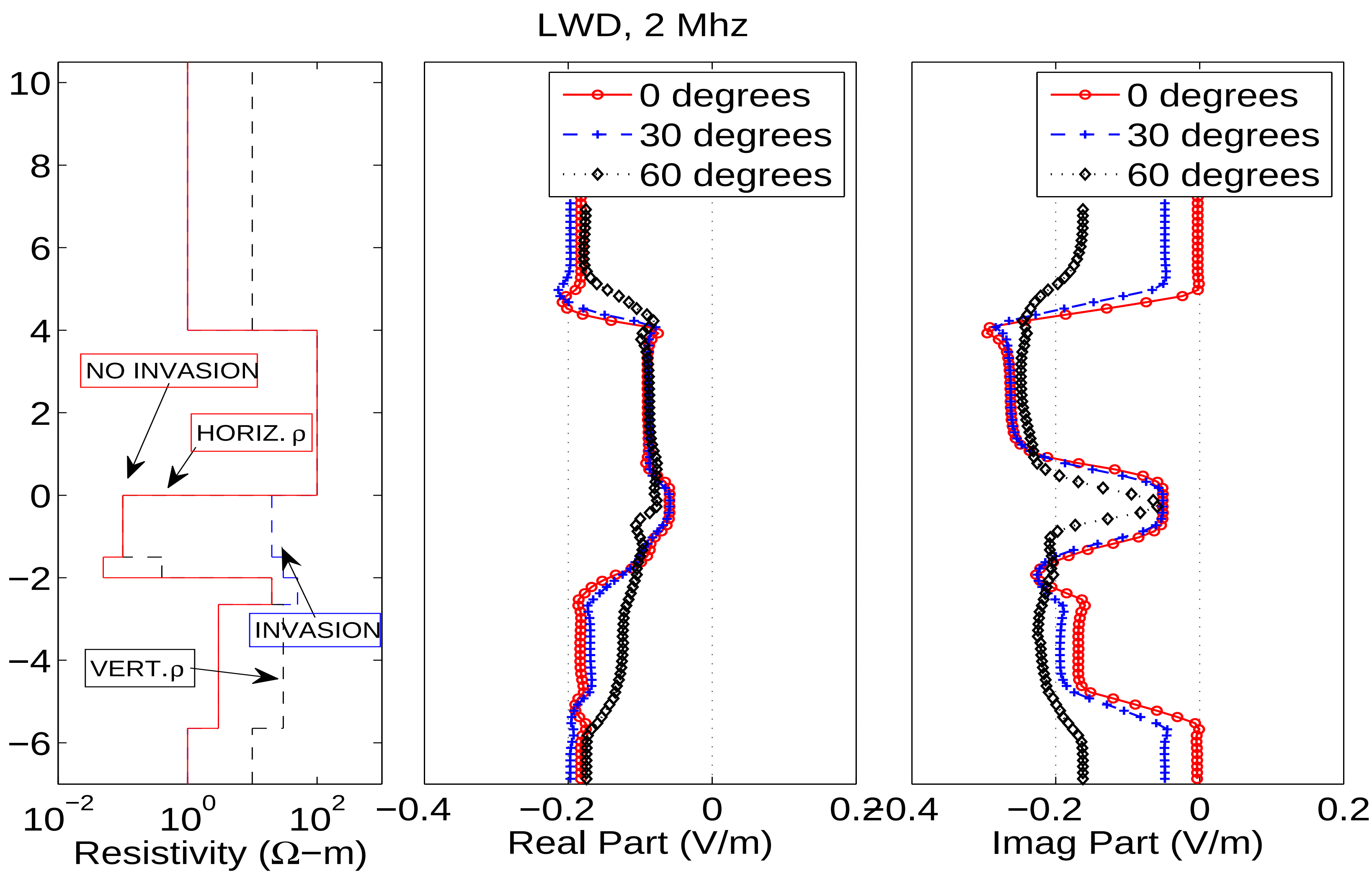

3D: ELECTROMAGNETIC SIMULATIONS

60-Degree Deviated Well

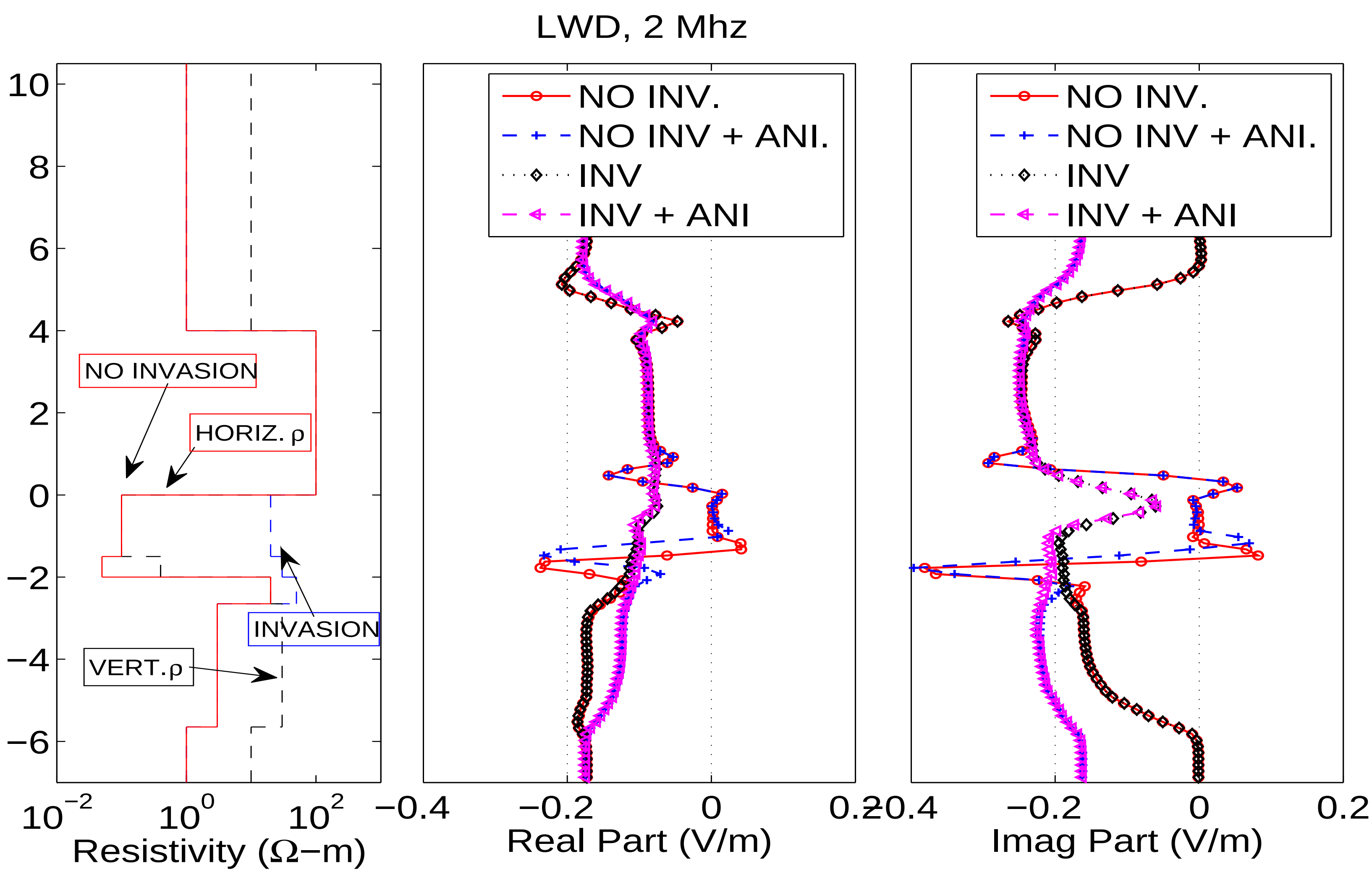

CONCLUSIONS AND FUTURE WORK

Conclusions:

- The goal-oriented hp-Finite Element Method (FEM) enables accurate solution of challenging problems that cannot be solver otherwise.
- A method based on combining a Fourier-series expansion in a non-orthogonal system of coordinates with a 2D hp-FEM can be succesfully employed to simulate problems in deviated wells.

Future Work:

- Time domain simulations.
- Fluid-flow simulations.
- Inverse multi-physics problems.

ACKNOWLEDGMENTS

Sponsors of UT Consortium on Formation Evaluation

Anadarko Petroleum Corporation
Saudi Aramco
Baker Hughes
Baker Atlas
bhpbilliton
bp
Chevron
ConocoPhillips
Agip
Eni
ExxonMobil
HALLIBURTON
IMP innovar
INSTITUTO MEXICANO DEL PETRÓLEO
Marathon Oil Corporation
HYDRO
OXY occidental petroleum corporation
BR PETROBRAS
Schlumberger
Shell
STATOIL
TOTAL
Weatherford